THE PYRETHROID DELTAMETHRIN WHICH CAUSES CHOREOATHETOSIS WITH SALIVATION (CS-SYNDROME) ENHANCES CALCIUM ION INFLUX VIA PHOSPHORYLATED $CA_V2.2$ EXPRESSED IN *XENOPUS LAEVIS* OOCYTES

A Thesis Presented

by

ANNA-MARIA F. ALVES

Submitted to the Graduate School of the
University of Massachusetts-Amherst in partial fulfillment
of the requirements for the degree of

MASTER OF SCIENCE

February 2012

Molecular and Cellular Biology

THE PYRETHROID DELTAMETHRIN WHICH CAUSES CHOREOATHETOSIS WITH SALIVATION (CS-SYNDROME) ENHANCES CALCIUM ION INFLUX VIA PHOSPHORYLATED $CA_V2.2$ EXPRESSED IN *XENOPUS LAEVIS* OOCYTES

A Thesis Presented

by

ANNA-MARIA F. ALVES

Approved as to style and content by:

_____
John M. Clark, Chair

_____
Kathleen F. Arcaro, Member

_____
Steven B. Symington, Member

_____
Barbara A. Osborne, Program Head
Molecular and Cellular Biology

DEDICATION

To my family and friends for their guidance and support.

ACKNOWLEDGMENTS

I would like to thank my advisor, Dr. John M. Clark, who has been an outstanding mentor and who has taught me many valuable skills that will allow me to succeed in my research career and future endeavors.

I would also like to thank my committee members, Dr. Kathleen Arcaro, Dr. Steven Symington, who have been invaluable resources throughout my undergraduate and graduate career while at the University of Massachusetts-Amherst.

Special thanks to “Clark Lab” members who so selflessly trained me and provided me with invaluable support: Kyong-Sup Yoon, Domenic Previte, Hilliary Hodgdon, Joseph Strycharz and Richard Frisbie.

And to the faculty and staff of the Molecular and Cellular Biology Program who have made my time at the University of Massachusetts-Amherst a truly memorable experience.

ABSTRACT

THE PYRETHROID DELTAMETHRIN WHICH CAUSES CHOREOATHETOSIS WITH SALIVATION (CS-SYNDROME) ENHANCES CALCIUM ION INFLUX VIA PHOSPHORYLATED $CA_V2.2$ EXPRESSED IN *XENOPUS LAEVIS* OOCYTES

FEBRUARY 2012

ANNA-MARIA F. ALVES

B.S., UNIVERSITY OF MASSACHUSETTS AMHERST

M.S., UNIVERSITY OF MASSACHUSETTS AMHERST

Directed by: Professor John M. Clark

Pyrethroids are insecticides used since the 1970s. They are favored for their low mammalian toxicity, improved environmental stability and insecticidal potency. Voltage-gated sodium channels (VGSCs) are a known target but *in vitro* evidence indicates that voltage-gated calcium channels (VGCCs) are also targets. Site-directed mutagenesis of $Ca_V2.2$ (N-type), altering threonine 422 to glutamate (T422E), produces a mutant channel that acts as if permanently phosphorylated. Deltamethrin increases peak current of T422E $Ca_V2.2$ compared to its antagonistic action on wild type $Ca_V2.2$ when expressed in *Xenopus* oocytes. Phosphorylation of wild type $Ca_V2.2$ is evoked by the phorbol ester PMA by activating endogenous protein kinase C (PKC) in oocytes. Under steady-state conditions, deltamethrin increases transient peak current and slows deactivation kinetics of the PKC phosphorylated channel thereby increasing Ca^{2+} influx and neurotransmitter release. Conversely, deltamethrin treatment resulted in no effect on the deactivation kinetics of the unphosphorylated or T422E channels. Under voltage-dependent conditions, deltamethrin enhances peak current, and causes a hyperpolarizing shift in

activation midpoint potential of the PKC phosphorylated channel which is consistent with enhanced Ca^{2+} influx. The hyperpolarizing shift of activation midpoint potential was not observed when deltamethrin was applied to the T422E mutant channels indicating that the other phosphorylation sites on $Ca_V2.2$ may be playing a role in the differential effects observed in the action of deltamethrin on the unphosphorylated channel, the T422E mutant and the PMA-activated PKC phosphorylation channel.

TABLE OF CONTENTS

LIST OF TABLES

Table Page

LIST OF FIGURES

Figure Page

CHAPTER 1

INTRODUCTION

1.1 Pyrethroid Insecticides

Pyrethroids are a class of synthetic insecticides used widely since the 1970s both in agriculture and urban environments. They are derived from the naturally-occurring insecticide pyrethrum, which is isolated from the flower heads of the chrysanthemum flower *Chrysanthemum cinerariaefolium*. Pyrethrum is highly labile due to its instability in sunlight and water caused by spontaneous cleavage of the central ester bond by photolysis and hydrolysis, respectively (Soderlund et al., 2002; Hossain et al., 2004). It is a mixture of six pyrethrin esters: pyrethrin I (Fig. 1) and II, cinerin I and II, and jasmolin I and II. Pyrethroids (synthetic pyrethrins) were developed to meet the need for potent insecticides with low mammalian toxicity but without the drawbacks of environmental instability, which limited the effectiveness of pyrethrum in crop protection and vector control (Soderlund et al., 2002). Among the pyrethroids, there is no specific substructure, reactive entity, or molecular moiety that can be identified as the common toxophore conferring pyrethroid-like insecticidal activity. Instead, toxicity results from the goodness of fit of the entire molecule at its site of action (Soderlund et al., 2002).

Pyrethroids target the voltage-gated sodium channels (VGSC) of insect pests as well as those of mammals, although mammalian VGSC vary in their biophysical and pharmacological properties from the insect channel. These differences result in different sensitivities of the various mammalian VGSC to pyrethroids (Soderlund et al., 2002). To date, the binding site of pyrethroids to VGSCs has yet to be elucidated.

The voltage-gated calcium channels (VGCC) and voltage-gated chloride channels (VGClC) are also pyrethroid targets and almost assuredly contribute to the overall neurotoxicity of the pyrethroids (Soderlund et al., 2002). A subset of α-cyano containing pyrethroids increased neurotransmitter release in the mammalian brain under depolarizing conditions. This effect is blocked by ω-conotoxin GVIA, a specific blocker of N-type VGCC, thereby implicating this subset of VGCC. The exact binding site on these channels has likewise yet to be elucidated (Brooks and Clark, 1987; Clark and Brooks, 1989; Soderlund and Lee, 2001; Hossain et al., 2004; Shafer and Meyer, 2004).

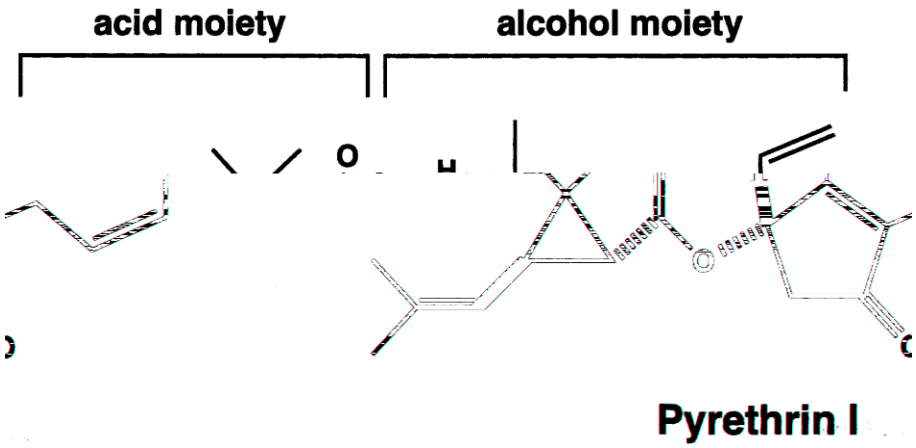

Figure 1. The chemical structure of pyrethrin I, the most toxic ester of pyrethrum. This structure is the basis for all pyrethroids (reproduced from Soderlund et al., 2002) (Soderlund et al., 2002).

1.2 Tremor (T-) and Choreoathetosis with Salivation (CS-) Syndromes

Based on their structure and generally on their ability to produce either a tremor (T) or a choreoathetosis with salivation (CS) intoxication syndrome, pyrethroids have been classified into two groups (Soderlund et al., 2002). For the most part, Type I (non α-

cyano) pyrethroids elicit the T-syndrome and Type II (α-cyano) pyrethroids cause the CS-syndrome of intoxication in mammals. T-syndrome symptoms include hypersensitivity, stimulus-induced bouts of general tremors, convulsive twitching, coma and death. CS-syndrome symptoms include salivation, jerking leg movements, progressive writhing convulsions and death (Soderlund et al., 2002). Using a functional observational battery (FOB), bifenthrin, tefluthrin, β-cyfluthrin and λ-cyhalothrin, which had been previously uncategorized, were placed within the T/CS-syndrome system (Choi and Soderlund, 2006; Weiner et al., 2009). Based on FOB data, two functional groups were proposed. Group 1 (T-syndrome) includes pyrethrins, resmethrin, permethrin, S-bioallethrin, bifenthrin, and tefluthrin. Group 2 (CS-syndrome) includes cypermethrin, deltamethrin, esfenvalerate, β-cyfluthrin and λ-cyhalothrin (Weiner et al., 2009). By exhibiting features of both groups, fenpropathrin, an α-cyano pyrethroid which had been previously described as causing a mixture of T- and CS-syndrome symptomologies and therefore not definitely a member of either class, remains unclassified (Breckenridge et al., 2009; Weiner et al., 2009).

1.3 Pyrethroid Neurotoxicity

The differences between how T- and CS-syndrome pyrethroids cause mammalian neurotoxicity apparently lay in their three-dimensional chemistry. The absence (Type I) or presence (Type II) of an α-cyano group in the 3-phenoxybenzyl alcohol moiety provides one of the key differences between the two types of pyrethroid structures. The presence of the α-cyano moiety provides Type II pyrethroids with a much greater level of insecticidal potency than their non α-cyano Type I counterparts, while maintaining the

same level of photostability (Soderlund et al., 2002). Type II pyrethroids are also less sensitive to ester bond hydrolysis (Brooks and Clark, 1987; Hossain et al., 2004).

Previous studies have shown that Type I pyrethroids that produce the T-syndrome and Type II pyrethroids that cause the CS-syndrome cause differential effects on the release of acetylcholine (ACh) from both whole brain and cerebellum of rats (Aldridge et al., 1978). The study compared the effects of cismethrin (a Type I pyrethroid that causes T-syndrome) with those of deltamethrin (a Type II that causes CS-syndrome) and found that only deltamethrin caused significantly more ACh release compared to cismethrin. In another study, freely moving rats were dosed with allethrin (a Type I pyrethroid that causes T-syndrome) and deltamethrin and λ-cyhalothrin (Type II pyrethroids that cause CS-syndrome) (Hossain et al., 2004). In this study, allethrin had a dose-dependent effect on ACh efflux. Low doses caused an increase in ACh efflux whereas high doses caused a decrease. Deltamethrin and λ-cyhalothrin had opposite results from one another: deltamethrin caused a dose-dependent increase in ACh release and λ-cyhalothrin caused a dose-dependent decrease. The differences apparent in the amount of neurotransmitter release in the presence of allethrin versus deltamethrin support the contention that some Type I and Type II pyrethroids may have different sites of action. The differences between the actions of λ-cyhalothrin and deltamethrin on ACh release despite both being Type II pyrethroids may, in part, be due to the differences in their three-dimensional configurations. β-cyfluthrin and λ-cyhalothrin, both close structural analogs of deltamethrin, prolongs Na^+ channel activation and deactivation kinetics beyond that of deltamethrin (Choi and Soderlund, 2006). Together with the FOB data, the prolongation of channel kinetics by β-cyfluthrin and λ-cyhalothrin, places the two pyrethroids within

the CS-syndrome class (Weiner et al., 2009).

The aquatic ciliate *Paramecium tetraurelia* has been shown to be one of the most sensitive organisms to pyrethroids, especially deltamethrin (Clark et al., 1995), despite their lack of VGSCs, long considered a major pyrethroid target (Symington et al., 1999b). Electrophysiological experiments showed that deltamethrin was toxic to *P. tetraurelia* under depolarizing conditions because they caused a significant increase in Ca^{2+} influx via their voltage-gated calcium channel, which control cilia motor function. When exposed to Type-II pyrethroids, *P. tetraurelia* exhibit increased backwards swimming behavior, which is controlled explicitly by increased Ca^{2+} influx via VGCCs (Symington et al., 1999a; Symington et al., 1999b). Pawn mutants, which lack VGCCs, were unaffected by deltamethrin and wild type cells were unaffected by the inactive 1*S* enantiomer of deltamethrin. Lastly, deciliated paramecia are no longer sensitive to the toxic action of deltamethrin. In summary, these biochemical and behavioral studies have shown that: 1) there is a difference in the action of pyrethroids based on the presence or absence of an α-cyano group, and 2) in addition to VGSCs, VGCCs are also pyrethroid targets.

1.4 Structure-Activity Relationships

The structure-activity relationship (SAR) for pyrethroids is based on the physical properties and three-dimensional configuration of the entire molecule. Thus, the activity of a pyrethroid is based upon how well the entire molecule fits at the site of action and there exists a wide range of structures that satisfy this requirement (Elliott et al., 1974; Soderlund et al., 2002).

The stereospecificity at the C1 carbon of the cyclopropane ring of the acid moiety is a major SAR that confers insecticidal action. Pyrethroids that have the *R* configuration at C1 (1*R*) have high insecticidal activity whereas pyrethroids in the *S* configuration (1*S*) have no insecticidal activity despite being chemically identical to the 1*R* enantiomer (Elliott et al., 1974). For fenvalerate, which does not have a cyclopropane in its acid moiety, a *S* configuration around the C2 carbon of the 3-methyl butyrate moiety, which mimics the 1R configuration of cyclopropane-containing pyrethroids, confers insecticidal activity whereas the *R* configuration is not insecticidal (Soderlund et al., 2002).

1.5 Voltage-gated Ion Channels

Members of the voltage-gated ion channel family include sodium (Na^+), potassium (K^+), chloride (Cl^-) and calcium (Ca^{2+}) ion channels and are found in various tissues (e.g., skeletal muscle, pancreas, cochlea, kidney, liver and nerve) where they provide a number of regulatory functions. VGSCs and VGCCs share substantial structural homology between their pore-forming α-subunits (Catterall, 1997; Shafer and Meyer, 2004). When either channel is activated, there is an influx of extracellular cations via the "opened" channel, which is positioned in the plasma membrane, thereby depolarizing the membrane. The voltage-gated potassium channel (VGPC) assist in rectifying membrane potential after depolarization by transporting K^+ ions out of the cell to counteract the increase of positive charge on the inside due to the influx of cations (Na^+, Ca^{2+}) through VGSCs and VGCCs (Martinez-Pinna et al., 2000). Ca^{2+}-activated Cl^- channels also assist in rectifying membrane potential by transporting Cl^- ions into the cell in response to the increase in intracellular Ca^{2+} (Hartzell et al., 2005).

1.6 Structure and Function of VGSCs

VGSCs play a central role in the initiation and propagation of action and generator potentials of electrically excitable cells, such as neurons (Yu and Catterall, 2003). VGSCs are multimeric proteins made up of an ion conducting pore (α-subunit) and the two auxiliary β-subunits, β_1 and β2. VGSC α-subunits contain four internally homologous domains, each made up of six α-helical transmembrane segments. β subunits are membrane-bound subunits connected to α-subunits by disulfide bonds.. Co-expression of β subunits with the α subunit increases the level of functional expression, causes a shift in the voltage-dependence of activation, and greatly accelerates channel inactivation (Isom et al., 1992; Isom et al., 1995).

Voltage dependence of the VGSCs plays a central role in the initiation and propagation of action potentials in nerve axons and in the production of electrical impulses in other electrically excitable cells. There are three functional characteristics that are used to identify VGSCs electrophysiologically. The first functional characteristic of VGSCs is activation which occurs via the outward movement of the positive "gating" charges on the helical S4 transmembrane segment of each transmembrane domain in response to changes in the membrane electric field (going from positive to negative on the outside surface of the membrane during depolarization) (Hodgkin and Huxley, 1952; Armstrong, 1981; Catterall, 2000a; Catterall, 2000b). The VGSC S4 transmembrane segment contains a cylindrical α-helix of repeating motifs consisting of one positive followed by two negative amino acids. When the ion-conducting pore of the channel is closed, the negatively charged internal electric field of the channel pulls the positively

charged amino acids of the S4 helix into the cell. In response to depolarization of the membrane, the S4 segment moves outward from the cell changing the conformation of the channel from a closed state to an open state thus allowing for the movement of ions through the ion conducting pore (Catterall, 2000b). The influx of Na^+ ions through the pore formed by the activated α-subunit further depolarizes the membrane and initiates the rising phase of the action potential. The conformational change of VGSC from a closed to an open state (activation) as the result of the S4 segments response to membrane depolarization occurs within a few milliseconds. The influx of Na^+ ions through the open channel into the cell is characterized by a measured transient peak current.

The second functional attribute is channel inactivation, which occurs under steady-state depolarization in response to channel activation, is characterized by the decay of "transient peak current". Under steady-state depolarization, VGSC inactivates when the inactivation gate, the intracellular III-IV transmembrane loop of the α-subunit, moves to block the ion-conducting pore by binding to a receptor on the intracellular mouth of the pore (Armstrong, 1981; Kellenberger et al., 1996; Catterall, 2000b; Kass, 2004). In sodium channels, inactivation is biphasic with the initial phase τ_{fast} and the slower secondary phase τ_{slow} and is measured as "late current" (Tan and Soderlund, 2009). Fast inactivation (τ_{fast}) is regulated by the inactivation gate and is coupled to channel activation whereas slow inactivation (τ_{slow}) is voltage-dependent (Kass, 2004).

The third functional attribute is deactivation. The current that occurs after the removal of steady state membrane depolarization (repolarization) is termed "tail current" and is a measure of deactivation.

In mammals, multiple VGSC isoforms exist that are encoded by a family of

homologous genes. Each isoform varies in its sensitivity to pyrethroids, both within and between the α- and non-cyano structural classes, which make the characterization of mammalian VGSCs complicated (Goldin et al., 2000; Soderlund et al., 2002; Yu and Catterall, 2003). The complete VGSC sequences for mammalian isoforms are designated as $Na_V1.1$-$Na_V1.9$ and each has been functionally characterized as encoding a voltage-gated ion channel (Goldin et al., 2000). The expression patterns of the different VGSC isoforms are tissue dependent and developmentally regulated (Choi and Soderlund, 2006). VGSCs are expressed in cardiac muscles, skeletal muscles and different anatomical regions of the central and peripheral nervous systems (Yu and Catterall, 2003) and exist in several states of alertness: closed resting state, open activated state, inactive open state, and inactive closed state (Rossie, 1999).

1.7 Neuropharmacology of Mammalian VGSC

VGSCs located in the rat dorsal root ganglion neurons can be formally divided into three groups. VGSCs whose currents are blocked by the neurotoxin tetrodotoxin (TTX) are TTX-sensitive (TTX-S), VGSCs whose currents are not blocked by TTX (TTX-resistant; TTX-R) and VGSCs whose currents are partially sensitive to TTX (TTX-partially sensitive; TTX-PS) (Roy and Narahashi, 1992; Ginsburg and Narahashi, 1993; Ogata and Tatebayashi, 1993; Choi and Soderlund, 2006). Analysis of VGSC isoforms determined that carriers of TTX-R currents are very sensitive to pyrethroids and had much faster activation and inactivation rates than VGSC carriers of TTX-S currents (Ginsburg and Narahashi, 1993; Ogata and Tatebayashi, 1993). $Na_V1.8$, the principle carrier of TTX-R current is located in the small diameter of the rat dorsal root ganglion

neuron (DRG), which is part of the peripheral nervous system (Akopian et al., 1996).

1.8 Pyrethroid Neurotoxicity to Mammalian VGSCs

Pyrethroids alter the normal function of VGSC by acting as channel agonists. Type I pyrethroids (e.g. allethrin, permethrin, tefluthrin, bifenthrin and cismethrin) have been shown to slow activation and inactivation kinetics of VGSC moderately while deactivation kinetics (tail current) decayed rapidly. On the other hand, Type II pyrethroids (e.g., deltamethrin, cypermethrin) slow activation and inactivation kinetics more than Type I pyrethroids and significantly slow deactivation, leading to extensive prolongation in the Na^+ tail current. Fenvalerate and fenpropathrin, both α-cyano pyrethroids, changed VGSC kinetics to a degree that was intermediate between the Type I and Type II pyrethroids. Although fenvalerate has been classified as a Type II pyrethroid based on other criteria and fenpropathrin has been characterized as a Type II pyrethroid structurally but is intermediate in its action in a FOB study (Weiner et al., 2009). Fenvalerate and fenpropathrin slow activation and inactivation kinetics much like Type II pyrethroids, but tail currents rapidly decay like Type I pyrethroids. Cyhalothrin and cyfluthrin (α-cyano) also cause extremely slow deactivation kinetics allowing pronounced tail current. In fact, cyhalothrin effect was greater than that of deltamethrin, which makes it an extreme example of a Type II pyrethroid that produces the CS-syndrome. The effect of cyfluthrin on tail current was also greater than deltamethrin, but was not as significant as that of cyhalothrin (Choi and Soderlund, 2006).

VGSCs mediate the transient Na^+ permeability of the cell membrane that is associated with the production of rising phase of the action potential in vertebrate and

invertebrate nerves and in vertebrate skeletal and cardiac muscles. Type I pyrethroids increase the rate of VGSC activation by causing a hyperpolarizing shift of the membrane potential at which VGSC activate (Shafer et al., 2005), moderately slow channel inactivation and cause rapidly decaying deactivation kinetics (Choi and Soderlund, 2006). These effects on VGSC kinetics by Type I pyrethroids produce transient depolarizing after potentials and result in repetitive firing of action potentials (repetitive discharges), which are the cause of the T-syndrome (Shafer et al., 2005; Choi and Soderlund, 2006; Ray and Fry, 2006). Type II pyrethroids in general slow the rate of channel activation and inactivation but result in persistent tail currents. This prolonged opening of the channel allows excess Na^+ ions to enter the nerve resulting in rapid and substantial membrane depolarization to the point that the generation of action potentials is no longer possible, a condition called conduction block (Soderlund and Bloomquist, 1989; Soderlund et al., 2002; Hildebrand et al., 2004; Shafer and Meyer, 2004; Ray and Fry, 2006).

1.9 Classification and Function of VGCCs

VGSCs are not the only channels affected by pyrethroids. VGCCs, which play a role in nerve cell excitability, calcium homeostasis, synaptic signaling and gene expression modulation, are also affected. VGCC are heteromeric protein complexes made up of α_1, β, $\alpha_2\delta$, and sometimes λ subunits. There are as many as ten α_1 subunit isoforms of VGCCs (Catterall et al., 2003). Each forms the ion conducting pore of the channel and contains major determinants for functional and pharmacological properties of VGCCs. All α_1 subunits have four repeating domains, each consisting of six transmembrane α helical segments (S). There is a membrane associated loop between S5

and S6 in each domain. The S4 segment of each homologous domain serves as the voltage sensor for activation (Catterall, 2000a). There are four the β subunit isoforms and unlike the α_1-subunit, all are entirely cytoplasmic. The β subunit modulates functional characteristics and membrane expression of the α- subunits (Hanlon and Wallace, 2002; Shafer and Meyer, 2004).

There are five types of VGCC that exist and they are classified based upon their biophysical, electrophysiological and pharmacological properties (Table 1). VGCC channel types are functionally characterized into two groups: those that activate under large depolarizations (high voltage activated; HVA) and those that activate under small depolarizations (low voltage activated; LVA). HVA channels are further divided based on the basis of tissue distribution, biophysical and pharmacological properties into two different gene families; $Ca_V1.2$ (L-Type), $Ca_V2.1$ (P/Q-type), $Ca_V2.2$ (N-Type), and $Ca_V2.3$ (R- type) channels. $Ca_V3.1$ (T-type) channels are the only form of LVA channels. The Ca_v2 channels are responsible for the release of neurotransmitters in the neocortex, hippocampus, cerebellum, neuromuscular junction and the peripheral autonomic effectors (Soderlund et al., 2002; Catterall et al., 2003).Ca_v1 channels, under certain conditions or at certain synapses, will also mediate neurotransmitter release (Xu et al., 1998). VGCC expression is developmentally regulated. Ca_v2 channels express early during the development of the nervous system and are most critical in cerebellar granule migration, gene activation and neurotransmitter release. $Ca_V2.2$ from rat brain is the most important of the VGCCs in neurotransmitter release and in pain transmission pathways (Drean et al., 1995; Finkbeiner and Greenberg, 1998; Vance et al., 1998; Shafer and Meyer, 2004).

VGCCs are further defined based on the pharmacological profile and functional

characteristics of each of their α_1 subunits. The Ca_V1 subfamily conducts L-type currents of the 1S, C, D and F α_1 subunits. The Ca_V2 family conducts N (α_{1B}), P/Q (α_{1A}) and R-type (α_{1E}) Ca^{2+} currents. T-type calcium currents are conducted by the Ca_V3 family of α subunits (α_{1G}, α_{1H} and α_{11}) (Perez-Reyes, 2003; Shafer and Meyer, 2004). Of these, the focus of our investigation will be on the $Ca_V2.2$, or N-type channel, which is localized at low density dendrites and high density nerve terminals of many classes of central neurons, and is the most important VGCC regulating Ca^{2+} dependent neurotransmitter release following depolarization of presynaptic nerve terminals (Catterall, 1997).

1.10 Effects of Pyrethroids on VGCCs

In general, pyrethroids decreased transient peak current of VGSC, prolonged channel inactivation under depolarizing conditions, and slow VGSC closure after repolarization (deactivation) (Narahashi, 1992). To assess what effect pyrethroids have on mammals, freely moving rats were dosed with cismethrin (Type I pyrethroid that produces the T-syndrome) and deltamethrin (Type II pyrethroid that produces the CS-syndrome) (Aldridge et al., 1978). Analysis of neurotransmitter content of the hippocampus and the whole brain after dosing revealed that deltamethrin significantly decreased the amount of ACh in each brain region whereas cismethrin did not. Rats similarly treated with DDT in the same study had no significant increase of ACh release from either of the brain regions studied compared to the control (Aldridge et al., 1978). Deltamethrin administered to freely moving rats caused a dose-dependent increase in the release of ACh from the hippocampus (Hossain et al., 2004).

Together, these studies showed that the CS-syndrome displayed with the dosing of

most Type II pyrethroids is likely due to target sites other than VGSCs. A hyperpolarizing shift in membrane potential of VGSCs due to the presence of Type I pyrethroids and DDT slow channel inactivation and increase late current causing depolarizing after potentials (DAP). DAP cause spontaneous firing of action potentials and long trains of repetitive discharges which are related to the tremors produced by T-type pyrethroids. Type II pyrethroids cause use-dependent conduction block of the action potential and a depolarizing shift in the resting membrane potential by prolonging deactivation kinetics and increasing tail currents (Narahashi and Yamasaki, 1960; Soderlund and Bloomquist, 1989; Narahashi, 1992).

The studies in which rats are dosed with Type II pyrethroids, such as deltamethrin, showed that there was significant neurotransmitter release, a process which is not controlled by VGSCs, and furthermore these studies showed that Type II poisoning caused CS-syndrome. These studies also showed that Type I pyrethroids, like DDT, caused tremors and other symptoms classified under T-syndrome poisoning. It follows from these studies, therefore, that there are alternative targets for Type II pyrethroids, in particular VGCCs which do control neurotransmitter release. Comparatively, decreased peak current and prolongation of activation and inactivation kinetics were observed in deltamethrin-treated N-type VGCC ($Ca_V2.2$), but deactivation kinetics remained unmodified (Symington and Clark, 2005). In rabbit striatal slices, cypermethrin, deltamethrin, and fenvalerate evoked neurotransmitter release 3- to 5-fold above the spontaneous release. Furthermore, fenvalerate also elicited a stereospecific and concentration-dependent release of neurotransmitters from the rabbit striatal slices (Eells and Dubocovich, 1988). In mouse spermatogenic cells, fenvalerate reduced T-type Ca^{2+}

current and caused a hyperpolarizing shift in the current-voltage relationship of the channel as well as the steady-state inactivation of the channel (Xiao et al., 2006).

Pyrethroids also block distinct classes of VGCCs in a variety of non-neuronal mammalian systems. Two distinct VGCC types from mouse neuroblastoma cells (N1E-115), a transient (T-type) and a long lasting (L-type) Ca^{2+} current, were examined (Narahashi et al., 1987). Tetramethrin, a T-syndrome pyrethroid, preferentially blocked T-type calcium current by 75% but only 30% of the L-type current (Yoshii, 1985). More recent electrophysiological studies using $Ca_V3.1$ (T-type), $Ca_V1.2$ (L-type), and $Ca_V2.1$ (P/Q-type) expressed in non-neuronal HEK cells indicated that all three current types were effectively blocked by allethrin (a Type I, T-syndrome-producing pyrethroid). The block caused an increase in the rate of channel inactivation during steady-state depolarization as well as a hyperpolarizing shift in the voltage-dependent inactivation (Hildebrand et al., 2004). The contributions of these effects are consistent with the channel block observed.

The increase in the rate of inactivation and the insignificant change in tail current of $Ca_V3.1$, $Ca_V1.2$ and $Ca_V2.1$ in the presence of allethrin is inconsistent with earlier studies that have shown pyrethroids to delay inactivation and slow the deactivation of tail currents (Vais et al., 2000; Soderlund et al., 2002; Wang and Wang, 2003; Hildebrand et al., 2004)

Table 1. Voltage-gated calcium channel (VGCC) subunit compositions and functions (adapted from Catterall 2003 (Catterall et al., 2003)).

Ca^{2+} Channels	Ca^{2+} Current type	Primary Localizations	Cellular Functions
$Ca_V1.1$	L	Skeletal muscle	Excitation-contraction coupling Calcium homeostasis Gene regulation
$Ca_V1.2$	L	Cardiac muscle Endocrine cells Neurons	Excitation-contraction coupling Hormone secretion Gene regulation
$Ca_V1.3$	L	Endocrine cells Neurons	Hormone secretion Gene regulation
$Ca_V1.4$	L	Retina	Tonic neurotransmitter release
$Ca_V2.1$	P/Q	Nerve terminals Dendrites	Neurotransmitter release Dendritic Ca^{2+} transients
$Ca_V2.2$	N	Nerve terminals Dendrites	Neurotransmitter release Dendritic Ca^{2+} transients
$Ca_V2.3$	R	Cell bodies Dendrites Nerve terminals	Ca^{2+} -dependent action potentials Neurotransmitter release Repetitive firing
$Ca_V3.1$	T	Cardiac muscle Skeletal muscle Neurons	Repetitive firing
$Ca_V3.2$	T	Cardiac muscle Neurons	Repetitive firing
$Ca_V3.3$	T	Neurons	Repetitive firing

al., 2004). Comparatively, deltamethrin has been shown to partially block $Ca_V2.2$ (N-type) currents heterologously expressed in *Xenopus* oocytes, which was accompanied by a slight hyperpolarizing shift in the voltage dependence of activation and a slowing of channel activation and inactivation (Symington and Clark, 2005). Peak, end, and tail currents of L-type (Ca_V1) Ca^{2+} channels expressed in PC12 cells significantly increased in the presence of allethrin and voltage-dependent peak current was shifted to more hyperpolarizing potentials(Neal et al., 2010). Neal et al (2010) also showed allethrin caused a shift in voltage-dependent activation and inactivation kinetics. The differential effects of allethrin on VGCCs indicate that Type I pyrethroids target some VGCC subtypes, but not others, in addition to targeting VGSCs. The differential effects may be due to the phosphorylation states of the channels or other forms of post-translational modifications. Type II pyrethroids certainly have an effect on VGCCs but again, the degree to which they have an effect appears to be based on the post-translational modification state of the channel.

1.11 Role of $Ca_V2.2$ in Neurotransmitter Release

$Ca_V2.2$ is expressed in presynaptic nerve terminals and is the predominant channel that regulates calcium-dependent, vesicle-mediated neurotransmitter release during membrane depolarization. The treatment of isolated presynaptic nerve terminals (synaptosomes) with deltamethrin causes an increase in neurotransmitter release as a result of Ca^{2+} influx via $Ca_V2.2$ (Augustine et al., 1987). Treatment of deltamethrin, a Type II/CS-syndrome pyrethroid, on $Ca_V2.2$ expressed in *Xenopus* oocytes resulted in a hyperpolarizing shift of the midpoint potential of activation, prolonged inactivation, and

decreased peak current. These effects were stereospecific and dose-dependent (Symington and Clark, 2005). Enhanced activation and prolonged inactivation kinetics of heterologously expressed $Ca_V2.2$ is consistent with increased neurotransmitter release observed from the treatment of synaptosomes with deltamethrin. However, the inhibition of peak current may be inconsistent with the enhanced neurotransmitter released observed in treated synaptosomes (Symington and Clark, 2005).

$Ca_V2.2$ exists either in a "willing" or a "reluctant" state. In the willing state, the channel undergoes rapid activation during depolarization to voltages within its physiological range. In the reluctant state, the channel undergoes slow activation at more positive voltages beyond its normal range of physiological membrane potential (Catterall, 2000a). Channel conductance is regulated by two separate processes: activation and inactivation. Activation controls the time and voltage dependence required to open the channel after depolarization and inactivation measures the voltage and time dependence of channel closure during maintained depolarization (Catterall, 1997; Hanlon and Wallace, 2002). Deactivation is a third kinetic measurement that describes the time dependence of complete closure of channels that have activated but not inactivated after the removal of membrane depolarization (Kostyuk and Shirokov, 1989).

Activation and inactivation kinetics can be modified by several proteins and through phosphorylation of the α-subunit by protein kinases. The $G_{\beta\gamma}$ subunit of the heteromeric G-proteins and SNARE proteins can modify channel kinetics by direct binding to the transmembrane domains of the α_1 subunit. Modulation by $G_{\beta\gamma}$ causes a hyperpolarizing shift in voltage dependence and slows channel activation. Phosphorylation of the α_{1D} channel at T422 or S425 (Fang et al., 2006) downstream of

where $G_{\beta\gamma}$ interacts on the I-II intracellular loop or a strong depolarization can reverse the $G_{\beta\gamma}$ inhibitory effect, resulting in increase Ca^{2+} currents. Unlike $G_{\beta\gamma}$, channel regulation by SNARE is Ca^{2+} dependent. Regulated by Ca^{2+}, presynaptic $Ca_V2.2$ interacts directly with SNARE proteins and synaptotgamin. The interaction of SNARE proteins and $Ca_V2.2$ is required to dock synaptic vesicles near Ca^{2+} channels for fast and effective exocytosis and the interaction is considered crucial for synaptic transmission (Catterall, 2000a). Locations on the synaptolemma where these processes co-organize are called "active release zones". When both $G_{\beta\gamma}$ and SNARE proteins become phosphorylated, they no longer have an effect on the channel. All members of the Ca_V2 subfamily are blocked by ω-conotoxin GVIA but $Ca_V2.2$ has the highest affinity for this channel blocker. Inhibition of $Ca_V2.2$ by ω-conotoxin GVIA causes a hyperpolarizing shift in voltage dependence and a slowing of channel activation, which can be alleviated by a strong depolarization resulting in Ca^{2+} current facilitation (Catterall, 2000a).

1.12 Differences between *in vivo* and *in vitro* Action of Deltamethrin on $Ca_V2.2$

Assays involving isolated presynaptic nerve terminals (synaptosomes) treated with deltamethrin were analyzed for enhanced Ca^{2+} influx and neurotransmitter release. Deltamethrin caused a significant increase in Ca^{2+} influx and glutamate release from synaptosomes in a concentration-dependant and stereospecific manner. No decrease in Ca^{2+} influx was observed when synaptosomes pretreated with the VGSC blocker tetrodotoxin (TTX), showing that Ca^{2+} influx was not VGSC-dependent and that there are additional sites at which deltamethrin is acting (Symington and Clark, 2005). The increase in Ca^{2+} influx that was the result of deltamethrin treatment and the deltamethrin-

enhanced release of glutamate were abolished when synaptosomes were pretreated with the N- and P/Q- type Ca^{2+} channel blocker ω-conotoxin MVIIC (Symington and Clark, 2005).

The N-type VGCC isolated from rat brain ($Ca_V2.2$) were heterologously expressed in *Xenopus* oocytes, a non-neuronal expression system, to determine the specific effects of deltamethrin on this channel. Deltamethrin stereospecifically reduced the Ba^{2+} peak current in a concentration dependent manner. Treatment of $Ca_V2.2$ with deltamethrin caused a hyperpolarizing shift in the voltage-dependent activation kinetics of the channel as well as prolonging inactivation gating characteristics. The hyperpolarizing shift in the voltage-dependent activation of $Ca_V2.2$ as well as the prolongation of the inactivation kinetics means that the channel is more sensitive to opening at lower potentials and stays open longer allowing for more Ba^{2+} ions to influx through the channel (Symington and Clark, 2005).

1.13 Protein kinase C (PKC)

Phosphorylation also plays an important role in the modulation of $Ca_V2.2$. Phosphorylation of $Ca_V2.2$ can reverse $G_{\beta\gamma}$ inhibition and cause an up regulation of Ca^{2+} currents via $Ca_V2.2$ expressed in intact neurons and transient expression systems. Protein kinase C (PKC) is responsible for the phosphorylation of $Ca_V2.2$ and the subsequent antagonism of G protein-mediated inhibition of the channel. This interaction between PKC and $G_{\beta\gamma}$ is termed “cross talk” (Swartz, 1993; Zamponi et al., 1997; Cooper et al., 2000; Doering et al., 2004).

PKC takes part in cellular responses to various agonists including hormones,

neurotransmitters and some growth factors. Agonist-induced hydrolysis of inositol phospholipids by phospholipase C produces $IP_{3,}$ which releases Ca^{2+} stores from endoplasmic reticulum. Cytosolic free Ca^{2+} and membrane-bound diacylglycerol (DAG) react to activate PKC. Metabolically-stable, tumor-promoting phorbol esters, such as phorbol ester 12-myristrate, 13-acetate (PMA), mimic DAG activity in a Ca^{2+} independent manner and are capable of activating PKC for longer periods of time than DAG and several doses of DAG are required to achieve the same effect as one dose of a phorbol ester (Nishizuka, 1992; Mosior and Newton, 1996; Newton, 2001).

The protein kinase C (PKC) enzyme family consists of ten Ser/Thr phosphotransferases and is divided into three subfamilies: conventional (PKC_{α}, $PKC_{\beta1}$, $PKC_{\beta2}$, PKC_{γ}), novel (PKC_{δ}, PKC_{σ}, PKC_{ε}, PKC_{η}) and atypical (PKC_{ζ}, PKC_{λ}). Every PKC has a regulatory domain and a catalytic domain. Within their regulatory domains, conventional and novel PKCs contain two C1 domains and a C2 domain, both of which are targets for different second messengers. Atypical PKCs only contain a single C1 domain. Common to all three subfamilies of PKC are domains C3 and C4 which make up the catalytic domain of PKC. Phosphorylation of PKC occurs at threonine 567 on the activation loop by phosphoinositide-dependent kinase (PDK-1) quickly followed by phosphorylation of threonine 711 on the turn motif and serine 729 in the hydrophobic region by autophosphorylation. Phosphorylation and the binding of cofactors induce long range conformational changes that regulate the domain interactions.

PKC exists under acute structural and spatial regulation. Its state of phosphorylation, conformation and sub-cellular location must each be tightly controlled for PKC to function properly. The catalytic domain comprises a conserved kinase core

containing the ATP-binding site, consensus phosphorylation sites, substrate binding and phototransfer sites (Newton, 2001; Corbalán-García and Gómez-Fernández, 2006). In order for PKC to become catalytically active, phosphorylation has to occur at three sites in the catalytic domain of the enzyme. Sites on the activation loop (Thr567), turn motif (Thr711), and hydrophobic motif (Ser729) of the PKC catalytic domain are phosphorylated via different mechanisms. The cofactors that regulate PKC conformation are phosphatidylserine (PS), DAG and Ca^{2+}. Not all of the cofactors regulate all of the PKCs. Conventional PKCs are regulated by PS, DAG and Ca^{2+}. Novel PKCs are regulated by PS and DAG. Atypical PKCs are regulated by just PS. Despite phosphorylation of its catalytic domain and its translocation to the membrane via binding of DAG and PS, PKC can still be held in an inactive state by the occupation of its kinase core by its pseudosubstrate (Newton, 2001). In order for unimpaired signaling of PKC to occur, its catalytic domain needs to be phosphorylated, PKC needs to translocate from the cytosol to the membrane via binding of its C1 and C2 domains to DAG and PS, respectively, and the allosterically regulating pseudosubstrate needs to be released from the kinase core.

DAG, a product of phospholipase C (PLC) hydrolysis of phosphatidyl inositol-biphosphate (PIP_2), is a second messenger phospholipid that binds to the C1 region of PKC and in the process of activating the protein, sequesters it to the plasma membrane (Liu and Heckman, 1998). The effects of phorbol esters on PKC are slightly different from the effects of DAG although they operate by the same mechanism (Newton, 2001). Their biological effects differ for two reasons: 1) membrane recruitments and activation by DAG is short lived because DAG is rapidly metabolized whereas phorbol esters are

not, and 2), phorbol esters are two times more potent than DAG on a molar basis in recruiting PKC to membranes.

Several different isozymes of PKC exist in neuronal channels and each has its own particular set of substrates. It has been shown that novel PKC, PKCε, is specific to phosphorylating $Ca_V2.2$ through the adaptor protein enigma homolog (ENH) (Newton, 2001; Maeno-Hikichi et al., 2003), but in many cases, the presence of ENH is not required to phosphorylate the Ca^{2+} channel (Stea et al., 1995; García-Ferreiro et al., 2001; Maeno-Hikichi et al., 2003). PKCε has also been confirmed to be present in *Xenopus* oocytes although it remains inactive unless activated by PMA (Maeno-Hikichi et al., 2003).

1.14 Dephosphorylation by Protein Phosphatases

Multiple families of Ser/Thr protein phosphatases (PP) have been identified in the brain and include PP1, PP2a, PP2b and PP2c. Just as individual kinases are capable of mediating unique cellular functions by adding phosphate groups to proteins, PPs are capable of removing phosphate groups from $Ca_V2.2$. However, much less is understood about which PP is responsible in regulating neuronal Ca^{2+} channel activity (Li et al., 2005).

It is yet to be determined which PP removes the phosphate group from T422 on $Ca_V2.2$. Of the five possible phosphorylation sites on the I-II and II-III intracellular loops of $Ca_V2.2$ for PKC_ε to interact with (Maeno-Hikichi et al., 2003; Fang et al., 2006), Li *et al*. (Li et al., 2005) have demonstrated that the protein phosphatase PP2cα was more effective in dephosphorylating the II-III intracellular loop than its PP counterparts. As for

the I-II intracellular loop, which includes T422, none of the PPs examined by Li *et al.* were effective in their individual ability to dephosphorylate the region, but when combined, the dephosphorylation rate of the I-II loop increased.

1.15 Effect of PMA-activated PKC modulation on Wild Type $Ca_V2.2$

PKC is a regulatory enzyme that phosphorylates serine and threonine residues. PMA up regulates PKC phosphorylation, which results in the addition of phosphate groups to residues Thr422 (T422), Ser425 (S425), Ser1757 (S1757), Ser2108 (S2108) and Ser2132 (S2132) (Stea et al., 1995; Fang et al., 2006). Phosphorylation of $Ca_V2.2$ removes G-protein mediated inhibition via the $G_{\beta\gamma}$ subunit, which allows increased Ca^{2+} influx and a subsequent increase in neurotransmitter release (Nichols et al., 1987; García-Ferreiro et al., 2001). Stea *et al.* (Stea et al., 1995) showed that within *Xenopus* oocytes, PMA-activated endogenous PKC phosphorylates heterologously expressed $Ca_V2.2$, which elicits a time-dependent increase in peak current. PMA enhancement of PKC activity in rat brain caused enhanced excitatory synaptic transmission (Swartz et al., 1993), reduced suppression by metabotropic glutamate receptor (G-protein mediated) agonists (Barrett and Rittenhouse, 2000), enhanced whole cell current amplitude in sympathetic neurons (García-Ferreiro et al., 2001) and increased Ca^{2+}-dependent neurotransmitter release from synaptosomes (Nichols et al., 1987; García-Ferreiro et al., 2001). Thus, VSCCs are modulated by direct phosphorylation that alter channel sensitivities to changes in membrane potential or channel ability to undergo conformational changes from an open state to inactive or closed states (Rossie, 1999). Treatment of synaptosomes with phorbol esters stimulated endogenous PKC activity,

which resulted in enhanced Ca^{2+}-dependent neurotransmitter release (Nichols et al., 1987). These results are consistent with the contention that PKC phosphorylation changes VSCC sensitivity to membrane depolarization and causes an increase in Ca^{2+} influx and neurotransmitter release.

1.16 Mutant $Ca_V2.2$

It has been shown that deltamethrin has an agonistic effect on Ca^{2+} influx and neurotransmitter release in rat brain synaptosomes (Aldridge et al., 1978; Hossain et al., 2004; Symington and Clark, 2005; Symington et al., 2007b). However, deltamethrin inhibits Ba^{2+} peak current when $Ca_V2.2$ is heterologously expressed in *Xenopus* oocytes (Symington and Clark, 2005). This difference in channel response to deltamethrin treatment, depending on the expression system, is believed to be due, in part, to the lack of active post-translational modifications in the non-neuronal oocytes versus active post-translational modifying enzymes, such as protein kinases, within rat brain synaptosomes.

The intracellular loop between domains I and II on the $Ca_V2.2$ α_1 subunit is a highly regulated domain (the alpha-subunit interacting domain, AID), which contains T422 and the overlapping binding sites for PKC, $G_{\beta\gamma}$ and the VGCC β subunit (Cooper et al., 2000). A specific phosphorylation of $Ca_V2.2$ by PMA-activated PKC can be mimicked by an amino acid substitution in the PKC regulatory site within the I-II intracellular domain. Conversion of threonine 422 to glutamic acid (T422E) results in a channel that functions as if it were permanently phosphorylated since glutamic acid is negatively charged at physiological pH. This mutation produces a $Ca_V2.2$ phosphoform that mimics the effect of PMA up-regulation and is no longer sensitive to $G_{\beta\gamma}$ inhibition

(Hamid et al., 1999; Cooper et al., 2000; Symington et al., 2007a).

Using this approach, it has been shown that the T422E mutation alters the action of deltamethrin on $Ca_V2.2$ expressed in *Xenopus* oocytes (Symington et al., 2007a). Deltamethrin significantly enhanced peak current via the T422E channel compared to the wild type, the solvent-treated control and a T422A (permanently unphosphorylated mutant) channel. This effect was stereospecific and concentration dependent. Additional effects of deltamethrin on T422E included a more positive activation midpoint potential, a depolarizing shift in the voltage dependence of activation. However, no change in the activation or inactivation tau values was observed as seen previously on the wild type channel. As demonstrated in the mutant T422E experiments, $Ca_V2.2$ is clearly modified by deltamethrin but the resulting perturbation is highly dependent upon the phosphorylation state of T422.

1.17 The Effect of PMA-activated PKC Phosphorylation on Wild Type $Ca_V2.2$ is enhanced by Deltamethrin Treatment

Post-translational modifications of $Ca_V2.2$ have been suggested to be the cause of the differences between the agonistic effect deltamethrin elicited in rat brain synaptosomes versus its antagonistic effect on the Ba^{2+} peak current via heterologously expressed $Ca_V2.2$ in *Xenopus* oocytes. The increase in peak current following deltamethrin treatment of T422E is highly suggestive that the phosphorylation state of $Ca_V2.2$ determines its response to deltamethrin (Symington et al., 2007a).

Using PMA to up regulate PKC activity in *Xenopus* oocytes, $Ca_V2.2$ is readily phosphorylated, although phosphorylation of the channel is nonspecific (Cooper et al.,

2000). It is our contention that deltamethrin enhances Ca^{2+} influx and subsequent neurotransmitter release only when acting upon a phosphorylated channel. By activating PKC with PMA, we are able to nonspecifically phosphorylate $Ca_V2.2$, which was heterologously expressed in *Xenopus* oocytes, and enhance channel conductance. We expect that the addition of deltamethrin and other CS-syndrome pyrethroids will further enhance the conductance of phosphorylated $Ca_V2.2$ in a stereospecific manner. By analyzing peak current and channel kinetics, such as activation, inactivation, deactivation, we will investigate which channel properties are influenced by phosphorylation in the presence and absence of pyrethroids.

CHAPTER 2

MATERIALS AND METHODS

2.1 Materials

Technical grade deltamethrin ((*S*)-α-cyano-3-phenoxybenzyl (1*R*,3*R*)-3-(2,2-dibromovinyl)-2,2-dimethylcyclopropanecarboxylate; isomeric composition: 95.0% (*Z*)-(1*R*)-*cis*-)) was provided by Aventis CropScience (Dublin, NJ), a member of the Pyrethroid Working Group (PWG); a conglomerate of the major pyrethroid manufactures in the United States and United Kingdom and includes Valent USA Corp. (Montvale, CA) and Syngenta (Cheshire, UK), FMC (Philadelphia, PA), DuPont Agricultural Products (Newark, NJ), and Bayer Corp. (Kansas City, MO). Phorbol 12-myristate, 13-acetate (PMA; ≥99% pure) was purchased from Calbiochem (# 524400; La Jolla, CA). 4α-phorbol 12-myristate, 13-acetate (4α-PMA; 98%) was purchased from Sigma-Aldrich (# 79352; St. Louis, MO). An isomeric mixture of cypermethrin was provided by Shell Corp (Houston, TX). Pyrethroid, PMA and 4α-PMA stocks were prepared in dimethyl sulfoxide (DMSO) and diluted with either DMSO or $BaCl_2$ recording solution as required. Chemical structures for pyrethroids and phorbol esters used in this study are included in Appendix A.

2.2 Animals

Female *Xenopus laevis* frogs (7.5-9 cm) were purchased from Nasco (Fort Atkinson, WI) and maintained on a 12:12 hr day and night light cycle in a 19 ^{o}C incubator. Animals were housed in plastic bins (61.54 cm x 41.45 cm x 32.47 cm) in 5 gallons of dechlorinated water at 5 females per bin. Animal procedures were conducted in

accordance with the Institutional Animal Care and Use Committee (IACUC) guidelines (Protocol #: 27-09-06R) entitled "Pharmacological and toxicological effects of pesticides on ion channels and ABC transporters expressed in *Xenopus laevis* oocytes" submitted by J.M. Clark, principle investigator.

2.3 $Ca_V2.2$ RNA Preparation

Full length $Ca_V2.2$ cDNA α_1 and β_3 clones were provided as a gift from Dr. Diane Lipscombe (Brown University, Providence, R.I.). Linearized cDNA was checked by electrophoresis on a 0.8 % agarose gel against a High Mass DNA Ladder (10496-016; Invitrogen). cDNA isolation and purification were performed following manufacturer's instructions for the QIAquick® Gel Extraction Kit (QIAGEN, Valencia, CA). *In vitro* transcription was performed using the mMessage mMachine® High Yield Capped RNA Transcription Kit (# AM1344; Ambion Inc., Austin TX) (Lin et al., 1997; Symington and Clark, 2005; Symington et al., 2007a).

Specifically, $Ca_V2.2$ α subunit cRNA was prepared for oocyte injection from the cDNA clone $RN_{\alpha 1B\text{-}d}$ (vector pBSTA rscg$\alpha_{1B\text{-}b,}$ 3.19 kb). The β_3 auxiliary subunit cRNA was prepared from the cDNA clone (vector pcDNA3.1zeo+, 5 kb). $Ca_V2.2$ and β_3 cDNAs were checked on a 0.8% agarose gel (0.4 g agarose, 50 ml 1X Tris-Acetate EDTA (TAE) buffer and 1 µl ethidium bromide (10 mg/ml)) run at 100 mV for 1 hr and measured against a High Mass DNA Ladder.

cDNA isolation and purification was performed using the QIAquick® Gel Extraction Kit. Three volumes of Buffer QG and 1 volume of isopropanol were added to the reaction mixture and mixed by repetitive pipetting until homogenous. The entire

sample was applied to the supplied spin column and centrifuged for 1 min at 15,690g. The flowthrough was removed from the catch tube. PE buffer (0.75 ml) was added to the spin column and after a 1 min equilibration interval the column was recentrifuged as before. The spin column was transferred to a new centrifuge tube. The concentration of cDNA was determined by gel electrophoresis on a 0.8% agarose gel stained with ethidium bromide and measured against a High Mass DNA Ladder prior to isolation and purification so that an appropriate amount of elution buffer (EB) could be added to ensure that the cDNA concentration after isolation and purification was equal to 1 μg/μl (20-50 μl). The appropriate amount of EB was added and the spin column was recentrifuged. The purity of the eluted cDNA was checked by electrophoresis on a 0.8% agarose gel stained with ethidium bromide at 100 mV for 1 hr and measured against a High Mass DNA Ladder. The remainder of the cDNA was stored at -20^{o}C until used for *in vitro* transcription. cDNA concentration was determined using a ND-1000 UV-Vis Spectrophotometer (Thermo Fisher Scientific Wilmington, DE). The ND-1000 UV-Vis Spectrophotometer forms a column of sample (2 μl of purified DNA) between the sample pedestal and the arm of the spectrophotometer. The pedestal moves to automatically adjust the length of the sample column for an optimal path length (0.05 mm to 1.0 mm) for measurement of the optical density (absorbance) of the sample at 260 nm. Concentration of the sample is calculated using the Beer-Lambert Law (Equation 1):

Equation 1

$$\mathbf{A = \varepsilon c \ell}$$

Where:
A = the absorbance of the sample at 260 nm

ε = the absorption coefficient of DNA (50)
c = the concentration of the sample
ℓ = the path length

In vitro transcription was performed using the mMessage mMachine® High Yield Capped RNA Transcription Kit. To the $Ca_V2.2$ α_1 and β_3 reaction mixtures, 1 µl of 30 mM GTP cap, 2 µl of 10X Reaction Buffer, 1 µg of either α_1 or β_3 $Ca_V2.2$ DNA, 10 µl of 2X NTP cap, 2 µl of 2X Enzyme mix and RNase-free ddH_2O (diethyl pyrocarbonate (DEPC)-treated) up to 20 µl were added and mixed. The reaction was incubated at 37°C for 2 hr, 2 U/µl Turbo DNase was added, and the mixture incubated for an additional 15 min. The reaction was stopped by adding 30 µl nuclease free ddH_2O and 30 µl of the $LiCl_2$ solution provided to precipitate the cRNA. Reaction mixtures were chilled for approximately 30 min at -20°C before pelleting the cRNA by centrifuging at 4° C for 15 min at 16,170g. After decanting the supernatant, the cRNA pellet was washed with 70% ethanol and re-centrifuged. Ethanol was removed via pipette and the cRNA resuspended in 12 µl RNase free ddH_2O. cRNA was electrophoressed on a 1% agarose gel (0.5 g RNase free agarose, 36 ml of 0.01% DEPC-treated ddH_2O) and measured against a RNA marker (0.2- 10 kb, R-7020; Sigma Aldrich St. Louis, MO). The gel was run at 50 mV for 3-5 hr at 4°C. The running buffer was 450 ml of 0.01% DEPC-treated ddH_2O and 50 ml of 10X MOPS (Swanson and Folander, 1992). cRNA concentration was determined using a ND-1000 UV-Vis Spectrophotometer (RNA absorption coefficient = 40) as described above and cRNA was stored at -80°C.

2.4 *Xenopus* Surgery and Oocyte Preparation

Oocytes were obtained surgically from a female *Xenopus laevis* frog anesthetized

in a 3-aminobenzoic acid ethyl ether (tricane) solution (2 g/L). Excised oocyte lobes were washed with OR2 solution (82.5 mM NaCl, 2 mM KCl, 1 mM $MgCl_2$, 5 mM N-(2-hydroxyethyl)piperazine-N′-2-ethanesulfonic acid (HEPES), pH 7.5). Most of the oocyte follicle membranes were digested with equal parts collagenase solution (Sigma Type 1A collagenase; 0.5 U/ml (2 mg/ml)) and OR2 solution. The remaining follicle membranes were removed manually using fine forceps under a stereomicroscope. Healthy stage V-VI oocytes were maintained at 19^{o}C in oocyte supplemental media (ND96 media (96 mM NaCl, 2 mM KCl, 1.8 mM $CaCl_2 \cdot 2H_2O$, 1 mM $MgCl_2 \cdot 6H_2O$, 5 mM HEPES, pH 7.5) supplemented 1% sodium pyruvate, 2% antibiotics (penicillin, streptomycin) and 5% horse serum) (Goldin, 1992).

Surgery was done under semi-sterile conditions following IACUC procedures outlined in Protocol No. 27-09-06R. A female frog (7.5-9 cm) was placed into a tricane solution (2 g/L) for 10-15 min. Anesthesia was checked by placing the frog upside down to see if she could right herself and by lack of foot-pinch reflex. If anesthesia was not complete, the frog was left in the tricane solution for up to 30 min. The anesthetized frog was placed on its back on a clean, wet surface. A 1.0 cm incision was made from the lower medial to lateral abdomen toward the head using a sterile surgical blade cutting through both the skin and underlying membrane. Ovary lobes were pulled through the incision with a pair of forceps until a sufficient number of oocytes (about 200-300) were exposed and removed by cutting the connective follicle membrane with a pair of dissecting scissors. The remaining ovary lobes were placed back into the frog's abdomen and the inner and outer membrane incisions were closed separately using a surgical suture (4-0 chromic gut, Angiotech, Reading, PA) (Goldin, 1992). Excised oocyte lobes were

washed three times with 20-30 ml of OR2 solution, placed in a 15 ml conical vial containing 5 ml collagenase solution (Type 1A collagenase; 0.5 U/ml (2 mg/ml)) and 5 ml OR2 solution, and incubated on an orbital shaker at 35 rpm at room temperature for 15-18 min or until the solution became cloudy. Collagenase/OR2 solution was discarded, replaced every 7-9 min with fresh solution, and treatment was continued until approximately half the oocytes were fully defollicated. The remaining follicle membranes were removed manually using fine forceps under a stereomicroscope. Healthy stage V-VI oocytes were selected based on uniform pigmentation, size and shape. They were maintained at 19^{o}C in oocyte supplemental media.

2.5 cRNA Injection

Stage V and VI oocytes were co-injected with 46 nl of a cRNA solution containing the α_1 (stock solution 1 μg/μl) and the β_3 (stock solution 0.33 μg/μl) subunits of $Ca_V2.2$ using a nanoliter 2000 injector (World Precision Instruments, Sarasota FL) in 25 nl increments. Injected oocytes were stored in oocyte supplemental media at 19^{o}C until used in expression experiments (Shih et al., 1998).

2.6 Electrophysiology

The function of wild type $Ca_V2.2$ α1B subunit co-expressed with the β3 subunit in the *Xenopus* oocytes was assayed using the two-electrode voltage clamp (TEVC) technique by measuring inward Ba^{2+} currents. The function of wild type $Ca_V2.2$ α1B subunit co-expressed with the β3 subunit in the *Xenopus* oocytes was assayed using the two-electrode voltage clamp (TEVC) technique by measuring inward Ba^{2+} currents.

The function of wild type $Ca_V2.2$ α1B subunit co-expressed with the β3 subunit in the *Xenopus* oocytes was assayed using the TEVC technique. Recordings were made in siliconized culture well oocyte recording chambers (250 µl bath volume; C7485-20EA, Sigma-Aldrich, St. Louis, MO) containing Ba^{2+} recording solution (5 mM $BaCl_2$, 85 mM tetraethylammonium, 5 mM KCl, 5 mM HEPES, adjusted to pH=7.4 with methanesulfonic acid) using a GeneClamp 500B amplifier (Axon Instruments, Union City, CA). Voltage and current microelectrodes with resistances between 0.5-3.0 MΩ were made from borosilicate glass using a Narishige PP-83 electrode puller and filled with 3 M KCl. The electrodes were coated with silver conductive paint (CW2200STP, Chemtronics®, Kennesaw, GA), over coated with insulating resin (CW3300C, Chemtronics®), and shielded with grounded aluminum foil to minimize noise. Data were digitized at 20 kHz using the Digidata 1322A digitizer, stored by the pClamp (ver. 9.2, Axon Instruments, Union City, CA) software, and capacitive transient current subtracted online using the P4 protocol.

Waveform protocols for the Transient, Activation, Inactivation and Deactivation Test Protocols are shown in Figure 2. To test for $Ca_V2.2$ channel expression, the Transient Test Protocol was applied to each oocyte by depolarizing the plasma membrane from a resting potential of -80 mV to 10 mV for 150 ms and returning to resting potential (Fig. 2A). Recordings were made every minute for 10 minutes to judge the time course of the effects of each of the pyrethroids and PMA on Ba^{2+} peak current via expressed $Ca_V2.2$. From these recordings, the treatments effects on transient peak current (the most

Figure 2. Waveform protocols for Transient, Activation, Inactivation and Deactivation tests. (A) Transient peak current, activation tau and deactivation tau can be measured directly from the Transient Test Protocol. (B) V_{50}inact and Inactivation tau, the rate of closure during depolarization, are best measured from the Inactivation Test Protocol. V_{50}inact is measured as a function of increasing levels of long-term (2 s) depolarizations. (C) The Deactivation Test Protocol measures the rate of channel closure (deactivation tau) as a function of decreasing levels of repolarization. (D) To best measure activation tau (ms), the Activation Test Protocol measures the rate of activation as a function of increasing levels of depolarization. Orange lines indicate a sample sweep from the Activation, Inactivation and Deactivation Test Protocols.

A.

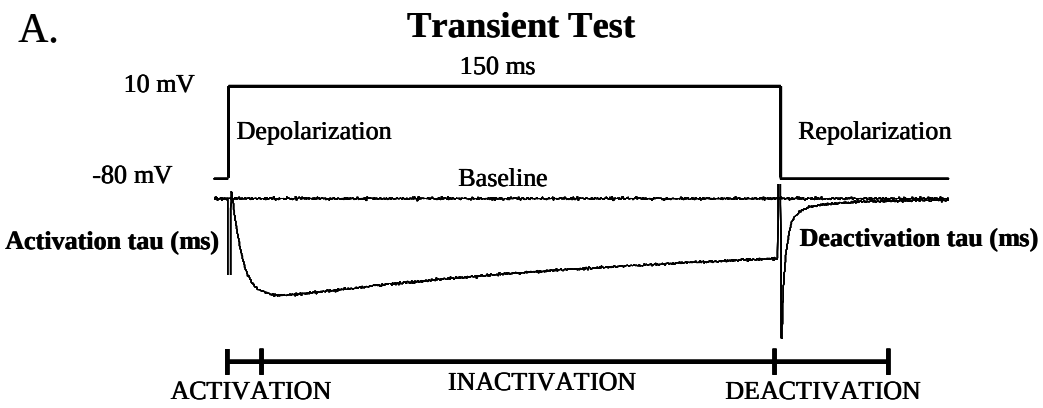
Transient Test
150 ms
10 mV
Depolarization
Repolarization
-80 mV
Baseline
Activation tau (ms)
Deactivation tau (ms)
ACTIVATION
INACTIVATION
DEACTIVATION

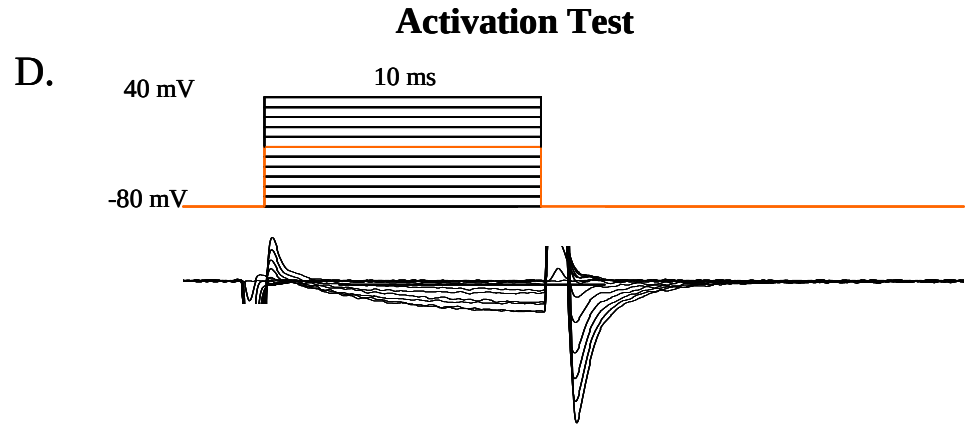
Activation Test
D.
40 mV
10 ms
-80 mV

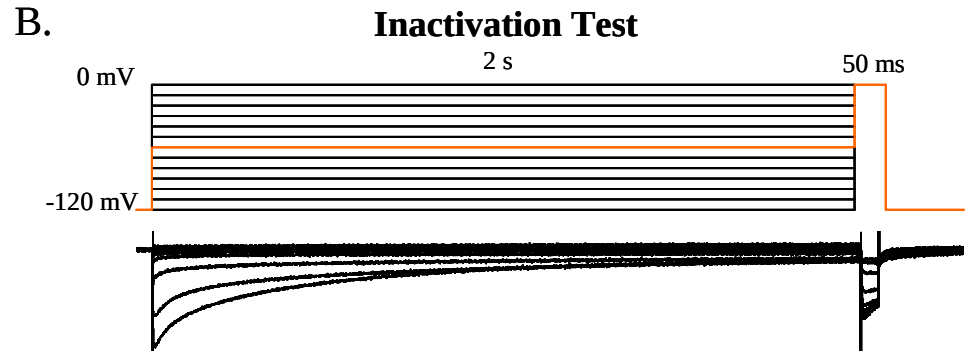
B.
Inactivation Test
2 s
50 ms
0 mV
-120 mV

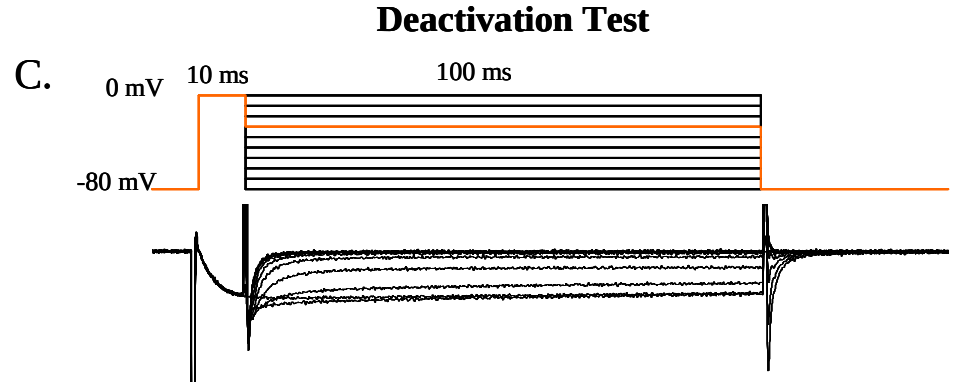
Deactivation Test
C.
0 mV
10 ms
100 ms
-80 mV

negative amplitude of current evoked from the depolarization step; μA), steady-state activation tau (the rate of channel opening during the depolarization step; ms), steady-state inactivation tau (the rate of channel inactivation during the depolarization step; ms) and steady state deactivation tau (the rate of channel closing after the removal of the depolarization step; ms) at 4 min and 10 min post treatment were obtained and used for statistical analysis.

In the Activation Test Protocol, the membrane potential was step-depolarized in 10 mV increments from a resting potential of -80 mV to a final level of 40 mV. The duration of each depolarization step is 10 ms before the membrane potential is repolarized back to -80 mV (Fig. 2B). The Activation Test Protocol was used to determine the effect our treatments have on $Ca_V2.2$ voltage dependent peak current, voltage-dependent activation taus, and voltage-dependent activation midpoint potentials (V_{50act}).

The Inactivation Test Protocol has two depolarization phases. The first lasts for 2 s and undergoes step-depolarization by an additional 10 mV per sweep starting at -120 mV and ends with a final step depolarization to 0 mV. Each sweep of the first phase of the Inactivation Test Protocol is immediately followed by the second phase of the protocol, which is the depolarization of the membrane from the current level of the first phase to 0 mV for 50 ms (Figure 2C). Recordings were made at 4 min and 10 min post application of treatment. Using the Inactivation Test Protocol, we were able to determine what effects our treatments had on $Ca_V2.2$ voltage-dependent inactivation midpoint potential ($V_{50inact}$) based on the measurement of late current.

The Deactivation Test Protocol also has two phases: a depolarization phase and a

repolarization phase. During the depolarization phase of the protocol, the membrane is depolarized from a resting potential of -80 mV to 0 mV for 10 ms. The repolarization phase occurs immediately following the depolarization phase. During the repolarization phase, the membrane is repolarized in decreasing steps by 10 mV starting with the repolarization step to -80 mV during the first sweep and ending at 0 mV during the last sweep. Each repolarization level is held for 100 ms and recordings were made at 4 min and 10 min post treatment (Figure 2D). The Deactivation Test Protocol was designed to determine what effects our treatments have on voltage-dependent deactivation taus.

2.7 Measuring PMA and Pyrethroid Effects on $Ca_V2.2$ Inward Transient Peak Current

Initially, a Transient Test Protocol was applied to the oocyte to determine VGCC expression (Fig. 2). Non-treated peak current (amperage, A), activation (ms), and deactivation tau (ms) values were obtained from oocytes when $Ca_V2.2$ expression levels produced peak currents ≥ 0.5 μA. Peak current (I_{Ca}^{2+}) was determined as the most negative amplitude value from the raw current trace produced by the Transient Test. Activation and deactivation taus were measured using the exponential standard (zero-shift) curve (Clampfit ver. 9.2, Axon Instruments) by Equation 2:

Equation 2

$$\mathbf{f(t) = \sum_{i=1}^{n} A_i e^{-\tau i} + C}$$

Where:
A = Amplitude
τ = time constant

C = constant *y*-offset
i = component to be measured

Activation measures the part of the current curve from the start of depolarization to peak current amplitude and activation tau (τ) represents the amount of time required to open 50% of the channels during membrane depolarization. Deactivation tau measures the part of the current curve displaying channel activity after membrane depolarization was removed (repolarization step) and represents the amount of time required to close 50 % of the channels (Clampfit 9.2). Midpoint potentials for activation and steady-state inactivation were determined by least squares fits of current-voltage relationship from individual experiments to the Boltzmann equation (Equation 3) using GraphPad Prism.

Equation 3

$$Y = \text{Bottom} + \frac{(\text{Top} - \text{Bottom})}{1+\exp\left(\frac{V_{50} - X}{\text{slope}}\right)}$$

Treated values (DMSO, PMA and pyrethroid) were obtained from $Ca_V2.2$ test protocols that were run after application of treatments. Only one type of treatment was applied to each oocyte. Pulse protocols were applied at 4 min and 10 min post treatment and the raw traces that resulted from each pulse were saved to obtain data values specific to each time point (Clampex). Raw data values were obtained using Clampfit 9.2. Data obtained from each time point (min post treatment) were normalized to the non-treated control using Equation 2.

Equation 4

$$\textbf{Normalized Value} = \frac{\textbf{Treated value}}{\textbf{Non-treated value}} \cdot 100\%$$

2.8 Statistical Analysis of Data

Analysis of the electrophysiology data was conducted using a combination of Clampfit 9.2 and Graph Pad Prism (GraphPad Software, Inc, San Diego CA) and Microsoft Excel (2003 Microsoft Corporation, Seattle WA). Averages and standard error means were calculated for normalized values from each individual treatment. Averages were statistically compared to the averaged normalized DMSO control values from each corresponding time point and step depolarization using a one-way ANOVA with a Bonferonni Post test comparing selected pairs of treatments (GraphPad Prism, P= 0.05 unless otherwise noted).

For example, peak current (PC) values are recorded as the highest current amplitude obtained during the Transient Test Protocol. From each oocyte, 11 recordings are made: no treatment (NT), and one recording per minute for 10 min post treatment. The 4 min post treatment (4 min) and 10 min post treatment (10 min) recordings are used for statistical analysis. Each oocyte is treated only once by direct application of the treatment compound to the recording solution after the NT recording is made. Four min and 10 min PC recordings are normalized to the NT from the same oocyte from which they were recorded (Equation 4). Normalized PC recordings are averaged together by time point and treatment and a standard error of the mean (SEM) was calculated for each average. Unless otherwise noted, the average and SEM data from each treatment were

statistically compared to normalized DMSO PC using one-way ANOVA with Bonferonni Post test.

In the Activation, Inactivation, and Deactivation Test Protocols, recordings are made at 4 min and 10 min post treatment using 5 mM Ba^{2+} as the charge carrier. From the Activation Test Protocol, voltage dependent peak current (mV ± SEM), activation midpoint potential (mV^{-1} ± SEM), and voltage-dependent activation (mV^{-1} ± SEM) data were collected. Activation midpoint potential and voltage-dependent activation are reported as V_{50} act and $\tau_{activation}$ (ms), respectively. The slope and intercept for determining voltage-dependent activation are reported as $\tau_{activation}$ slope (mV^{-1} ± SEM) and $\tau_{activation}$ y-intercept. From the Inactivation Test Protocol, the inactivation midpoint potential data were collected and reported as $V_{50inact}$ (mV± SEM). From the Deactivation Test Protocol, voltage-dependent deactivation data were calculated and reported as the $\tau_{deactivation}$ (ms). The slope and intercept for determining voltage-dependent deactivation are reported as $\tau_{deactivation}$ slope (mV^{-1} ± SEM) and $\tau_{deactivation}$ y-intercept. Data from the Activation, Inactivation and Deactivation Test Protocols were statistically compared using the Student's T-test. Unless otherwise reported, $P < 0.05$).

Figure 3: Overview of the method used to express and analyze $Ca_V2.2$. α- and β- subunit cDNAs are cloned, amplified and purified and used to produce cRNAs by *in vitro* transcription. α- and β-subunit cRNAs are injected in to *Xenopus laevis* oocytes for heterologous expression which is verified using two-electrode voltage clamp (TEVC) technique. Using TEVC, $Ca_V2.2$ is subjected to Transient, Activation, Inactivation and Deactivation Test Protocols from which measurements are taken to determine the transient peak current, activation taus, inactivation taus, deactivation taus, current-voltage relationships, voltage-dependent peak current, voltage-dependent activation rate, activation midpoint potential, inactivation midpoint potential and voltage-dependent deactivation rate under control and treated conditions, Values are statistically compared using either One-way ANOVA with Bonferonni Post Test or Student's T-test ($P < 0.05$).

$Ca_V2.2$ and β_3 cDNAs obtained for amplification and purification.

↓

$Ca_V2.2$ and β_3 cRNAs produced by *in vitro* transcription (Symington 2005)

↓

Xenopus laevis oocytes injected with cRNAs (Shih *et al.* 1998; Soderlund *et al.* 2002).

↓

Expression of $Ca_V2.2$ verified using the TEVC technique

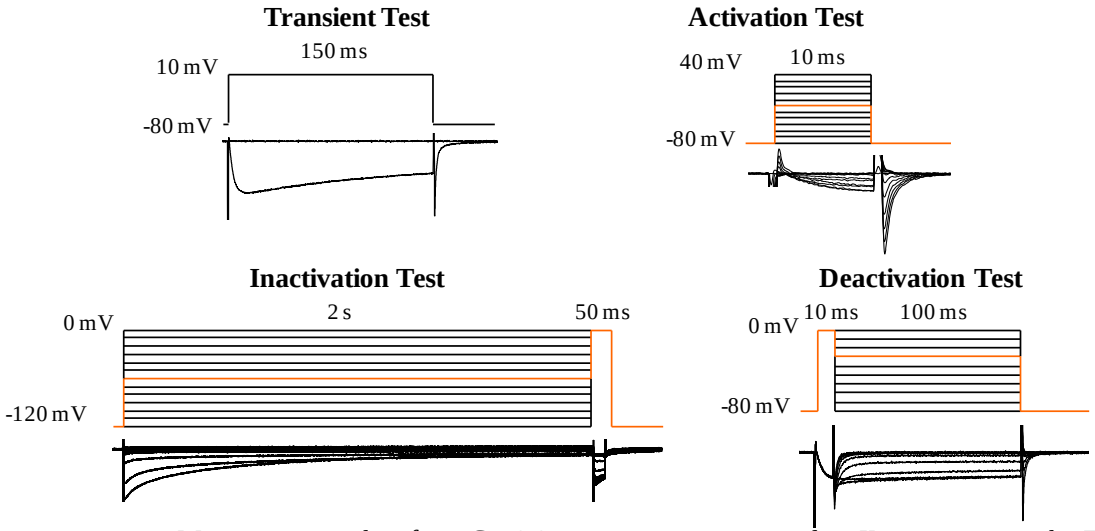

Measurements taken from $Ca_V2.2$ current traces expressed in *Xenopus* oocytes by TEVC.

↓

Values were normalized to either their respective No Treatment values or DMSO. Steady-state data was analyzed using one-way ANOVA with Bonferonni post-test was used to determine the statistical differences between treatments ($P<0.05$) and voltage-dependent data was statistically analyzed using T-tests ($P<0.05$).

Table 2: Types of data endpoints obtained from the Transient, Activation, Inactivation, and Deactivation Test protocols.

	Protocol			
	Transient	Activation	Inactivation	Deactivation
Endpoints	Transient Peak Current ($\mu A_T/\mu A_{NT}$ x 100)	Voltage-dependent peak current (mV)	Inactivation MPP (mV ± SEM)	Voltage-dependent deactivation ($\tau_{deactivation}$)
	Activation tau ($msec_T/msec_{NT}$ x 100)	Activation MPP (mV ± SEM)		$\tau_{deactivation}$ slope (mV^{-1} ± SEM)
	Inactivation tau ($msec_T/msec_{NT}$ x 100)	Voltage-dependent activation ($\tau_{activation}$)		$\tau_{deactivation}$ y-intercept
	Deactivation tau ($msec_T/msec_{NT}$ x 100)	$\tau_{activation}$ slope (mV^{-1} ± SEM)		
		$\tau_{activation}$ y-intercept		

CHAPTER 3

PMA INCREASES TRANSIENT PEAK CURRENT AND CHANGES THE GATING KINETICS OF $CA_V2.2$

3.1 Results

3.1.1 Steady-state Peak Current

Using the Transient Test Protocol, maximal effects on transient peak current under steady-state depolarization were observed for wild type $Ca_V2.2$ in the presence of DMSO, PMA and 4α-PMA over the course of a 10 min incubation period (Fig. 4A). PMA treatment of expressed $Ca_V2.2$ phosphorylates the channel due to the activation of PKC. Under basal conditions in the absence of PMA $Ca_V2.2$ is unphosphorylated (Stea et al., 1995). The presence of PMA at 4 min post treatment caused the largest and most significant difference in transient peak current (49%) compared to the DMSO control. At 4 min post treatment, transient peak current in the presence of 4α-PMA was significantly less (-31%) than transient peak current in the presence of PMA. The presence of PMA caused a significant 40% increase compared to the effect of DMSO on transient peak current at 10 min post treatment. In the presence of 4α-PMA at 10 min post treatment, transient peak current was not significantly different from transient peak current in the presence of DMSO or PMA (Fig. 4B; Table 3).

Figure 4. The effects of 0.1 % DMSO, the phorbol ester PMA (8 x 10^{-7} M) and its enantiomer 4α-PMA (8 x 10^{-7} M) on relative transient peak current of wild type $Ca_V2.2$ over 10 min. A diamond (♦) indicates significant difference from DMSO treatment. A circle (●) indicates significant difference from PMA treatment. The number of eggs (n) used for these treatments are: DMSO (n = 39); PMA (n = 51); 4α-PMA (n = 12). Significance was calculated using One-way ANOVA with Bonferroni's Multiple Comparison post test ($P<0.05$).

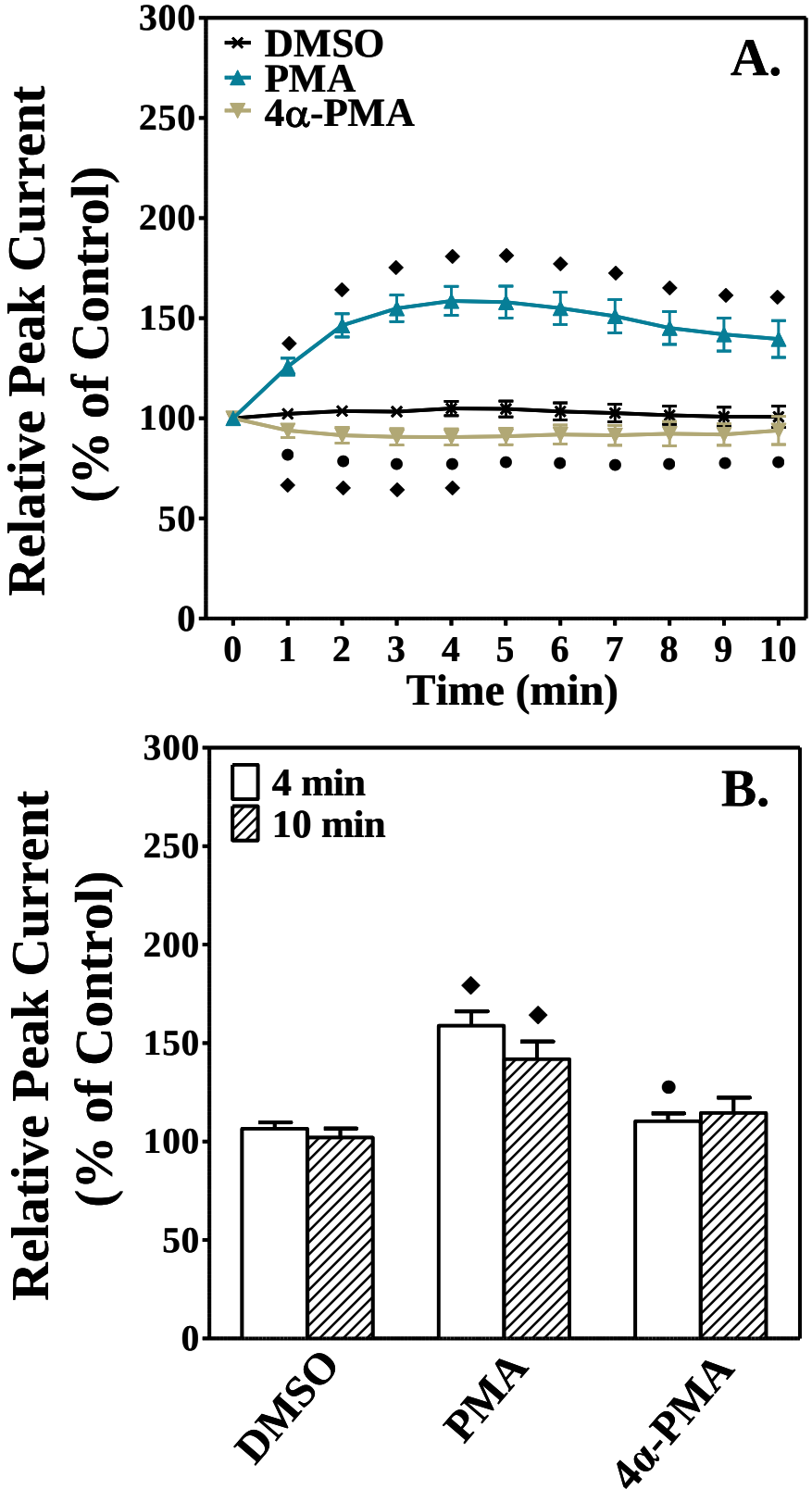
A.
DMSO
PMA
4α-PMA
Relative Peak Current
(% of Control)
300
250
200
150
100
50
0
0 1 2 3 4 5 6 7 8 9 10
Time (min)
B.
4 min
10 min
Relative Peak Current
(% of Control)
300
250
200
150
100
50
0
DMSO
PMA
4α-PMA

3.1.2 Steady-state Gating Kinetics

Steady-state activation, inactivation and deactivation taus were obtained using the Transient Test Protocol (Fig. 2). At 4 min post treatment, activation taus in the presence of PMA were not significantly different from the DMSO control, but at 10 min post treatment, there was a 21% significant increase in the activation tau in the presence of PMA (Fig. 5B). In the presence of 4α-PMA at both 4 and 10 min post treatments, activation taus were not significantly different from DMSO control (Fig. 5A and 5B and Table 3).

The rate of the inactivation tau did not change significantly in the presence of either PMA or 4α-PMA at both 4 min and 10 min post treatments (Fig. 5C and 5D and Table 3). Although not statistically different, the inactivation tau at 4 min post treatment decreased (-42%) compared to the DMSO control, indicating that there may be a trend that $Ca_V2.2$ inactivates faster in the presence of PMA (Fig. 5C).

Steady-state deactivation taus in the presence of PMA at 4 and 10 min post treatment were increased by 41 and 54%, respectively, compared to the DMSO controls (Fig. 5E and 5F) indicating that the rate of channel closure after removal of the depolarization step was slowed. In the presence of 4α-PMA, deactivation taus were not statistically different compared to those in the presence of DMSO at 10 min post treatment. However, at 4 min post treatment, 4α-PMA significantly reduced the deactivation tau 4 min post treatment by 28% compared to the effect of PMA.

Figure 5. The effects of 0.1 % DMSO, the phorbol ester PMA (8×10^{-7} M) and its inactive enantiomer 4α-PMA (8×10^{-7} M) on steady-state kinetics of wild type $Ca_V2.2$ at 4 and 10 min post treatment. Activation (A and B), inactivation (C and D) and deactivation (E and F) taus were normalized to their respective no treatment controls. The number of eggs (n) used to calculate activation and deactivation taus at 4 min post treatment were DMSO (n = 38); PMA (n=51); 4α-PMA (n=11) and at 10 min were DMSO (n=38); PMA (n=50); 4α-PMA (n=12). The number of eggs (n) used to calculate inactivation taus at 4 min post treatment were DMSO (n=16); PMA (n=16); 4α-PMA (n=3) and at 10 min post treatment, were DMSO (n=12); PMA (n= 17); 4α-PMA (n=4). Significance was calculated using One-way ANOVAs with Bonferroni's Multiple Comparison post test ($P<0.05$).

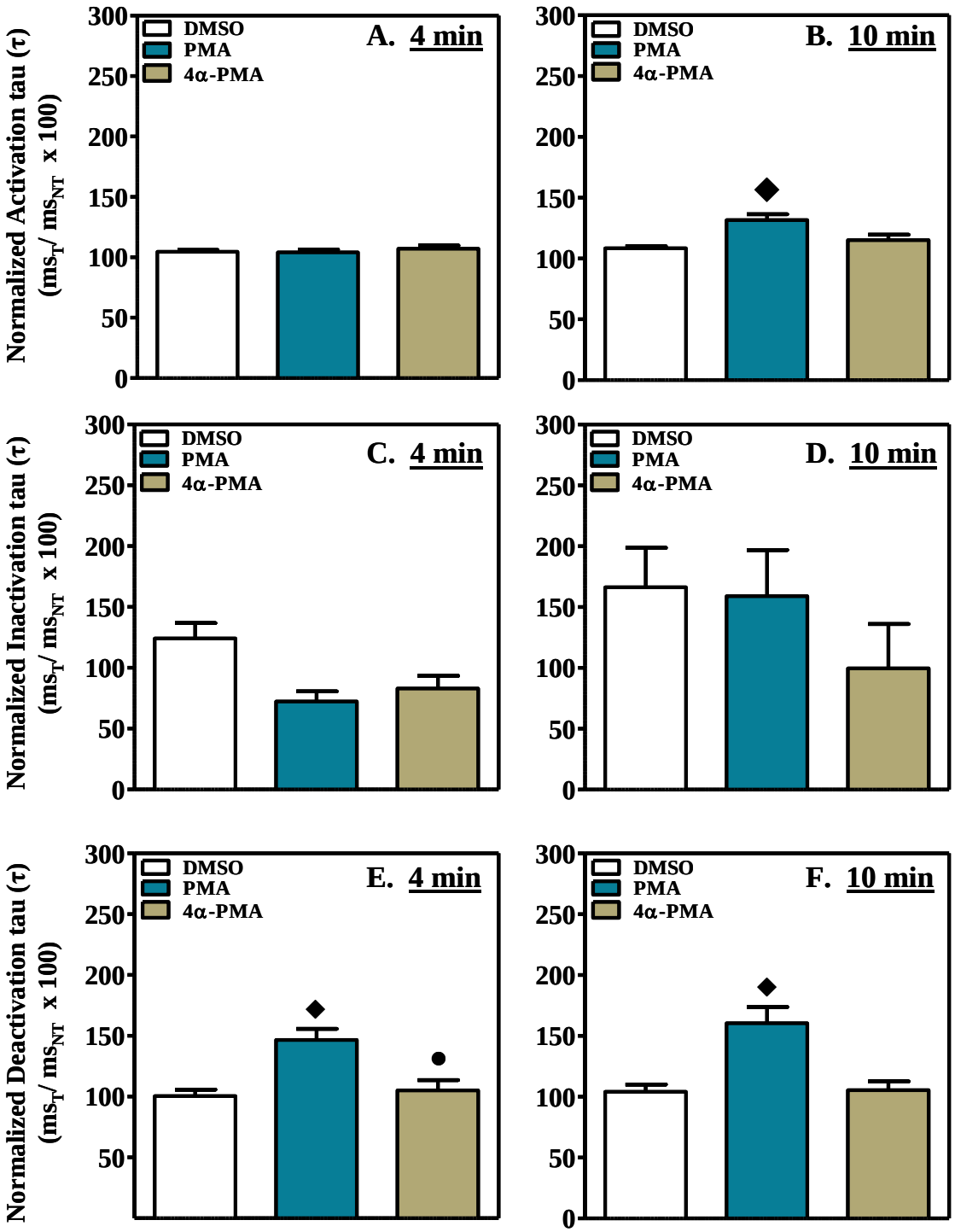
A. 4 min
B. 10 min
C. 4 min
D. 10 min
E. 4 min
F. 10 min
DMSO
PMA
4α-PMA
Normalized Activation tau (τ)
(msT/ msNT x 100)
Normalized Inactivation tau (τ)
(msT/ msNT x 100)
Normalized Deactivation tau (τ)
(msT/ msNT x 100)
300
250
200
150
100
50
0

3.1.3 Voltage-dependent Peak Current

The effects of PMA on average voltage-dependent kinetics of $Ca_V2.2$ were determined using current-voltage relationships (I/V curves) obtained using the Activation Test Protocol (Fig. 2). Voltage-dependent peak current significantly increased by 44% and 64%, in the presence of PMA compared to the normalized No Treatment and DMSO controls respectively at 4 min post treatment (Fig. 6A and Table 4). At 10 min post treatment, voltage-dependent peak current significantly increased in the presence of PMA by 39% at 10 min post treatment (Fig 6B). The increases in peak current in the presence of PMA at both 4 and 10 min post treatment are consistent with previous reports (Stea *et. al*, 1995). Treatment with 4α-PMA also resulted in significant 24% increase in voltage-dependent peak currents at 4 min post treatment (Fig. 6A and Table 4). The difference in the average voltage-dependent peak current in the presence of PMA and in the presence of 4α-PMA at 4 min post treatment was not significantly different (Table 4). The effect of 4α-PMA on peak current at 10 min post treatment was greater but was not significantly different from the effect of 4α-PMA 4 min post treatment. At 10 min post treatment, the effect of 4α-PMA treatment on average peak current was not significantly different from that of the PMA treatment.

3.1.4 Voltage-dependent Gating Kinetics

The activation midpoint potential (V_{50act}) at 4 min post treatment was not altered by any of the treatments compared to the no treatment control (Table 4). Significant depolarizing shifts in the activation midpoint potential, however, were observed for both the DMSO (88%) and 4α-PMA (238%) treatments compared to the no treatment control

Table 3. The effects of DMSO, PMA and 4α-PMA on $Ca_V2.2$ steady-state transient peak current, activation, inactivation and deactivation taus at 4 and 10 min post treatment.

		Treatment (10^{-7} M)			
		No Treatment	DMSO	PMA	4α-PMA
4 min	Transient Peak Current ($\mu A_T/\mu A_{NT}$ x 100)	100 ± 0.0	106.6 ± 3.2	158.9 ± 7.3 ♦(49)	110.3 ± 4.0 ●(-31)
	Activation tau (τ) ($msec_T/msec_{NT}$ x 100)	100 ± 0.0	108.4 ± 1.8	104.1 ± 2.2	107.1 ± 2.6
	Inactivation tau (τ) ($msec_T/msec_{NT}$ x 100)	100 ± 0.0	124.1 ± 12.5	72.24 ± 8.4 ♦(-42)	82.9 ± 10.5
	Deactivation tau (τ) ($msec_T/msec_{NT}$ x 100)	100 ± 0.0	104.0 ± 6.6	146.6 ± 9.1 ♦(41)	105.0 ± 8.6 ● (-28)
10 min	Transient Peak Current ($\mu A_T/\mu A_{NT}$ x 100)	100 ± 0.0	102.1 ± 4.5	141.9 ± 8.9 ♦(40)	114.5 ± 7.8 ●(-19)
	Activation tau (τ) ($msec_T/msec_{NT}$ x 100)	100 ± 0.0	108.4 ± 1.8	131.6 ± 4.8 ♦(21)	115.2 ± 4.5
	Inactivation tau (τ) ($msec_T/msec_{NT}$ x 100)	100 ± 0.0	166.3 ± 32.5	158.9 ± 38.1	99.54 ± 36.5
	Deactivation tau (τ) ($msec_T/msec_{NT}$ x 100)	100 ± 0.0	104.0 ± 6.6	160.3 ± 13.3 ♦(54)	105.4 ± 7.1

A closed diamond (♦) indicates significant difference from DMSO. A closed circle (●) indicates significant difference from PMA. Both were determined by one-way ANOVA ($P < 0.05$). Values in parentheses are percent increases or decreases.

value (Fig. 5D) at 10 min post treatments. The effects of PMA and 4α-PMA treatments on V_{50acts} were not significantly different from the DMSO treatment or from each other at 10 min post treatment.

Treatments with PMA and 4α-PMA did modify the voltage-dependent inactivation kinetics compared to the controls (Fig. 6, Table 4). A hyperpolarizing shift in $V_{50inact}$ is an indication that the channels are inactivating at lower potentials allowing for decreased Ca^{2+} influx. At 4 min post treatment, DMSO caused a significant 25% hyperpolarizing shift in $V_{50inact}$ compared to the no treatment control (Fig. 6E). There was no significant effect, however, at 10 min post treatment. In the presence of PMA, at 4 min post treatment significant 40% and 24% hyperpolarizing shifts in the $V_{50inact}$ compared to the no treatment and DMSO control, respectively, were observed (Fig. 6E, Table 4). The presence of PMA at 10 min post treatment (Fig. 6F) caused an even greater hyperpolarizing shift of $V_{50inact}$ compared to no treatment (80%) and DMSO (69%) values.

4α-PMA did not significantly alter the voltage-dependent inactivation kinetics compared to the no treatment control, however, a 34% depolarizing shift in $V_{50inact}$ was observed in the presence of 4α-PMA at 4 min post treatment compared to DMSO treatment. 4α-PMA did result in significant depolarizing shifts in the $V_{50inact}$ compared to the PMA treatment at 4 (49%) and 10 (50%) min post treatment (Table 4).

The effects of PMA on the activation and deactivation kinetics of $Ca_V2.2$ are shown in Figure 7 and Table 5. At 4 min post treatment, there were no significant differences between treatments on the voltage-dependent rates of activation ($\tau_{activation}$) (Table 5). In the presence of DMSO at 10 min post treatment, $\tau_{activation}$ was significantly

Figure 6. Effects of 0.02% DMSO, PMA (1×10^{-7} M) and its inactive analog 4α-PMA (1×10^{-7} M) on voltage-dependent peak current, activation midpoint potential and inactivation midpoint potential at 4 and 10 min post treatment. (A and B) Voltage-dependent peak current was normalized to the DMSO control (value of DMSO treatment normalized to 1). (C and D) Activation midpoint potentials (V_{50act}) and (E and F) inactivation midpoint potential ($V_{50inact}$) were determined by the least-squares fits of the current-voltage relationship from individual experiments of the Activation and Inactivation Test Protocols using the sigmoidal dose-response (variable slope) equation. The number of eggs (n) used for the calculations of voltage-dependent peak currents, and V_{50act} were no treatment (n= 40); DMSO (n = 19); PMA (n = 17); 4α-PMA (n = 5). (E and F). The number of eggs (n) used for the calculations of $V_{50inact}$ were no treatment (n= 30) DMSO (n = 13); PMA (n = 13); 4α-PMA (n = 5). Statistical analysis was conducted using Student's T-test ($P < 0.05$).

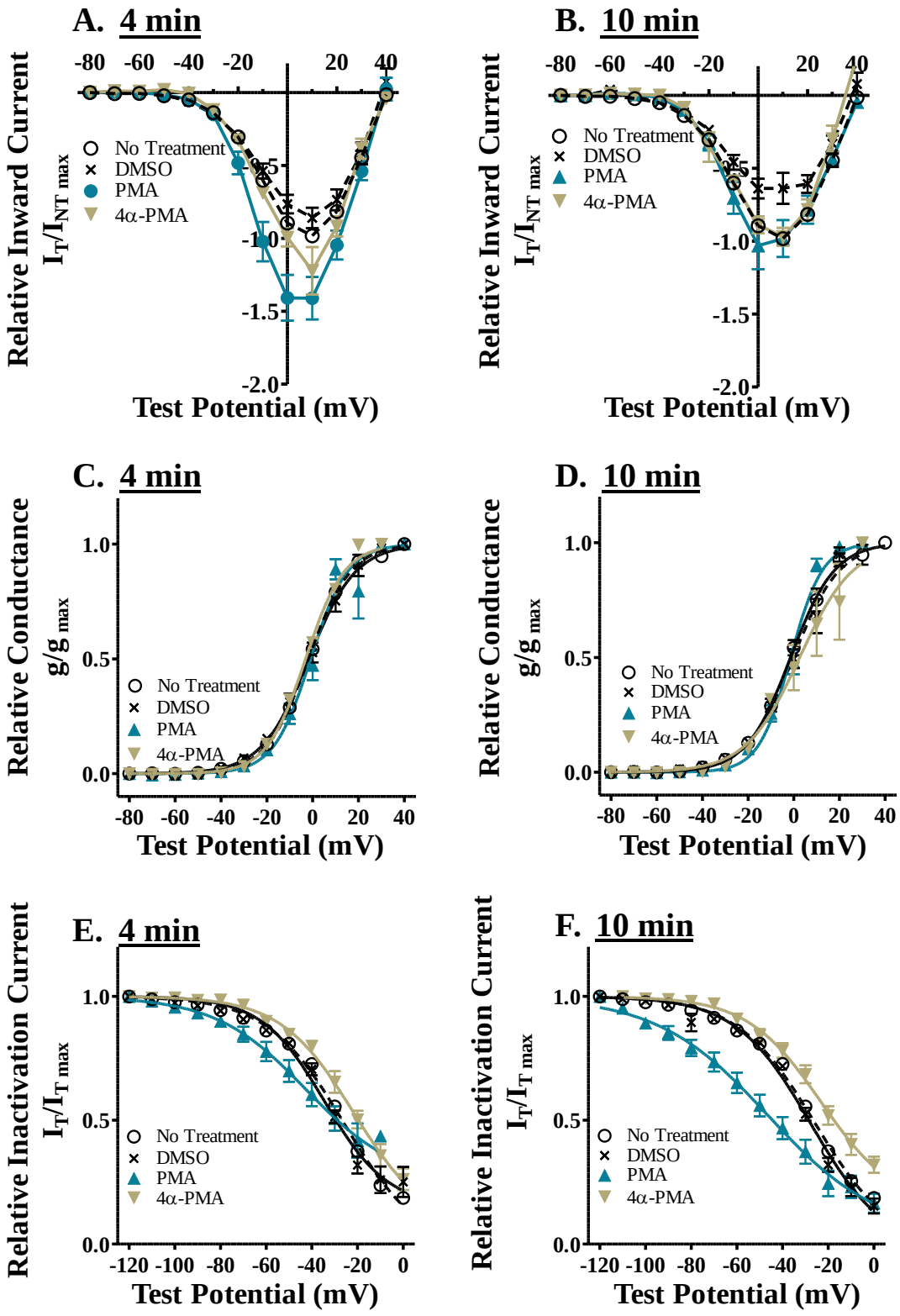
A. 4 min
B. 10 min
C. 4 min
D. 10 min
E. 4 min
F. 10 min
Relative Inward Current
$I_T/I_{NT\ max}$
Relative Conductance
g/g_{max}
Relative Inactivation Current
$I_T/I_{T\ max}$
Test Potential (mV)
No Treatment
DMSO
PMA
4α-PMA

greater than no treatment control by 14% at 30 mV. In the presence of PMA at 10 min post treatment, there were significant increases in $\tau_{activation}$ values that ranged from 16-29% following membrane depolarizations from -20 mV to 30 mV of 16-29% compared to DMSO control values. Conversely, 4α-PMA caused significant decreases in $\tau_{activation}$ values at 10 min post treatment that ranged from 21-27% following membrane depolarization from -30 mV to -10 mV compared to DMSO control values. The $\tau_{activation}$ values in the presence of 4α-PMA at 10 min post treatment were significantly less than those following PMA treatment and ranged from 18-37% following membrane depolarizations from -10 mV to 20 mV.

At 4 min post treatment, $\tau_{activation}$ slope in the presence of DMSO was significantly different from the no treatment control (Table 6). In the presence of PMA, $\tau_{activation}$ slope had no significant effect compared to the DMSO control at 4 min post treatment (Figure 7). The $\tau_{activation}$ slope in the presence of 4α-PMA was significantly different compared to either DMSO or PMA treatments at 4 min post treatment (Table 6).

At 4 and 10 min post treatment, $\tau_{activation}$ y-intercept in the presence of DMSO was significantly different from the no treatment control treatment (Table 6). The effect of PMA on $\tau_{activation}$ y-intercept was not significant at 4 min post treatment but was significantly different at 10 min post treatment from DMSO. The $\tau_{activation}$ y-intercept in the presence of 4α-PMA was significantly different from both DMSO and PMA at 4 and 10 min post treatments.

The effect of PMA on the voltage-dependent $\tau_{deactivation}$ at 4 min post treatment was significantly greater than the voltage-dependent $\tau_{deactivation}$ in the presence of DMSO at -40 mV and -30 mV by 29% and 41% respectively (Table 7). The effect of 4α-PMA on

Table 4. The effects of DMSO, PMA and 4α-PMA on $Ca_V2.2$ voltage-dependent peak current, activation and inactivation midpoint potentials.

		Treatment (10^{-7} M)			
		No Treatment	DMSO	PMA	4α-PMA
4 min	Voltage-dependent peak current	-0.98 ± 0.01	-0.86 ± 0.07 ◊(-12)	-1.41 ± 0.15 ◊(44) ♦(64)	-1.22 ± 0.16 ◊(24) ♦(42)
	Activation MPP (mV ± SEM)	-1.85 ± 0.43	-1.71 ± 0.65	-0.93 ± 0.75	-3.09 ± 0.40
	Inactivation MPP (mV ± SEM)	-27.73 ± 2.21	-34.40 ± 2.34 ◊(25)	-42.62 ± 9.31 ◊(-40) ♦(-24)	-21.58 ± 4.21 ♦(34) ●(49)
10 min	Voltage-dependent peak current	-0.98 ± 0.01	-0.64 ± 0.07 ◊(35)	-1.03 ± 0.16 ♦(39)	-0.97 ± 0.06
	Activation MPP (mV ± SEM)	-1.42 ± 0.52	-0.22 ± 0.74 ◊(88)	-1.40 ± 0.47	2.56 ± 1.82 ◊(238)
	Inactivation MPP (mV ± SEM)	-25.78 ± 2.28	-27.49 ± 2.62	-46.36 ± 6.01 ◊(-80) ♦(-69)	-23.19 ± 4.46 ●(50)

An open diamond (◊) indicates significant difference from no treatment. A closed diamond (♦) indicates significant difference from DMSO. A closed circle (●) indicates significant difference from PMA. Statistical differences were determined by using Student's T-test ($P < 0.05$). Values in parentheses are percent increases or decreases.

$\tau_{deactivation}$ at 4 min post treatment was significantly less than DMSO treatment by 40% at -30 mV. At 10 min post treatment the presence of DMSO caused significant increases in $\tau_{deactivation}$ values that ranged from 20-21% following membrane depolarizations from -50 mV to -30 mV.

The $\tau_{deactivation}$ values in the presence of PMA at 10 min post treatment were significantly greater than those following DMSO treatment and ranged from 44%-86% following membrane depolarizations from -50 mV to -30 mV. $\tau_{deactivation}$ in the presence of 4α-PMA was not significantly different from either DMSO or PMA treatments at 10 min post treatment.

The $\tau_{deactivation}$ slope following PMA treatment was significantly greater than the DMSO control value 4 min (Fig. 7C) and 10 min (Fig. 7D) post treatment (Table 6). In the presence of 4α-PMA at both the 4 and 10 min post treatment, the $\tau_{deactivation}$ slope was reduced by -65% and -70%, respectively, compared to the effect of PMA treatment (Table 6). The effect of PMA on the $\tau_{deactivation}$ y-intercept was significantly greater than the effect of the DMSO control at both 4 min and 10 min post treatments. The $\tau_{deactivation}$ y-intercept in the presence of 4α-PMA was significantly less than the effect of PMA at either 4 or 10 min post treatment by -70% or -49%, respectively (Table 6).

3.2 Discussion

3.2.1 Steady-state peak current

Our results confirm earlier reports that under steady-state conditions, the phorbol ester PMA is a potent activator of the endogenously expressed PKC in *Xenopus* oocytes resulting in altered $Ca_v2.2$ currents (Bourinet et al., 1992). PMA is capable of

Figure 7. Semi-logarithmic plots of the activation tau (A and C) and deactivation tau (C and D) values resulting from the effects of 0.02% DMSO, PMA (1 x 10^{-7} M) and its inactive analog 4α-PMA (1 x 10^{-7} M) at 4 min (A and B) and 10 min (C and D) post treatment using the Activation and Deactivation Test Protocols, respectively. Activation and deactivation tau values are obtained from linear regression fits to the data. The voltage dependence of activation and deactivation are represented by slope. The rates of activation and deactivation are represented by the y-intercept. The number of eggs (n) used for A and C are: no treatment (n = 41); DMSO (n = 18); PMA (n = 17); 4α-PMA (n = 5). The number of eggs (n) for B and D are: no treatment (n = 30); DMSO (n = 21); PMA (n = 11); 4α-PMA (n = 5). Statistical analysis was conducted using Student's T-test ($P < 0.05$).

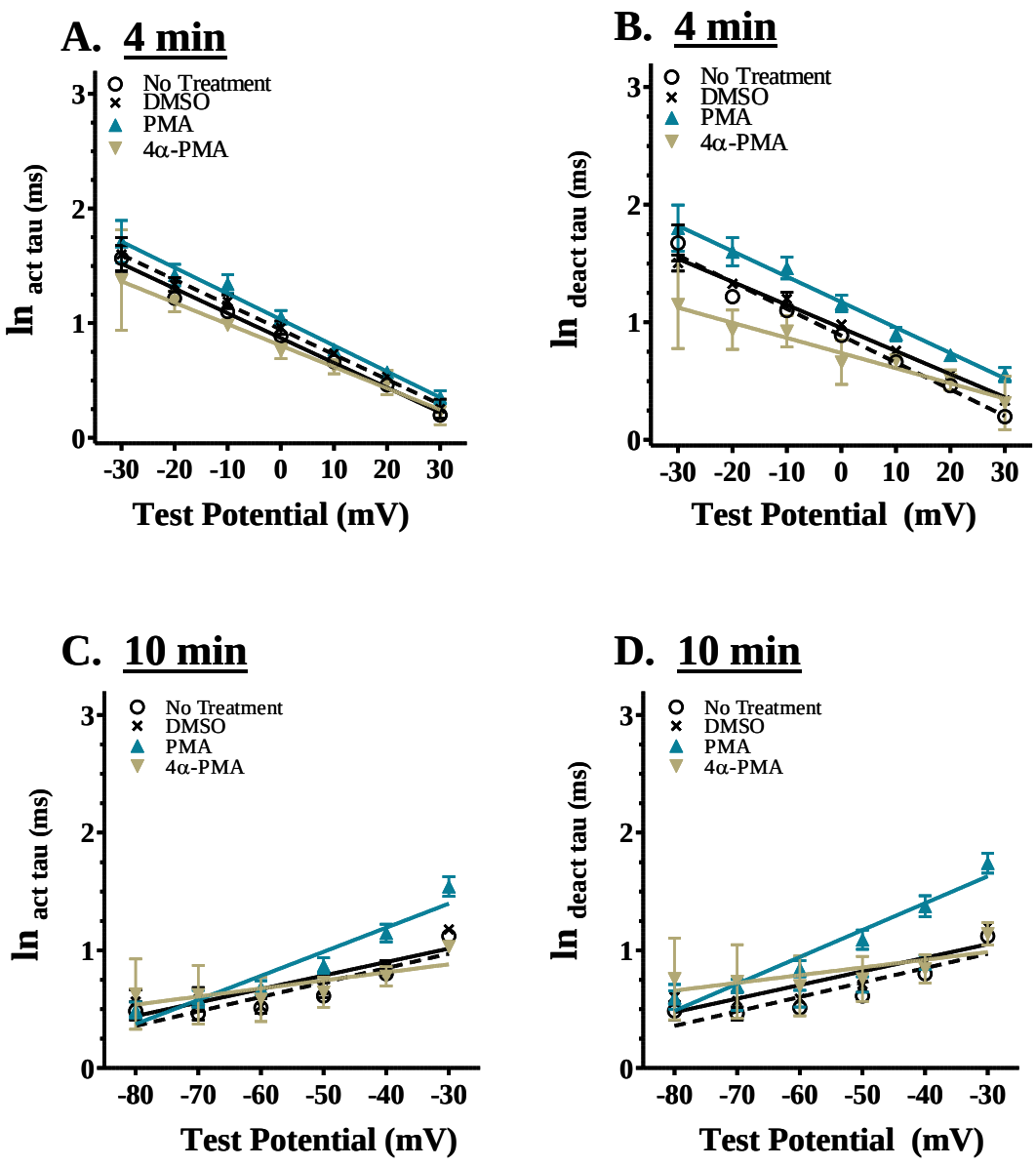
A. 4 min
No Treatment
DMSO
PMA
4α-PMA
ln act tau (ms)
Test Potential (mV)
B. 4 min
ln deact tau (ms)
C. 10 min
D. 10 min

phosphorylating several different sites on the intracellular loops of $Ca_V2.2$ and result in a variety of altered expression patterns and kinetic properties of this channel (Fang et al., 2006).

In support of previous findings (Stea et al., 1995), phosphorylated $Ca_V2.2$ allowed an increase of transient Ba^{2+} peak current under steady-state depolarizing conditions. The same time-dependent effects of phosphorylated $Ca_V2.2$ transient peak current observed by Stea *et. al.* (1995) were seen in our assay with a similar run down of Ba^{2+} currents by the 10 min time point and a maximal effect on peak current occurring at 4 min post treatment.

4α-PMA, the inactive structural analog of PMA, had no effect on Ba^{2+} influx. A similar effect of 4α-PMA on transient peak current was also reported by Stea *et al*. (1995), but using the R-type Ca^{2+} channels α_{1E}. Although the *Xenopus* oocyte system is a non neuronal heterologous expression system, our findings are consistent with other studies where neuronal tissue preparations were used to show PMA-activated PKC increased transient peak current using superior cervical ganglion, and dorsal root ganglion nerve preparations that also show an increase in peak current in the presence of PMA-activated PKC(Swartz, 1993). When neuronal cell preparations were treated with PMA under depolarizing conditions, an increase in whole cell current and neurotransmitter release was observed (Swartz, 1993; Zhu and Ikeda, 1994; Barrett and Rittenhouse, 2000; García-Ferreiro et al., 2001). Thus, increases in Ba^{2+} peak current from heterologously expressed phosphorylated $Ca_V2.2$ in *Xenopus* oocytes under steady state depolarizing conditions is consistent with previous reports finding that PMA activates PKC endogenously expressed within the oocyte allowing phosphorylation of

Table 5. The effects of DMSO, PMA and 4α-PMA on $Ca_V2.2$ voltage-dependent activation ($\tau_{activation}$).

	Treatment (10^{-7}M)	Test Potential (mV) -30	-20	-10	0	10	20	30
		$tau_{activation}$ (ms)						
	No Treatment	5.05 ± 0.41	3.93 ± 0.24	3.10 ± 0.15	2.46 ± 0.09	1.97 ± 0.07	1.58 ± 0.06	1.28 ± 0.05
4 min	DMSO	5.09 ± 0.28	4.08 ± 0.20	3.27 ± 0.14	2.64 ± 0.10	2.13 ± 0.07	1.73 ± 0.06	1.41 ± 0.05
	PMA	5.78 ± 0.69	4.57 ± 0.46	3.63 ± 0.30	2.90 ± 0.20	2.33 ± 0.13	1.89 ± 0.10	1.53 ± 0.08
	4α-PMA	4.25 ± 0.77	3.43 ± 0.52	2.78 ± 0.33	2.28 ± 0.21	1.88 ± 0.14	1.56 ± 0.13	1.31 ± 0.15
10 min	DMSO	4.78 ± 0.24	3.91 ± 0.17	3.20 ± 0.13	2.62 ± 0.10	2.15 ± 0.08	1.77 ± 0.07	1.46 ± 0.06
	PMA	6.48 ± 0.87	5.07 ± 0.55 ♦(29)	4.00 ±0.35 ♦(25)	3.18 ± 0.21 ♦(21)	2.55 ± 0.13 ♦(19)	2.13 ± 0.11 ♦(20)	1.70 ± 0.08 ♦(16)
	4α-PMA	3.51 ± 0.79 ♦(-27)	2.96 ± 0.58 ♦(-24)	2.52 ± 0.40 ♦(-21) ●(-37)	2.16 ± 0.27 ●(-18)	1.87 ± 0.17 ●(-25)	1.64 ± 0.12 ●(-23)	1.45 ± 0.14

An open diamond (◊) indicates significant difference from no treatment. A closed diamond (♦) indicates significant difference from DMSO. A closed circle (●) indicates significant difference from PMA. Statistical differences were determined by Student's T-test (P

<0.05). Values in parentheses are percent increases or decreases.

$Ca_V2.2$ and producing a phosphoform that enhances Ca^{2+}-dependent neurotransmitter release. (Bourinet et al., 1992; Stea et al., 1995).

Conversely, we observed under steady-state conditions, that the inactive form of PMA, 4α-PMA, had no significant effect on transient peak current. This confirms previous studies showing that 4α-PMA does not activate PKC under steady-state conditions (Castagna et al., 1982; Stea et al., 1995; García-Ferreiro et al., 2001)

3.2.2 Steady-state Gating Kinetics

Apparent phosphorylation of $Ca_V2.2$ by PMA-activated PKC induced a slowing of activation under steady-state depolarization at the end of a 10 min treatment but there was no change in activation rate at 4 min post treatment when we observed the maximal effect of PMA on transient peak current. This increase of activation taus following PMA treatment indicates that phosphorylated $Ca_V2.2$ takes more time to open than the unphosphorylated channel. The increase in activation tau observed at 10 min post treatment in the presence of PMA was not observed in the presence of DMSO or 4α-PMA at either the 4 or 10 min post treatments. This slowing of activation tau in the presence of PMA indicates that phosphorylated $Ca_V2.2$ opens at a slower rate than unphosphorylated $Ca_V2.2$. This slowing of the time it takes for the channel to open would, in an *in vivo* neuron would decrease Ca^{2+} influx and decrease subsequent Ca^{2+}-dependent neurotransmitter release.

Inactivation taus were measured from peak current to end of protocol and are an indication of how fast or slow $Ca_V2.2$ closes under depolarizing conditions. Inactivation taus of phosphorylated $Ca_V2.2$ significantly decreased at 4 min post treatment, indicating

Table 6. The effects of DMSO, PMA and 4α-PMA on $Ca_V2.2$ voltage-dependent activation and deactivation taus.

		$\tau_{actvation}$		$\tau_{deactvation}$	
	Treatment (10^{-7} M)	slope (mV^{-1} ± SEM)	y-intercept	slope (mV^{-1} ± SEM)	y-intercept
	No Treatment	-0.023 ± 0.001	0.890 ± 0.026	0.012 ± 0.001	1.340 ± 0.074
4 min	DMSO	-0.022 ± 0.001	0.944 ± 0.012	0.011 ± 0.002	1.359 ± 0.109
	PMA	-0.023 ± 0.001	1.031 ± 0.020	0.020 ± 0.002 ♦(45)	2.011 ± 0.104 ♦(32)
	4α-PMA	-0.019 ± 0.001 ♦(-14) ●(-17)	0.804 ± 0.012 ♦(-15) ●(-22)	0.007 ± 0.004 ●(-65)	1.087 ± 0.262 ●(-45)
10 min	DMSO	-0.020 ± 0.001	0.951 ± 0.013 ◊(7)	0.012 ± 0.002	1.399 ± 0.106
	PMA	-0.022 ± 0.001	1.171 ± 0.017 ♦(23)	0.023 ± 0.002 ♦(85)	2.315 ± 0.106 ♦(65)
	4α-PMA	-0.013 ± 0.001 ♦(-35) ●(-41)	0.737 ± 0.024 ♦(-22) ●(-37)	0.007± 0.005 ●(-70)	1.182 ± 0.311 ●(-49)

An open diamond (◊) indicates significant difference from no treatment. A closed diamond (♦) indicates significant difference from DMSO. A closed circle (●) indicates significant difference from PMA. (n) indicates percent increase or decrease. Student's T-test ($P < 0.05$).

that the phosphorylated channel takes less time to inactivate than the unphosphorylated channel. At 10 min post treatment, we did not observe a significant difference in average inactivation taus between phosphorylated and unphosphorylated $Ca_V2.2$. A decrease in average inactivation taus means that phosphorylated $Ca_V2.2$ takes less time to inactivate than unphosphorylated $Ca_V2.2$. This decrease in inactivation taus is not consistent with increased Ca^{2+} influx and neurotransmitter release observed in PMA-treated neuronal preparations because a fast inactivating channel does not allow for more Ca^{2+} to enter the cell.

The significant and pronounced increase in average steady-state deactivation taus of phosphorylated $Ca_V2.2$ is consistent with the data that shows increased Ca^{2+} influx and neurotransmitter release in *in vivo* neuron preparations when treated with PMA (Swartz, 1993; Zhu and Ikeda, 1994; García-Ferreiro et al., 2001). The larger the deactivation taus, the more time it takes for $Ca_V2.2$ to close after the removal of membrane depolarization and the greater the influx of Ca^{2+} and neurotransmitter release. Phosphorylated $Ca_V2.2$ takes longer to deactivate than unphosphorylated $Ca_V2.2$. We know that endogenous $Ca_V2.2$ in *in vivo* neurons and synaptosomes undergo post translational modifications that include phosphorylation. The addition of deltamethrin to rat brain synaptosomes resulted in an increase in Ca^{2+} influx and subsequent neurotransmitter release. We expect that the addition of deltamethrin to phosphorylated $Ca_V2.2$ expressed in *Xenopus* oocytes would result in an even greater increase in Ba^{2+} influx that is similar to what was observed when synaptosomes were treated with deltamethrin and Ca^{2+} enters the synaptosomes.

Fang *et al.* (2006) demonstrated that there are several residues on $Ca_V2.2$ α-subunit that regulate current in the presence of PMA. $Ca_V2.2$ mutant S425A had

Table 7. The effects of DMSO, PMA and 4α-PMA on voltage-dependent deactivation ($\tau_{deactivation}$).

		Test Potential (mV)					
		-80	-70	-60	-50	-40	-30
	Treatment (10^{-7}M)	$tau_{deactivation}$ (ms)					
	No Treatment	1.53 ± 0.16	1.66 ± 0.13	1.82 ± 0.10	2.02 ± 0.08	2.26 ± 0.08	2.56 ± 0.11
4 min	DMSO	1.81 ± 0.21	1.94 ± 0.19	2.10 ± 0.17	2.30 ± 0.16	2.55 ± 0.15	2.85 ± 0.17
	PMA	1.64 ± 0.21	1.89 ± 0.15	2.24 ± 0.14	2.69 ± 0.20	3.28 ± 0.32 ♦(29)	4.03 ± 0.48 ♦(41)
	4α-PMA	2.08 ± 0.66	2.08 ± 0.53	2.11 ± 0.40	2.17 ± 0.28	2.27 ± 0.15	2.41 ± 0.05 ●(-40)
10 min	DMSO	1.86 ± 0.23	2.03 ± 0.21	2.23 ± 0.20	2.46 ± 0.19 ◊(22)	2.74 ± 0.19 ◊(21)	3.07 ± 0.19 ◊(20)
	PMA	1.65 ± 0.09	2.08 ± 0.13	2.62 ± 0.19	3.31 ± 0.27 ♦(44)	4.20 ± 0.38 ♦(65)	5.32 ± 0.54 ♦(86)
	4α-PMA	2.5 ± 0.88	2.48 ± 0.75	2.49 ± 0.62	2.53 ± 0.49	2.60 ± 0.36	2.72 ± 0.23

An open diamond (◊) indicates significant difference from no treatment. A closed diamond (♦) indicates significant difference from DMSO. A closed circle (●) indicates significant difference from PMA. Statistical differences were determined using Student's T-test ($P < 0.05$). Values in parentheses are percent increases or decreases.

enhanced currents in the presence of PMA. $Ca_V2.2$ currents decreased in the presence of the unchanged S425 isoform. Although they did not show the effect of PMA on the kinetics of mutant forms of $Ca_V2.2$, we would expect that the kinetic profile of S425A $Ca_V2.2$ would be similar to PMA-treated $Ca_V2.2$. Some phosphorylation sites had more of an effect on peak current than others when phosphorylated. Phosphorylated S425 decreased peak current, whereas phosphorylated T422 increased peak current. Even in the presence of a S425A mutation, significant PMA enhancement of peak current occurs in the presence of not only phosphorylated T422 but phosphorylated S2108 as well. The findings show us that it is not just one phosphorylation site or the other that increases or decreases $Ca_V2.2$ current, but multiple phosphorylation sites work together to effect changes in the response of $Ca_V2.2$ to changes in membrane potential. The selective phosphorylation of these sites, alone and in combination, will be necessary in determining which sites, when phosphorylated, change the kinetic profile of $Ca_V2.2$.

3.2.3 Voltage-dependent peak current

Voltage-dependent peak current of phosphorylated $Ca_V2.2$ increased significantly at both the 4 and 10 min post treatments. A similar effect has been previously reported in the literature (Stea et al., 1995) and is consistent with enhanced Ca^{2+} influx and neurotransmitter release. Voltage-dependent peak current of phosphorylated $Ca_V2.2$ also underwent a 10 mV hyperpolarizing shift from 10 mV to 0 mV. This shift means that under phosphorylating conditions, 50% of the channels are opening at lower levels of membrane depolarization than they would have in their unphosphorylated state.

Unlike under steady-state depolarization, voltage-dependent peak current in the presence of 4α-PMA is significantly increased compared to our No Treatment control. This was an unexpected result given that 4α-PMA is considered an inactive analog to PMA and has no effect on $Ca_V2.2$ peak current under steady-state conditions presented here and elsewhere (Stea et al., 1995; Barrett and Rittenhouse, 2000; García-Ferreiro et al., 2001). The effect of 4α-PMA on $Ca_V2.2$ voltage-dependent peak current, however, is not significantly different from the effect of PMA on voltage-dependent peak current. Thus, it is possible, that the increase in voltage-dependent peak current observed in the presence of 4α-PMA may be due to differential phosphorylation of PKC activity. It is possible that 4α-PMA does activate PKC, but the spectrum of phosphorylation activity of 4α-PMA-activated PKC may not be as broad as PMA-activated PKC would be. For example, S425 on the I-II intramembrane loop has been reported to down regulate $Ca_V2.2$ activity when phosphorylated and 4α-PMA-activated PKC could be selectively not phosphorylating S425. Another possibility could be that 4α-PMA-activated PKC could be selectively phosphorylating T422, a site that has been shown to increase voltage-dependent peak current (Fang et al., 2006; Symington et al., 2007a).

3.2.4 Voltage-dependent Gating Kinetics

The V_{50acts} of phosphorylated $Ca_V2.2$ were not significantly different from the DMSO solvent control. We expected that with increases in Ba^{2+} influx via phosphorylated $Ca_V2.2$, the V_{50act} would be hyperpolarized. A hyperpolarized channel means that 50% of the channels will activate at depolarization levels lower than unphosphorylated $Ca_V2.2$ thus making the channel more sensitive to changes in

membrane potential.

Significantly hyperpolarized $V_{50inacts}$ in the presence of PMA indicate that $Ca_V2.2$ was more sensitive to undergoing inactivation at smaller changes in membrane potential. The increased sensitivity to small changes in membrane potential is inconsistent with increase neurotransmitter release observed when nerve cell preparations are treated with PMA (Stea et al., 1995; García-Ferreiro et al., 2001). Our data is consistent, however, with a previous study in which PMA caused a significant 20 mV hyperpolarizing shift in $V_{50inact}$ (we reported a significant 19 mV shift compared to DMSO control) (García-Ferreiro et al., 2001).

We have reported the average voltage-dependent rate of activation ($\tau_{activation}$) of non-treated $Ca_V2.2$ to be 3.10 ± 0.15 ms at 10 mV. This $\tau_{activation}$ at is nearly identical with the $\tau_{activation}$ reported by Lin et al. (1997) using heterologous expression of $Ca_V2.2$ in *Xenopus* oocytes. The presence of PMA or 4α-PMA did not have a significant effect on the rates of activation ($\tau_{activation}$) at 4 min post treatment in the range of -30 mV to 30 mV indicating that the voltage-dependent rates of activation neither increased nor decreased at this time (Table 5). However, at 10 min post treatment, PMA caused a significant increase in $\tau_{activation}$ at -20 mV, -10 mV, 0 mV, 10 mV, 20 mV and 30 mV compared to DMSO. These increases in $\tau_{activation}$ mean that phosphorylated $Ca_V2.2$ was taking more time to activate under as the channel underwent increasing levels of depolarization. The 22% increase in $\tau_{activation}$ means that it took $Ca_V2.2$ 22% longer to activate when phosphorylated. Compared to the presence of PMA at 10 min post treatment, 4α-PMA treated $Ca_V2.2$ produced a channel that activated at a faster rate, which was, as expected, not significantly different compared to the DMSO control.

We observed that under steady-state depolarization, phosphorylated $Ca_V2.2$ required more time to activate at 10 min post treatment. Similarly, we have shown that $\tau_{activation}$ of phosphorylated $Ca_V2.2$ also increases significantly at 10 min post treatment and the time required to activate the channel remains significantly greater than the time required to activate unphosphorylated $Ca_V2.2$ under voltage-dependent conditions in the range of -20-30mV.

Steady-state inactivation for phosphorylated $Ca_V2.2$ was not significantly altered compared to steady-state inactivation of unphosphorylated $Ca_V2.2$. Here, we see that phosphorylated $Ca_V2.2$ is activating slower and the slowing of activation remains at increasing levels of depolarization, phosphorylated $Ca_V2.2$ does not take longer to inactivate. This slowing rate of activation and the unchanged rate of inactivation under phosphorylating conditions does not support the observation that phosphorylation increases Ba^{2+} and that the addition of PMA to neuronal cell cultures enhances Ca^{2+} influx. Thus, we can conclude that phosphorylation of $Ca_V2.2$ does not increase Ba^{2+} or Ca^{2+} through activation or inactivation gating kinetics of the channel.

In the presence of PMA, $\tau_{deactivation}$ was prolonged at 4 min post treatment at -40 mV and -30 mV (Table 7). This prolongation of the time it takes for $Ca_V2.2$ to close after the removal of the membrane depolarization pulse corresponds with increased Ca^{2+} influx and neurotransmitter release because more Ca^{2+} is able to flow through the channel in the time it takes for it to completely deactivate. Although $\tau_{deactivation}$ increased in the presence DMSO at 10 min post treatment at -50 mV, -40 mV and -30 mV compared to no treatment, PMA still further increased $\tau_{deactivation}$ significantly more than the effect of DMSO at the same potentials. The increase in $\tau_{deactivation}$ at -50 mV, -40 mV, and -30 mV

means that $Ca_V2.2$ is taking more time to deactivate at higher levels of depolarization, allowing more Ca^{2+} to influx, in the *in vivo* neuron would correspond to an increase in neurotransmitter release.

CHAPTER 4

EFFECTS OF DELTAMETHRIN ON PMA-ACTIVATED PKC-PHOPHORYLATED $CA_V2.2$

4.1 Results

4.1.1 Transient Peak Current

Using the Transient Test Protocol, maximal effects on transient peak current were observed for wild type $Ca_V2.2$ in the presence of deltamethrin, PMA + deltamethrin, and 4α-PMA + deltamethrin during a 10 min incubation period (Fig. 8A). The presence of deltamethrin significantly reduced transient peak current compared to the effect of DMSO at 4 min (-18%) and 10 (-29%) min post treatment. The presence of PMA + deltamethrin significantly increased transient peak current compared to DMSO by 69% at 4 min and 82% at 10 min post treatment.

The presence of PMA + deltamethrin significantly increased transient peak current by 107% at 4 min and 156% at 10 min post treatment compared to the effect of deltamethrin (Fig 8A). At 4 min post treatment, transient peak current in the presence of 4α-PMA + deltamethrin was significantly less (-42%) than transient peak current in the presence of PMA + deltamethrin, but was significantly greater (19%) than transient peak current in the presence of deltamethrin alone. At 10 min post treatment, the effect of 4α-PMA + deltamethrin on peak current was 47% less than the effect of PMA + deltamethrin.

Figure 8. The effects of 0.1 % DMSO, deltamethrin (2×10^{-7} M), PMA (8×10^{-7} M) + deltamethrin (2×10^{-7} M) and 4α-PMA (8×10^{-7} M) + deltamethrin (2×10^{-7} M) on transient peak current of wild type $Ca_V2.2$ over a 10 min incubation period. Significance was calculated using one-way ANOVA with Bonferroni's multiple comparison post test ($P<0.05$). A diamond (♦) indicates significant difference from DMSO treatment. A square (■) indicates significant difference from deltamethrin treatment. A circle (●) indicates significant difference from PMA treatment. The numbers of eggs (n) used for these treatments are as follows: DMSO (39); deltamethrin (18); PMA + deltamethrin (9); 4α-PMA + deltamethrin (10).

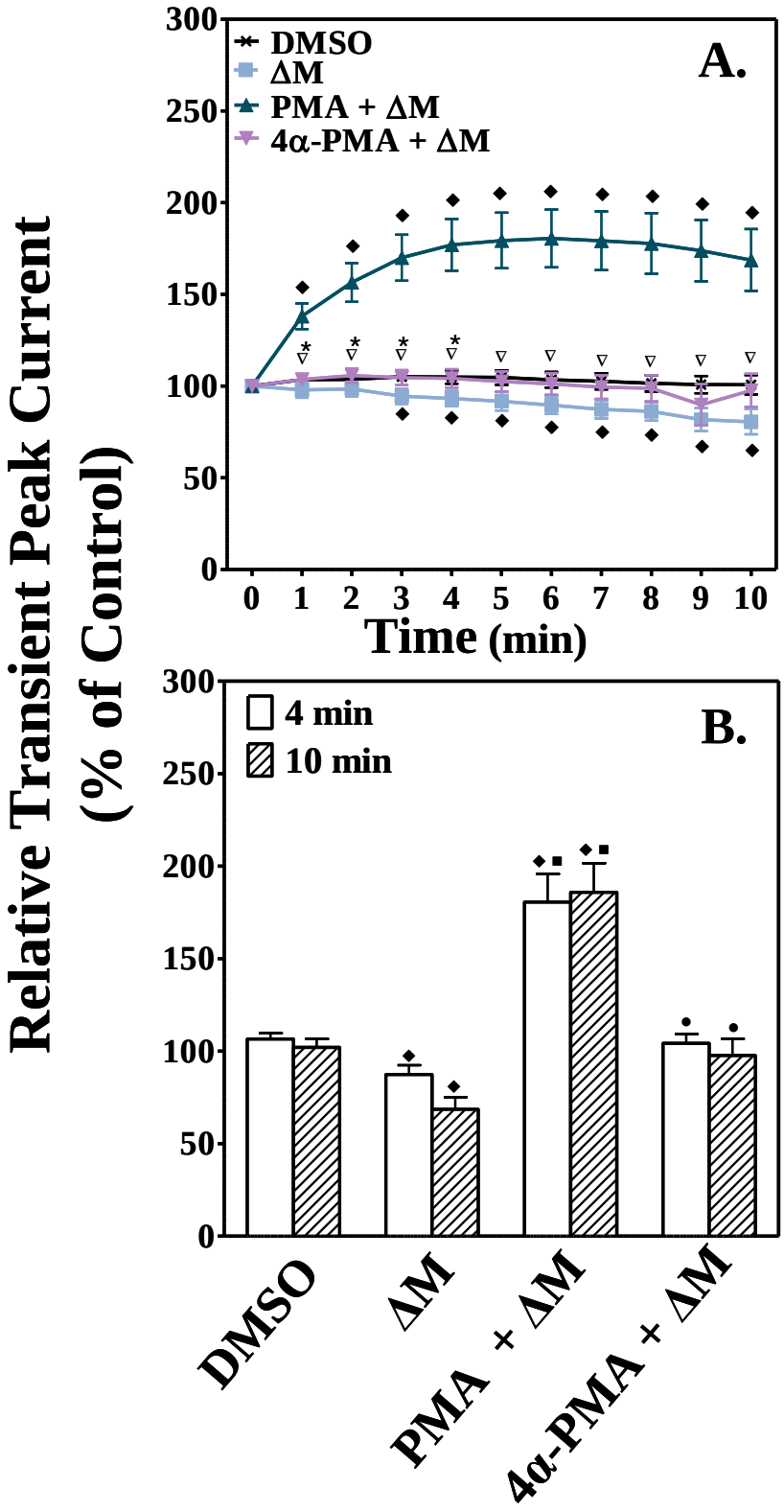
Relative Transient Peak Current
(% of Control)
A.
DMSO
ΔM
PMA + ΔM
4α-PMA + ΔM
Time (min)
B.
4 min
10 min
DMSO
ΔM
PMA + ΔM
4α-PMA + ΔM

4.1.2 Steady-state Gating Kinetics

In the presence of deltamethrin, steady-state activation taus were not significantly different from the DMSO controls at either the 4 min (Fig. 4A) or 10 min (Fig. 4B) post treatments. At 4 min post treatment, the PMA + deltamethrin treatment had no significant effect on activation taus compared to DMSO. The presence of PMA + deltamethrin significantly increased activation taus at 10 min post treatment (Fig 9B) compared to the effects of DMSO (27%) and deltamethrin (28%) (Table 8). The presence of 4α-PMA + deltamethrin had no significant effect on activation taus at either the 4 min or 10 min post treatments.

Steady-state inactivation taus were not significantly changed in the presence of deltamethrin following either 4 min (Fig. 9C) or 10 min (Fig. 9D) post treatments. At 4 min post treatment, average steady-state inactivation taus were significantly reduced by 53% in the presence of PMA + deltamethrin compared to DMSO and reduced by 52% compared to deltamethrin (Fig. 9D). In the presence of PMA + deltamethrin, steady-state inactivation taus were not significantly different from DMSO or PMA (Table 3) at 10 min post treatment, but were significantly less than steady-state inactivation taus in the presence of deltamethrin by 62% (Table 6).

There were no significant effects of deltamethrin on steady-state deactivation taus following either 4 min or 10 min post treatments compared to DMSO (Fig. 9E and F). At 4 and 10 min post treatment, the presence of PMA + deltamethrin significantly increased average deactivation taus by 79% and 54%, respectively, compared to DMSO (Fig. 9E). Although the difference in deactivation taus in the presence of PMA (Table 3) and PMA + deltamethrin were not significantly different at 4 min post treatment, the effect of PMA +

Figure 9. The effects of 0.1 % DMSO, deltamethrin (2×10^{-7} M), PMA (8×10^{-7} M) + deltamethrin (2×10^{-7} M) and 4α-PMA (8×10^{-7} M) + deltamethrin (2×10^{-7} M) on steady-state kinetics of wild type $Ca_V2.2$ at 4 min and 10 min post treatment. Activation (A and B), inactivation (C and D) and deactivation (E and F) taus were normalized to their respective No Treatment controls. The number of eggs (n) used for activation and deactivation taus at 4 min post treatment were DMSO (38); deltamethrin (25) PMA + deltamethrin (10); 4α-PMA + deltamethrin (9). The number of eggs (n) used for inactivation tau were DMSO (16); deltamethrin (19) PMA + deltamethrin (10); 4α-PMA + deltamethrin (9). Significance was determined by one-way ANOVA with Bonferroni's multiple comparison post test ($P < 0.05$). Symbols followed by asterisks (*) indicate that $P < 0.1$.

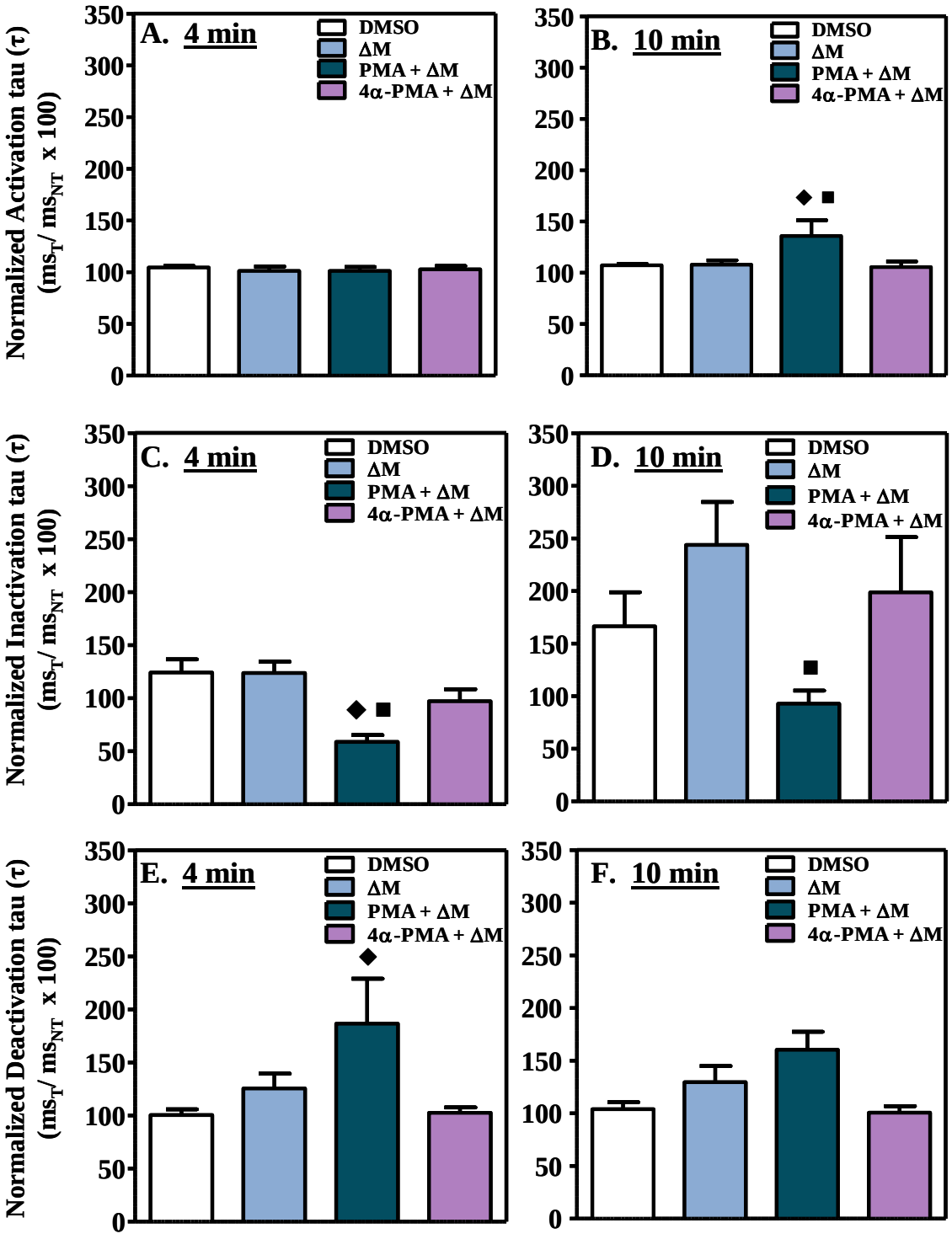
A. 4 min
B. 10 min
C. 4 min
D. 10 min
E. 4 min
F. 10 min
DMSO
ΔM
PMA + ΔM
4α-PMA + ΔM
Normalized Activation tau (τ)
(msT/ msNT x 100)
Normalized Inactivation tau (τ)
(msT/ msNT x 100)
Normalized Deactivation tau (τ)
(msT/ msNT x 100)
0
50
100
150
200
250
300
350

deltamethrin on deactivation taus was greater than the effect of PMA (Table 3). Deactivation taus in the presence of 4α-PMA+ deltamethrin at 4 min post treatment were 37% less than the effect of PMA + deltamethrin but deactivation taus were not significantly altered at 10 min post treatment.

4.1.3 Voltage-dependent Peak Current

The presence of deltamethrin caused significant decrease (-12%) in maximal voltage-dependent peak current compared to No Treatment at 10 min post treatment (Fig. 10B and Table 9). However, the decrease in maximal voltage-dependent peak current in the presence of deltamethrin was not significantly different from DMSO treatment at 10 min post treatment (Table 9). The presence of PMA + deltamethrin significantly increased maximal voltage-dependent peak current compared to No Treatment (47%), DMSO treatment (70%) and deltamethrin (46%) at 4 min post treatment. At 10 min post treatment, maximal voltage-dependent peak current in the presence of PMA + deltamethrin was reduced by -26% compared to the maximal peak current at 4 min post treatment. Compared to DMSO treatment at 10 min post treatment (Fig. 4), maximal voltage-dependent peak current in the presence of PMA + deltamethrin was significantly greater by 21%. The presence of 4α-PMA + deltamethrin significantly reduced maximal voltage-dependent peak current at 4 min post treatment by -16% compared to No Treatment and by -32% compared to 4α-PMA treatment. Maximal voltage-dependent peak current in the presence of 4α-PMA + deltamethrin was significantly less than the effect of PMA + deltamethrin treatment at 4 min post treatment by -43%. At 10 min post

Table 8. The effects of DMSO, deltamethrin, PMA + deltamethrin and 4α-PMA + deltamethrin on $Ca_V2.2$ steady-state transient peak current, activation, inactivation and deactivation taus.

		Treatment (10^{-7} M)			
		DMSO	Deltamethrin	PMA + deltamethrin	4α-PMA + deltamethrin
4 min	Transient Peak Current ($\mu A_T/\mu A_{NT}$ x 100)	106.6 ± 3.2	87.4 ± 5.1 ♦(-18)	180.6 ± 15.3 ♦(69) ■(107)	104.2 ± 5.0 ●(-42) ■(19)
	Activation tau (τ) ($msec_T/msec_{NT}$ x 100)	108.4 ± 1.8	100.9 ± 4.2	101.3 ± 3.8	102.7 ± 3.4
	Inactivation tau (τ) ($msec_T/msec_{NT}$ x 100)	124.1 ± 12.5	123.8 ± 10.7	58.8 ± 6.5 ♦(-53) ■(-52)	97.2 ± 11.2
	Deactivation tau (τ) ($msec_T/msec_{NT}$ x 100)	104.0 ± 6.6	125.6 ± 13.9	186.5 ± 42.5 ♦*(79)	102.5 ± 5.1 □(-37)
10 min	Transient Peak Current ($\mu A_T/\mu A_{NT}$ x 100)	102.1 ± 4.5	72.6 ± 15.8 ♦(-29)	185.8 ± 5.6 ♦(82) ■(156)	97.7 ± 9.1 ●(-47)
	Activation tau (τ) ($msec_T/msec_{NT}$ x 100)	108.4 ± 1.8	107.7 ± 4.3	135.8 ± 15.3 ♦(27) ■(28)	105.5 ± 5.4
	Inactivation tau (τ) ($msec_T/msec_{NT}$ x 100)	166.3 ± 32.5	243.7 ± 40.8	92.8 ± 12.5 ■(-62)	198.7 ± 52.5
	Deactivation tau (τ) ($msec_T/msec_{NT}$ x 100)	104.0 ± 6.6	129.6 ± 15.3	160.3 ± 17.2 ♦*(54)	100.6 ± 6.3

All values are normalized to the no treatment control (100.0). A closed diamond (♦) indicates significant difference from DMSO. A closed square (■) indicates significant difference from deltamethrin. A closed circle (●) indicates significant difference from PMA. An open square (□) indicates significant difference from PMA + deltamethrin. The values in parentheses (n) are percent increases or decreases. Significance was determined by One-way ANOVA with Bonferroni's multiple comparison post test ($P < 0.05$). Asterisks (*) indicates the $P < 0.10$.

treatment, deltamethrin treatment caused a significant -12% reduction in peak current compared to No Treatment, but the effect was not significantly different from the effect of DMSO (Table 4). PMA + deltamethrin treatment increased maximal peak current by 21% compared to DMSO. 4α-PMA + deltamethrin treatment significantly decreased peak current by -27% compared to No Treatment at 10 min post treatment. Compared to PMA + deltamethrin treatment at 10 min post treatment, 4α-PMA + deltamethrin treatment significantly reduced peak current by 33%. The presence of 4α-PMA + deltamethrin treatment significantly reduced peak current by -26% compared to 4α-PMA treatment at 10 min post treatment.

4.1.4 Voltage-dependent Gating Kinetics

The Activation Protocol was used to measure the midpoint activation potential (V_{50act}) in the presence of deltamethrin, PMA + deltamethrin and 4α-PMA + deltamethrin (Fig. 10C and D; Table 9). The presence of deltamethrin resulted in no significant effect on V_{50act} compared to DMSO at either 4 or 10 min post treatments. In the presence of PMA + deltamethrin, V_{50act} underwent significant 56% and 117% hyperpolarizing shifts at 4 and 10 min post treatments, respectively compared to the V_{50act} in the presence of PMA (Table 9). In the presence of 4α-PMA + deltamethrin at 4 min post treatment, significant depolarizing shifts in the V_{50act} compared to DMSO (175%), deltamethrin (171%), and 4α-PMA (142%) (Table 9) were apparent.

In the presence of deltamethrin at 4 and 10 min post treatment, there was no significant effect on the inactivation midpoint potential ($V_{50inact}$) compared to DMSO

Figure 10. Effects of 0.02% DMSO, deltamethrin (1 x 10^{-7} M), PMA (1 x 10^{-7} M) + deltamethrin (1 x 10^{-7} M) and 4α-PMA (1 x 10^{-7} M) + deltamethrin (1 x 10^{-7} M) on voltage-dependent peak current, activation midpoint potential and inactivation midpoint potential at 4 min and 10 min post treatment. (A and B) Voltage-dependent peak current was normalized to the DMSO control (value of DMSO treatment normalized to 1). (C and D) Activation midpoint potentials and (E and F) inactivation midpoint potentials were determined by the least-squares fits of the current-voltage relationship from individual experiments of the Activation and Inactivation Test Protocols using the sigmoidal dose-response (variable slope) equation. Significance was calculated using Student's T-test ($P < 0.05$). The number of eggs (n) used for A-D treatments are DMSO (19); deltamethrin (5); PMA + deltamethrin (5); 4α-PMA + deltamethrin (5). (E and F) The number of eggs (n) used for E-F treatments are DMSO (12); deltamethrin (5); PMA + deltamethrin (5); 4α-PMA + deltamethrin (5). Significance was calculated using Student's T-test ($P<0.05$).

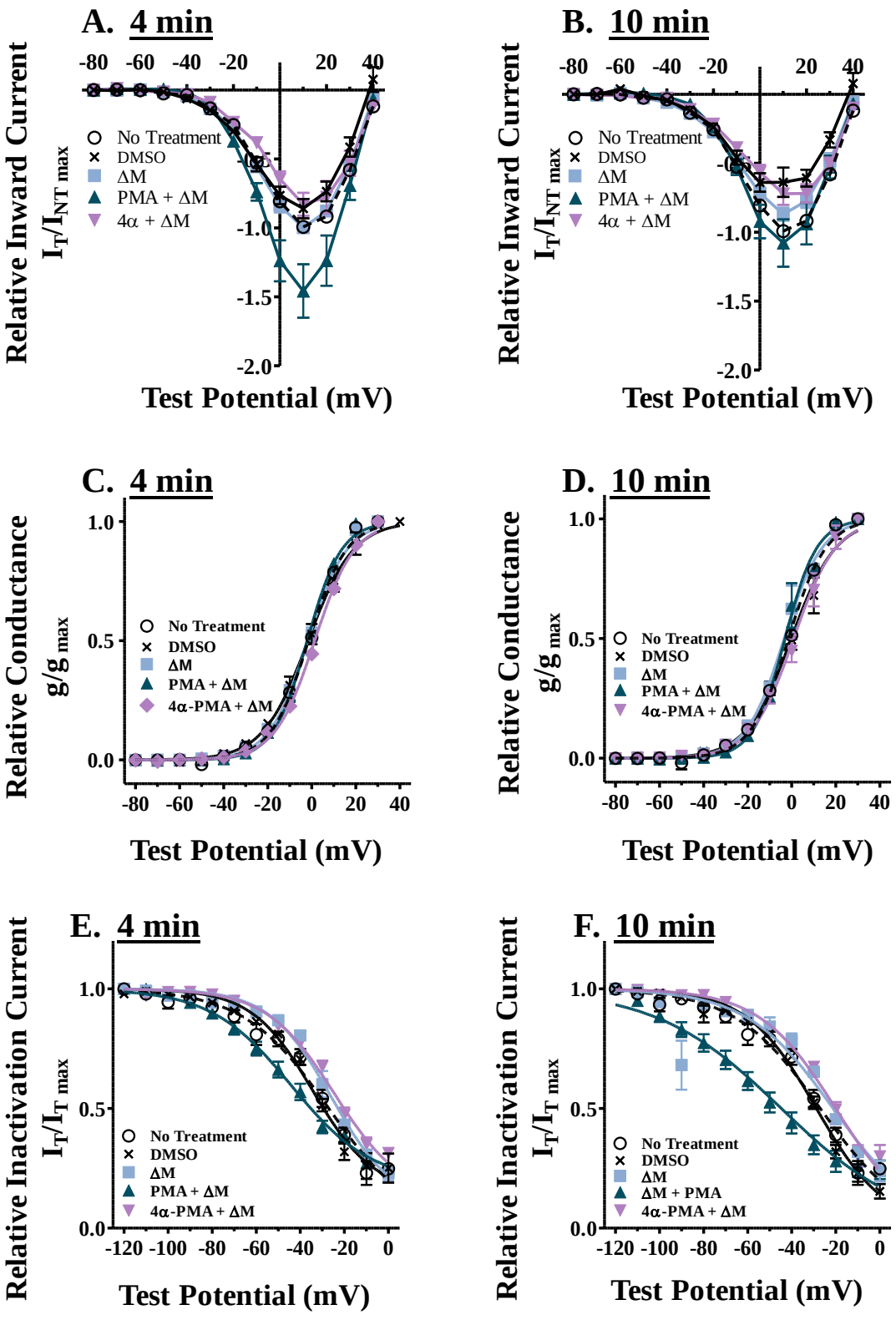
A. 4 min
B. 10 min
C. 4 min
D. 10 min
E. 4 min
F. 10 min
Relative Inward Current
$I_T/I_{NT\ max}$
Relative Conductance
g/g_{max}
Relative Inactivation Current
$I_T/I_{T\ max}$
Test Potential (mV)
No Treatment
DMSO
ΔM
PMA + ΔM
4α + ΔM
4α-PMA + ΔM
ΔM + PMA

(Table 9). The presence of PMA + deltamethrin at 4 min post treatment caused a hyperpolarizing shift in the $V_{50inact}$ that was significantly different from both DMSO (28%) and deltamethrin (71%). At 10 min post treatment, the presence of PMA + deltamethrin caused a significant 63% hyperpolarizing shift in $V_{50inact}$ compared to DMSO and a significant 111% hyperpolarizing shift in $V_{50inact}$ compared to PMA. The presence of 4α-PMA + deltamethrin caused a significant 29% depolarizing shift in $V_{50inact}$ compared to DMSO at 4 min post treatment.

Voltage-dependent rate constants for activation ($\tau_{activation}$) are shown in Table 10. Deltamethrin treatment resulted in no significant effect on $\tau_{activation}$ at either 4 or 10 min post treatment compared to DMSO. PMA + deltamethrin treatment resulted in no significant effect compared to DMSO at 4 min post treatment. However, PMA + deltamethrin significantly increased $\tau_{activation}$ by 33% (-20 mV), 28% (-10 mV), 20% (0 mV), 23% (10 mV) 21% (20 mV) and 20% (30 mV), respectively, at 10 min post treatment compared to the DMSO. The presence of deltamethrin on 4α-PMA-treated $Ca_V2.2$ had the unexpected effect of significantly increasing $\tau_{activation}$ at-30 mV by 90% and at -20 mV and -10 mV by 33% compared to DMSO. At -30 mV, the 4α-PMA + deltamethrin treatment increased $\tau_{activation}$ by 67% compared to deltamethrin alone. $\tau_{activation}$ in the presence of 4α-PMA + deltamethrin was significantly less than $\tau_{activation}$ in the presence of PMA + deltamethrin at 20 mV and 30 mV by 16% and 21%, respectively.

At 4 min post treatment, $\tau_{activation}$ slope in the presence of deltamethrin was not significantly different from DMSO (Fig. 11A). The $\tau_{activation}$ slope at 10 min post deltamethrin treatment, however, was significantly increased by 30% compared to DMSO control (Fig. 11C and Table 11). In the presence of PMA+ deltamethrin at 4 min

Table 9. The effects of DMSO, deltamethrin, PMA + deltamethrin and 4α-PMA + deltamethrin on voltage-dependent peak current, activation and inactivation midpoint potentials.

		Treatment (10^{-7} M)				
		No Treatment	DMSO	Deltamethrin	PMA + deltamethrin	4α-PMA + deltamethrin
4 min	Voltage-dependent peak current	-0.99 ± 0.01	-0.86 ± 0.07 ◊(-12%)	-1.00 ± 0.04	-1.46 ± 0.19 ◊(47) ♦(70) ■*(46)	-0.83 ± 0.08 ◊(-16) ○*(-43) Δ*(-32)
	Activation MPP (mV ± SEM)	-1.47 ± 0.33	-1.71 ± 0.65	-1.83 ± 0.35	-2.09 ± 0.29 ●(-56)	1.30 ± 0.61 ♦(175) ■(171) Δ(142)
	Inactivation MPP (mV ± SEM)	-27.35 ± 5.01	-34.38 ± 2.34 ◊(25)	-25.73 ± 2.47	-44.07 ± 3.45 ♦(-28) ■(-71)	-24.55 ± 3.06 ♦(29)
10 min	Voltage-dependent peak current	-0.99 ± 0.01	-0.64 ± 0.07 ◊(-35)	-0.87 ± 0.05 ◊(-12)	-1.08 ± 0.17 ♦(21)	-0.72 ± 0.08 ◊(-27) ○*(-33) Δ(-26)
	Activation MPP (mV ± SEM)	-1.47 ± 0.33	-0.22 ± 0.74 ◊(88)	-3.44 ± 0.69	-3.04 ± 0.61 ●(-117)	0.85 ± 0.72 ■(124)
	Inactivation MPP (mV ± SEM)	-27.02 ± 1.10	-28.79 ± 0.67	-21.21 ± 2.16	-44.69 ± 1.56 ♦(-63) ■(-111)	-20.07 ± 0.79

An open diamond (◊) indicates significant difference from No Treatment. A closed diamond (♦) indicates significant difference from DMSO. A square (■) indicates significant difference from deltamethrin. A circle (●) indicates significant difference from PMA. A triangle (Δ) indicates significant difference from 4α-PMA. A open circle (○) indicates significant difference from PMA + ΔM. The values in parentheses (n) are percent increases or decreases. Significance was calculated using Student's T-

test ($P<0.05$). Symbols followed by an asterisk (*) indicate that the significance level was $P < 0.1$.

post treatment, $\tau_{activation}$ slope was reduced by 14% compared to DMSO. 4α-PMA + deltamethrin treatment significantly reduced $\tau_{activation}$ slope by 35% compared to DMSO and by 38% compared to deltamethrin at 10 min post treatments.

Deltamethrin and PMA + deltamethrin treatments resulted in no significant effects on $\tau_{activation}$ y-intercept of $Ca_V2.2$ at 4 min post treatment but PMA + deltamethrin treatment significantly increased the $\tau_{activation}$ y-intercept compared to DMSO by 23% at 10 min post treatment. The $\tau_{activation}$ y-intercept was significantly reduced (-16%) by the 4α-PMA + deltamethrin treatment compared to DMSO at 4 min post treatment.

The 4 min deltamethrin treatment caused a significant increase (15%) in the voltage-dependent rate constant for deactivation ($\tau_{deactivation}$) at -30 mV (Table 12). At 10 min post deltamethrin treatment, there was no effect on $\tau_{deactivation}$. PMA + deltamethrin treatment also produced no significant effect on $\tau_{deactivation}$ at either 4 or 10 min post treatment. The 4 min post 4α-PMA + deltamethrin treatment caused significant reductions in $\tau_{deactivation}$ values at -60 mV (40%), -50 mV(32%), -40 mV(35%) and -30 mV (36%) compared to their respective DMSO $\tau_{deactivation}$ values. The 10 min post 4α-PMA + deltamethrin treatment, also reduced the $\tau_{deactivation}$ values by 43% (-60 mV), 36% (-50 mV), 39% (-40 mV) and 41% (-30 mV). Deltamethrin had no significant effect on $\tau_{deactivation}$ slope at either the 4 or 10 min post treatments compared to DMSO (Table 11). The effect of PMA + deltamethrin on $\tau_{deactivation}$ slope was significantly reduced by 50% compared to PMA at 4 min post treatment and by 30% at 10 min post treatment (Table 11).

Deltamethrin and PMA + deltamethrin resulted in no significant effects on the $\tau_{deactivation}$ y-intercepts at either 4 or 10 min post treatments compared to DMSO. The

Figure 11. Semi-logarithmic plots of the activation tau ($\tau_{activation}$) and deactivation tau ($\tau_{deactivation}$) values resulting from the effects of DMSO, deltamethrin (1×10^{-7} M), PMA (1×10^{-7} M) + deltamethrin (1×10^{-7} M) and 4α-PMA (1×10^{-7} M) + deltamethrin (1×10^{-7} M) + at 4 min (A and B) and 10 min (C and D) post treatment using the Activation Protocol (A and C) and the Deactivation Protocol (B and D), respectively. Activation tau and deactivation tau rate constants were obtained from linear regression fits to the data. The number of eggs (n) used for panels A and C are DMSO (n = 18); deltamethrin (n = 5); PMA + deltamethrin (n = 5); 4α-PMA + deltamethrin (n = 5). The number of eggs (n) used for panels B and D are DMSO (n = 18); deltamethrin (n = 5); and PMA + deltamethrin (n = 5); 4α-PMA + deltamethrin (n = 5). Significance was calculated using Student's T-test ($P<0.05$).

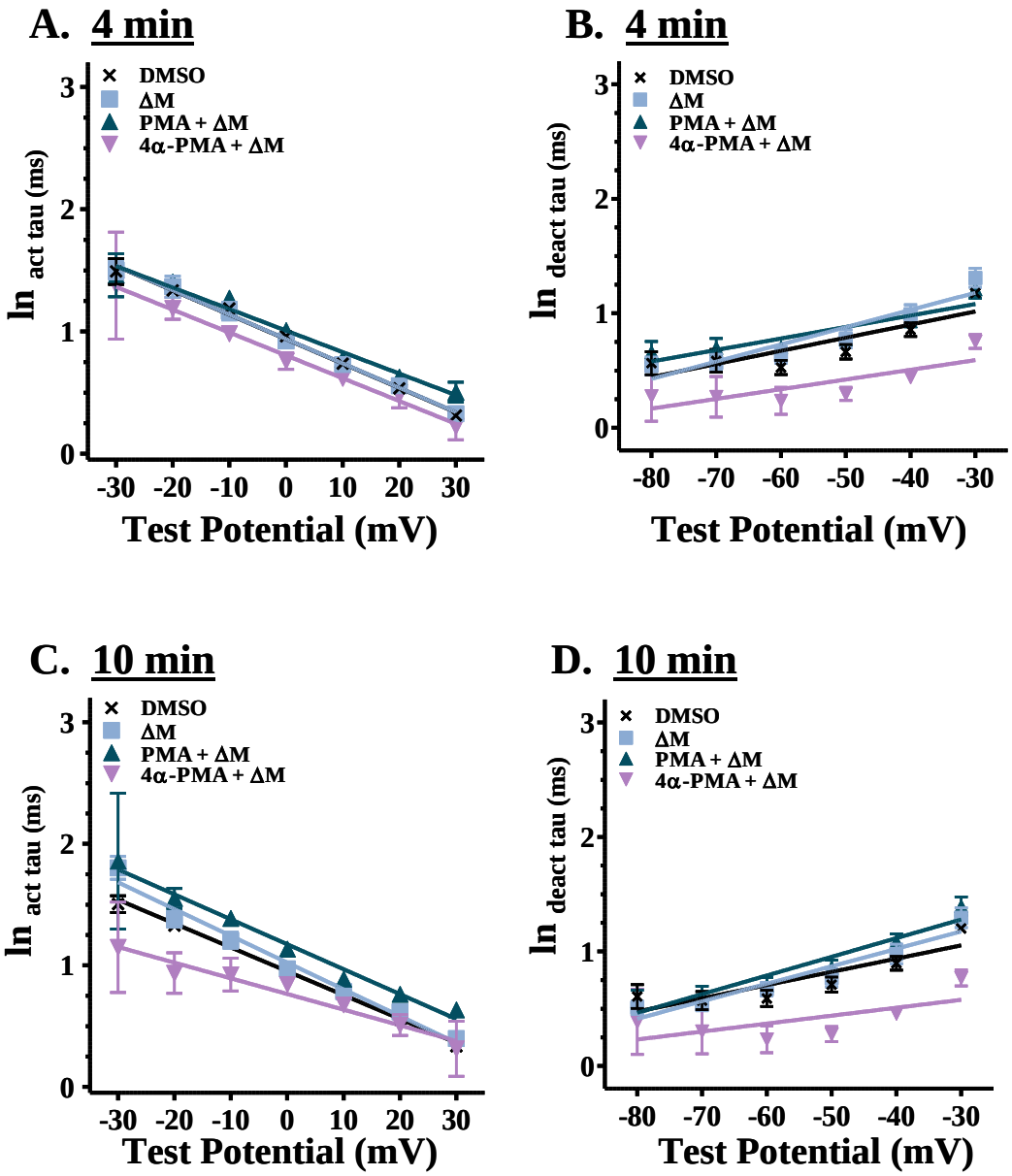
A. 4 min
DMSO
ΔM
PMA + ΔM
4α-PMA + ΔM
ln act tau (ms)
Test Potential (mV)
B. 4 min
ln deact tau (ms)
C. 10 min
D. 10 min

$\tau_{deactivation}$ y-intercept was reduced by 31% following the 4 min PMA + deltamethrin treatment compared to PMA (Table 6). The effects of PMA + deltamethrin treatment on the $\tau_{deactivation}$ y-intercepts were significantly less (-38% at 4 min and 44% at 10 min) than DMSO. 4α-PMA + deltamethrin treatment significantly reduced $\tau_{deactivation}$ y-intercept compared to deltamethrin by at both 4 (-38%) and 10 min (-52%) min post treatments (Table 6).

4.2 Discussion

4.2.1. Transient peak current

It is known that $Ca_V2.2$ undergoes post-translational modifications that include phosphorylation (Swartz, 1993; Swartz et al., 1993; Zhu and Ikeda, 1994). There are five sites located on the intracellular loops of $Ca_V2.2$ capable of being phosphorylated by PKC and it has been shown that, depending on which sites are phosphorylated, $Ca_V2.2$ will exhibit different functional characteristics (Fang et al., 2006). When $Ca_V2.2$ is phosphorylated by PMA-activated PKC, there is no control over which of the available sites are phosphorylated. The uncertainty of which sites are actually phosphorylated or not may have produced different phosphoforms from those produced in the synaptosomes and via mutagenesis and may have contributed to the different results obtained in the current study versus those obtained previously using different protocols (Symington and Clark, 2005; Symington et al., 2007a).

Nevertheless, the current data support, in part, previous findings, which suggest that deltamethrin modifies phosphorylated $Ca_V2.2$ and increases channel conductance.

Table 10. The effects of DMSO, deltamethrin, PMA + deltamethrin and 4α-PMA + deltamethrin on voltage-dependent activation ($\tau_{activation}$).

		Test Potential (mV)						
		-30	-20	-10	0	10	20	30
	Treatment (10^{-7}M)	$tau_{activation}$ (ms)						
	No Treatment	5.05 ± 0.41	3.93 ± 0.24	3.10 ± 0.15	2.46 ± 0.09	1.97 ± 0.07	1.58 ± 0.06	1.28 ± 0.05
4 min	DMSO	5.09 ± 0.28	4.08 ± 0.20	3.27 ± 0.14	2.64 ± 0.10	2.13 ± 0.07	1.73 ± 0.06	1.41 ± 0.05
	Deltamethrin	4.80 ± 0.36	3.90 ± 0.25	3.17 ± 0.17	2.58 ± 0.12	2.10 ± 0.09	1.72 ± 0.08	1.40 ± 0.08 ◊(10)
	PMA + deltamethrin	4.75 ± 0.39	3.96 ± 0.29	3.30 ± 0.21	2.75 ± 0.15	2.30 ± 0.11	1.92 ± 0.09	1.60 ± 0.07
	4α-PMA + deltamethrin	4.38 ± 0.41	3.63 ± 0.25	3.02 ± 0.15	2.52 ± 0.09	2.10 ± 0.09	1.76 ± 0.11	1.48 ± 0.13
10 min	DMSO	4.78 ± 0.24	3.91 ± 0.17	3.20 ± 0.13	2.62 ± 0.10	2.15 ± 0.08	1.77 ± 0.07	1.46 ± 0.06
	Deltamethrin	5.42 ± 0.32	4.34 ± 0.21	3.47 ± 0.13	2.78 ± 0.08	2.23 ± 0.06	1.79 ± 0.06	1.44 ± 0.06
	PMA + deltamethrin	5.07 ± 0.53	5.19 ± 0.99 ♦ (33)	4.11 ± 0.58 ♦(28)	3.28 ± 0.3 ♦(20)	2.64 ± 0.13 ♦(23) ■(18)	2.14 ± 0.03 ♦(21) ■(20)	1.75 ± 0.07 ♦(20) ■(22)
	4α-PMA + deltamethrin	9.07 ± 2.31 ♦(90) ■(67)	5.83 ± 1.24 ♦(33)	4.26 ± 0.71 ♦(33)	3.16 ± 0.37	2.36 ± 0.16	1.79 ± 0.06 □(-16)	1.38 ± 0.09 □(-21)

An open diamond (◊) indicates significant difference from No Treatment. A closed diamond (♦) indicates significant difference from DMSO. A square (■) indicates significant difference from deltamethrin. An open square (□) indicates significant difference from PMA + deltamethrin. The values in parentheses (n) are percent increases or decreases. Significance was calculated using Student's T-test ($P<0.05$).

As expected, when deltamethrin was applied to heterologously expressed unphosphorylated wild type $Ca_V2.2$ under steady-state conditions, peak current decreased. This finding was the same as that initially reported by Symington and Clark (2005). When deltamethrin was applied to $Ca_V2.2$ that had been phosphorylated in a PMA-activated PKC-dependent manner under steady-state conditions, however, peak current significantly increased (Alves et al., 2009).

The decrease in peak $Ca_V2.2$ current observed when deltamethrin was applied to unphosphorylated $Ca_V2.2$ was inconsistent with biochemical studies which showed that dosing with deltamethrin significantly increased neurotransmitter release from rat brain synaptosomes (Symington et al., 2007b). Dosing live rats with deltamethrin also increased neurotransmitter release (Aldridge et al., 1978; Hossain et al., 2004). The increase in neurotransmitter release was, therefore, consistent with the CS-syndrome observed during deltamethrin poisoning. The decrease in peak current caused by the dosing of deltamethrin on unphosphorylated $Ca_V2.2$ under steady state conditions is inconsistent with previous reports and led us to conclude that post translational modifications, which are not readily available in the non-neuronal *Xenopus* oocyte system, but are available in the *in vivo* system, may play a role in how deltamethrin acts upon the channel.

A permanently phosphorylated channel was created by site-directed mutagenesis, which converted a threonine at site 422 (T422) to a glutamate (T422E). This permanently phosphorylated channel, when heterologously expressed in *Xenopus* oocytes and treated with deltamethrin, mimicked the effect of deltamethrin in the live rat *in vivo* system, and

Table 11. The effects of DMSO, deltamethrin, PMA+ deltamethrin and 4α-PMA + deltamethrin on the slopes and intercepts of $Ca_V2.2$ voltage dependent activation and deactivation taus.

		$\tau_{actvation}$		$\tau_{deactvation}$	
	Treatment (10^{-7} M)	slope (mV^{-1} ± SEM)	y-intercept	slope (mV^{-1} ± SEM)	y-intercept
4 min	DMSO	-0.022 ± 0.001	0.944 ± 0.012 ◊(6)	0.011 ± 0.002	1.359 ± 0.109
	Deltamethrin	-0.023 ± 0.002	0.905 ± 0.046	0.015 ± 0.002	1.630 ± 0.115
	PMA + deltamethrin	-0.019 ± 0.001 ♦(14)	0.995 ± 0.026	0.010 ± 0.002 ●(-50)	1.381 ± 0.103 ●(-31)
	4α-PMA + deltamethrin	-0.020 ± 0.001	0.794 ± 0.0180 ♦(-16)	0.008 ± 0.003	0.844 ± 0.180 ♦(-38) ■(-48)
10 min	DMSO	-0.020 ± 0.001	0.951 ± 0.013 ◊(7)	0.012 ± 0.002	1.399 ± 0.106
	Deltamethrin	-0.026 ± 0.002 ♦(30)	0.987 ± 0.054	0.015 ± 0.002	1.630 ± 0.105
	PMA + deltamethrin	-0.021 ± 0.001 ■(19)	1.168 ± 0.022 ♦(23) ■(18)	0.016 ± 0.002 ●(-30)	1.770 ± 0.112 ●(-24)
	4α-PMA + deltamethrin	-0.013 ± 0.001 ♦(-35) ■(-50)	0.763 ± 0.021 ♦(-20) ■(-23)	0.007 ± 0.004	0.784 ± 0.217 ♦(-44) ■(-52)

An open diamond (◊) indicates significant difference from No Treatment. A closed diamond (♦) indicates significant

difference from DMSO. A square (■) indicates significant difference from deltamethrin. A circle (●) indicates significant difference from PMA. The values in parentheses (n) are percent increases or decreases. Significance was calculated using Student's T-test ($P<0.05$).

in intact synaptosomes by significantly increasing Ba^{2+}(Ca^{2+}), current (Symington et al., 2007a). To observe the effects of deltamethrin on wild type $Ca_V2.2$ under phosphorylating conditions, PMA was used to induce endogenous PKC activity in the *Xenopus* heterologous expression system with the expectation that PKC phosphorylation activity would not be selective. Under steady-state depolarization, PMA + deltamethrin treatment significantly increased Ba^{2+} current compared to DMSO and deltamethrin treatments at both 4 and 10 min post treatment. The increase in peak current via PMA-activated PKC-dependent phosphorylated $Ca_V2.2$ in the presence of deltamethrin supports the hypothesis that phosphorylation enhances the action of deltamethrin on $Ca_V2.2$.

4.2.2 Steady-state Gating Kinetics

Deltamethrin treatment produced no significant effect on steady-state activation of $Ca_V2.2$, but PMA + deltamethrin significantly increased activation taus at 10 min post treatment compared to DMSO and deltamethrin alone. The increase in steady-state activation taus indicates that phosphorylated $Ca_V2.2$, when treated with deltamethrin, is slow to activate completely causing a reduction in Ba^{2+} influx. This delay in activation is consistent with a study by Symington and Clark (2005), in which steady-state activation taus of $Ca_V2.2$ were significantly increased in the presence of deltamethrin. As expected, the treatment of 4α-PMA + deltamethrin resulted in no effect on steady-state activation.

The reduction in Ba^{2+} (or Ca^{2+}) influx due to the slowing of steady-state activation of phosphorylated $Ca_V2.2$ activation in the presence of deltamethrin is not consistent with increased neurotransmitter release. When applied to synaptosomes, deltamethrin caused

Table 12. The effects of DMSO, deltamethrin, PMA + deltamethrin and 4α-PMA + deltamethrin on voltage-dependent deactivation ($\tau_{deactivation}$).

		Test Potential (mV)					
		-80	-70	-60	-50	-40	-30
	Treatment (10^{-7}M)	$tau_{deactivation}$ (ms)					
	No Treatment	1.53 ± 0.16	1.66 ± 0.13	1.82 ± 0.10	2.02 ± 0.08	2.26 ± 0.08	2.56 ± 0.11
4 min	DMSO	1.81 ± 0.21	1.94 ± 0.19	2.10 ± 0.17	2.30 ± 0.16	2.55 ± 0.15	2.85 ± 0.17
	Deltamethrin	1.55 ± 0.12	1.8 ± 0.14	2.09 ± 0.16	2.43 ± 0.19	2.83 ± 0.22	3.29 ± 0.26 ♦(15)
	PMA + deltamethrin	1.82 ± 0.17	1.99 ± 0.14	2.19 ± 0.10	2.42 ± 0.09	2.68 ± 0.14	2.98 ± 0.23
	4α-PMA + deltamethrin	0.98 ± 0.05	1.11 ± 0.05	1.27 ± 0.06 ♦(-40)	1.57 ± 0.15 ♦(-32)	1.67 ± 0.09 ♦(-35)	1.80 ± 0.14 ♦(-36)
10 min	DMSO	1.86 ± 0.23	2.03 ± 0.21	2.23 ± 0.20	2.46 ± 0.19 ◊(22)	2.74 ± 0.19 ◊(21)	3.07 ± 0.19 ◊(20)
	Deltamethrin	1.52 ± 0.08	1.77 ± 0.1	2.06 ± 0.13	2.41 ± 0.17	2.81 ± 0.22	3.28 ± 0.28
	PMA + deltamethrin	1.62 ± 0.17	1.89 ± 0.15	2.22 ± 0.14	2.61 ± 0.15	3.08 ± 0.21	3.65 ± 0.33
	4α-PMA + deltamethrin	0.98 ± 0.05	1.11 ± 0.05	1.28 ± 0.06 ♦(-43)	1.57 ± 0.15 ♦(-36)	1.67 ± 0.09 ♦(-39)	1.80 ± 0.14 ♦(-41)

An open diamond (◊) indicates significant difference from No Treatment. A closed diamond (♦) indicates significant difference from DMSO. The values in parentheses (n) are percent increases or decreases. Significance was calculated using Student's T-test ($P<0.05$).

an increase in neurotransmitter release and this cannot be achieved if neurotransmitter release is dependent on channel activation alone. Thus, we can conclude that steady-state activation is not the process by which deltamethrin alters $Ca_V2.2$ conductivity to increase Ca^{2+}-dependent neurotransmitter release.

Although not statistically significant, the rate of inactivation of unphosphorylated $Ca_V2.2$ was slowed in the presence of deltamethrin (Table 6). This slowing of inactivation is consistent with a previous report in which deltamethrin significantly slowing down the rate of unphosphorylated $Ca_V2.2$ steady-state inactivation (Symington and Clark, 2005). PKC-phosphorylated $Ca_V2.2$ inactivates faster in the presence of deltamethrin when compared to the inactivation of unphosphorylated $Ca_V2.2$ in the presence of DMSO or deltamethrin. This reduction in steady-state inactivation taus indicates that phosphorylated $Ca_V2.2$ in the presence of deltamethrin takes less time to inactivate than its unphosphorylated form and reduces Ba^{2+} influx. Because Ba^{2+} influx via $Ca_V2.2$ under phosphorylating conditions was increased, we expected a slowing of inactivation may have occurred. However, we observed a slowing of inactivation in the presence of deltamethrin only when $Ca_V2.2$ was not undergoing PMA-activated PKC phosphorylation. When $Ca_V2.2$ is phosphorylated, we observed that deltamethrin significantly increased the rate at which the channel inactivated under steady-state depolarization. This finding is not consistent with increased Ca^{2+} influx necessary for increased neurotransmitter release. We can conclude from this data that, like steady-state activation, steady-state inactivation is not a process by which deltamethrin alters $Ca_V2.2$ conductance to increase Ca^{2+}-dependent neurotransmitter release.

Steady-state deactivation in the presence of PMA + deltamethrin was significantly

increased at both 4 and 10 min post treatments. An increase in deactivation taus indicates a slower rate of open channels going to the closed state after the removal of steady-state membrane depolarization signal (voltage change). This slower rate of closure means that more Ba^{2+} is able to enter the cell via $Ca_V2.2$. Within the *in vivo* system, this increase in Ba^{2+} (or Ca^{2+}) influx results in the increased release of neurotransmitters. Furthermore, the increase in neurotransmitter release is consistent with the symptoms observed in CS-syndrome as a result of deltamethrin poisoning (Hossain et al., 2004).

4α-PMA was used to test how deltamethrin would affect channel kinetics in the presence of a phorbol ester that does not activate PKC-phosphorylation. When deltamethrin was applied to 4α-PMA-treated $Ca_V2.2$, deactivation taus were reduced. This reduction in deactivation taus means that 4α-PMA-treated $Ca_V2.2$ deactivates faster than untreated $Ca_V2.2$ in the presence of deltamethrin. From this, we can conclude that deltamethrin alters $Ca_V2.2$ deactivation kinetics under phosphorylating conditions and that this change in deactivation gating kinetics increases Ba^{2+} influx. From this, we can infer that the addition of deltamethrin to the *in vivo* system would result in increased Ca^{2+}-depedent neurotransmitter release that is consistent with CS-syndrome.

The increase in transient peak current and the slowing of deactivation rates of phosphorylated $Ca_V2.2$, in the presence of deltamethrin, allow for increased Ba^{2+} influx via phosphorylated $Ca_V2.2$. Within the *in vivo* system, the increase in Ba^{2+} (or Ca^{2+}) influx would translate into to increased neurotransmitter release, an effect observed during deltamethrin poisoning.

4.2.3 Voltage-dependent peak current

Deltamethrin treatment produced a significant decrease in maximal voltage-dependent peak current at 10 min post treatment, which agrees with our steady-state data and previously reported results that deltamethrin reduces steady state and voltage-dependent peak current (Symington and Clark, 2005). The decrease in peak current indicates that less Ba^{2+} is entering the cell via $Ca_V2.2$, which would translate into a decrease in Ca^{2+} influx and a decrease in neurotransmitter release in the *in vivo* neuron.

We expected that the increase in peak current caused by PMA treatment would be augmented by the presence of deltamethrin due to the observation that deltamethrin increases neurotransmitter release from the *in vivo* neuron. We observed a significant increase in voltage-dependent peak current of phosphorylated $Ca_V2.2$ in the presence of deltamethrin. Within the *in vivo* neuron, this increase in peak current of phosphorylated $Ca_V2.2$ in the presence of deltamethrin would mean that a significantly greater amount of Ca^{2+} was flowing through the channel causing a significant increase in neurotransmitter release.

In the presence of deltamethrin, the $Ca_V2.2$ mutant T422E underwent an increase in maximal voltage-dependent peak current, which mimicked the effect of deltamethrin *in vivo* (Symington et al., 2007a). We observed a similar increase in voltage-dependent peak current of phosphorylated $Ca_V2.2$ in the presence of deltamethrin but the actual phosphorylation pattern of $Ca_V2.2$ resulting from PMA-activated PKC phosphorylation under experimental conditions is unknown. Using site-directed mutagenesis it was determined that Ser425 is inhibitory when phosphorylated while the other four PKC-dependent phosphorylation sites enhance Ba^{2+} influx (Fang et al., 2006). Our experiments

do not control for which phosphorylation sites on $Ca_V2.2$ are phosphorylated and which ones are not. Therefore using site-directed mutagenesis , we can "phosphorylate" the channel at single or multiple sites by replacing the wild type amino acid with glutamate and determine under which phosphorylation patterns we observe an increase in Ba^{2+} (Ca^{2+}) influx in the presence of deltamethrin.

Maximal peak current in the presence of 4α-PMA + deltamethrin decreased at both 4 and 10 min post treatment compared to No Treatment, 4α-PMA and PMA + deltamethrin. This reduction in peak current means that Ba^{2+} influx through unphosphorylated $Ca_V2.2$ in the presence is reduced. There was no significant difference between $Ca_V2.2$ peak current in the presence of deltamethrin and $Ca_V2.2$ peak current in the presence of 4α-PMA + deltamethrin indicating that the presence of the inactive phorbol ester does not change the action of deltamethrin on the channel.

We propose that the difference between the effect of PMA + deltamethrin on steady-state peak current versus voltage-dependent peak current may be due the multiple step depolarizations that occur during the Activation Test Protocol used to obtain voltage-dependent peak current versus the single step depolarization of the Transient Test Protocol. As $Ca_V2.2$ undergoes multiple step depolarizations, the channels that are opening at lower potentials are inactivating and remain in their unwilling state during subsequent depolarization steps. The inactivation of these channels may be a mechanism by which the maximal effect of deltamethrin on phosphorylated $Ca_V2.2$ during voltage-dependent protocols was not observed.

4.2.4 Voltage-dependent Gating Kinetics

Activation midpoint potentials (V_{50act}) obtained in our study are consistent with previous findings of enhanced neurotransmitter release. The V_{50act} of unphosphorylated $Ca_V2.2$ in the presence of deltamethrin underwent a hyperpolarizing shift at both 4 and 10 min post treatments. Phosphorylated $Ca_V2.2$ treated with deltamethrin had a significantly greater hyperpolarizing shift in V_{50act} compared to the V_{50act} of the untreated phosphorylated channels, indicating that the activation of phosphorylated $Ca_V2.2$ occurred at lower levels of depolarization. The increased sensitivity of deltamethrin-treated PKC-phosphorylated $Ca_V2.2$ to smaller levels of membrane depolarizations is consistent with increased Ba^{2+} influx within our heterologous expression system, and enhanced neurotransmitter release within the *in vivo* system. In the presence of 4α-PMA + deltamethrin, the V_{50act} underwent a depolarizing shift making the channel less likely to activate when the membrane undergoes depolarization consistent with less Ba^{2+} (or Ca^{2+}) influx and less neurotransmitter release.

Deltamethrin treatment had no significant effect on inactivation midpoint potentials ($V_{50inact}$) of unphosphorylated $Ca_V2.2$. In the presence of PMA+ deltamethrin, $V_{50inact}$ underwent a significant hyperpolarizing shift compared to the effects of DMSO and deltamethrin treatments. This hyperpolarizing shift indicates that $Ca_V2.2$ will inactivate at lower levels of depolarization thereby reducing the amount of Ba^{2+} influx. The reduction of Ba^{2+} (or Ca^{2+}) influx would translate into reduced neurotransmitter release within the *in vivo* system. With the increase in neurotransmitter release observed by Symington et al. (2007a), we expected to observe a depolarizing shift in $V_{50inact}$, which would indicate that $Ca_V2.2$ would require greater levels of depolarizations to inactivate.

Instead, a significant hyperpolarizing shift similar to what we observed in the presence of PMA was observed when phosphorylated $Ca_V2.2$ was treated with deltamethrin caused.

Deltamethrin also had no effect on voltage-dependent activation rate constants of unphosphorylated $Ca_V2.2$ ($\tau_{activation}$) following either the 4 or 10 min post treatments. The increase in $\tau_{activation}$ at 10 min post treatment in the presence of PMA + deltamethrin significantly increased at step potentials between -20 mV and 30 mV compared to DMSO and indicates that phosphorylated $Ca_V2.2$ took more time to activate in the presence of deltamethrin than the unphosphorylated channel. Also, the presence of deltamethrin on the phosphorylated channel caused an increase in the length of time required to activate the channel compared to the effect of deltamethrin on the unphosphorylated channel between 10 mV and 30 mV. The increase in $\tau_{activation}$ of phosphorylated $Ca_V2.2$ corresponds with the increase of activation tau under steady-state deactivation but in both cases, the increases in the time it takes for $Ca_V2.2$ to activate is not consistent with increase Ba^{2+} influx. Thus, we would not expect an increase in activation taus to increase Ca^{2+} influx and subsequent neurotransmitter release within the *in vivo* system. This result is not consistent with increased Ca^{2+} via $Ca_V2.2$ resulting in increased neurotransmitter release.

The effect of deltamethrin on 4α-PMA-treated $Ca_V2.2$ was a significant increase in $\tau_{activation}$ constants at -30 mV, -20 mV and -10 mV at 10 min post treatment. At -30 mV the $\tau_{activation}$ rate constant was nearly two times greater than the $\tau_{activation}$ rate constant of DMSO. Under steady-state depolarization, activation taus remain unchanged in the presence of 4α-PMA + deltamethrin , so the rate increase we observed under voltage-dependent activation was unexpected and contradictory to what we observed under

steady-state conditions especially considering previous reports of 4α-PMA being a non-active form of PMA (Castagna et al., 1982; García-Ferreiro et al., 2001). The rate increase would indicate, within the *in vivo* system, that $Ca_V2.2$ would take longer to activate and that the amount of neurotransmitter that would eventually be released as a result of Ca^{2+} influx once the channel opened would be reduced.

Under steady-state conditions, we observed that deltamethrin had no significant effect on the deactivation tau of unphosphorylated $Ca_V2.2$. We observed, likewise, that deltamethrin had almost no effect on voltage-dependent $\tau_{deactivation}$, in the absence of PMA the exception being an increase in the length of time required for the channel to close at -30 mV at 4 min post treatment. This means that within the *in vivo* system, the membrane would have to undergo a large depolarization in the presence of deltamethrin in order for there to be increased Ca^{2+} influx via unphosphorylated $Ca_V2.2$ followed by increased neurotransmitter release.

The presence of deltamethrin on phosphorylated $Ca_V2.2$ under steady-state conditions increased deactivation tau allowing for an increase in Ba^{2+} influx. There was no such increase, however, in voltage-dependent $\tau_{deactivation}$ rate constants. This means that in the presence of deltamethrin the amount of Ba^{2+} entering the cell via phosphorylated $Ca_V2.2$ does not significantly differ from Ba^{2+} influx of our No Treatment. We propose that the difference between the effect of PMA + deltamethrin on steady-state deactivation taus versus voltage-dependent $\tau_{deactivation}$ may be due the multiple step depolarizations undergone that occur the Activation Test Protocol used to obtain $\tau_{deactivation}$ versus the single step depolarization of the Transient Test Protocol. As $Ca_V2.2$ undergoes multiple step depolarizations, the channels that are opening at lower potentials

are inactivating and remain in their unwilling state during subsequent depolarization steps. The inactivation of these channels may be a mechanism by which the maximal effect of deltamethrin on phosphorylated $Ca_V2.2$ during voltage-dependent protocols was not observed

The presence of 4α-PMA + deltamethrin had no significant effect on steady-state deactivation taus at either 4 or 10 min post treatment, but caused significant decreases in $\tau_{deactivation}$ rate constants at both time points compared to the DMSO control at depolarization steps ranging from -60 mV to -30 mV. These decreases mean that the presence of deltamethrin on a 4α-PMA-treated channel causes the channel to close an average of 40% faster than it would in the presence of DMSO at step depolarizations at or above -60 mV, and these faster rates reduce the amount of Ba^{2+} entering the via $Ca_V2.2$. This faster rate of closure would translate as less Ca^{2+} uptake and less neurotransmitter released, which does not cause the effects we observe in CS-syndrome. These results differ from the steady-state data in that, under steady-state conditions, the presence of 4α-PMA + deltamethrin had no significant effect on steady-state deactivation gating kinetics.

CHAPTER 5

SUMMARY AND FUTURE DIRECTIONS

Consistent with a previous study by Symington *et al.* (2005), we observed a significant decrease in steady-state peak current when unphosphorylated $Ca_V2.2$ was treated with deltamethrin. The decrease in steady-state peak current itself is inconsistent with *in vivo* data, in which deltamethrin increased $Ca_V2.2$ currents and subsequent neurotransmitter release (Table 13). We also observed a decrease in voltage-dependent peak current of unphosphorylated $Ca_V2.2$ in the presence of deltamethrin. Although this is consistent with work by Symington *et al.* (2005), it is not consistent with *in vivo* data in which the presence of deltamethrin causes an increase in Ca^{2+} influx and subsequent neurotransmitter release. When deltamethrin is added to PMA-activated, PKC-dependent phosphorylated $Ca_V2.2$, steady-state and voltage-dependent peak current is significantly increased, which is consistent with the *in vivo* data. Additionally, we observed an increase in steady-state deactivation taus which is consistent with increased Ca^{2+} influx and neurotransmitter release. Also, consistent with enhanced neurotransmitter release, voltage-dependent activation midpoint potentials (V_{50act}) of phosphorylated $Ca_V2.2$ in the presence of deltamethrin underwent a hyperpolarizing shift. We have been able to confirm previous reports which show that deltamethrin causes an increase in both steady-state and voltage-dependent peak current of phosphorylated $Ca_V2.2$, but we have also reported novel changes in the kinetic profile of $Ca_V2.2$ (increased deactivation taus and hyperpolarizing shift in the V_{50act}) under the same conditions which support enhanced Ca^{2+} influx and subsequent neurotransmitter release.

Table 13. Summary of transient and voltage-dependent data endpoints of both unphosphorylated and phosphorylated $Ca_V2.2$ modified by deltamethrin.

			Unphosphorylated + ΔM		Phosphorylated + ΔM	
			Endpoint	Consistent w/ Neurotransmitter Release?	Endpoint	Consistent w/ Neurotransmitter Release?
4 min	Transient	Peak Current	87.4 ± 5.1 ♦(-18)	No	180.6 ± 15.3 ♦(69) ■(107)	Yes
		Activation tau	100.9 ± 4.2	No	101.3 ± 3.8	No
		Inactivation tau	123.8 ± 10.7	No	58.8 ± 6.5 ♦(-53) ■(-52)	No
		Deactivation tau	125.6 ± 13.9	No	186.5 ± 42.5 ♦*(79)	Yes
	Voltage-dependent	Peak Current	-1.00 ± 0.04	No	-1.46 ± 0.19 ◊(47) ♦(70) ■*(46)	Yes
		V_{50act}	-1.83 ± 0.35	No	-2.09 ± 0.29 ●(-56)	Yes
		$V_{50inact}$	-25.73 ± 2.47	No	-44.07 ± 3.45 ♦(-28) ■(-71)	No
10 min	Transient	Peak Current	72.6 ± 15.8 ♦(-29)	No	185.8 ± 5.6 ♦(82) ■(156)	Yes
		Activation tau	107.7 ± 4.3	No	123.6 ± 6.1 ♦(14) ■(15)	No
		Inactivation tau	243.7 ± 40.8	No	92.8 ± 12.5 ■(-62)	No
		Deactivation tau	129.6 ± 15.3	No	160.3 ± 17.2 ♦*(54)	Yes
	Voltage-dependent	Peak Current	-0.87 ± 0.05 ◊(-12%)	No	-1.08 ± 0.17 ♦(21%)	No
		V_{50act}	-3.44 ± 0.69	No	-3.04 ± 0.61 ●(-117)	Yes
		$V_{50inact}$	-21.21 ± 2.16	No	-44.69 ± 1.56 ♦(-63) ■(-111)	No

An open diamond (◊) indicates significant difference from No Treatment. A closed diamond (♦) indicates significant difference from DMSO. A square (■) indicates significant difference from deltamethrin. A circle (●) indicates significant difference from PMA. The values in parentheses (n) are percent increases or decreases. Significance was calculated using Student's T-test ($P<0.05$). Symbols followed by an asterisk (*) indicate that the significance level was $P < 0.1$.

Symington *et al.* (2005) reported a significant increase in steady-state inactivation taus of deltamethrin-treated unphosphorylated $Ca_V2.2$ expressed in *Xenopus* oocytes consistent with enhanced neurotransmitter release. PMA-activated PKC-dependent phosphorylation of $Ca_V2.2$ enhanced steady-state peak current, activation and deactivation taus but reduced steady-state inactivation taus (Table 13). We observed an increase in steady-state inactivation tau but the change was not significant. Likewise, when deltamethrin is added to the phosphorylated channel, inactivation tau is similarly decreased in a manner that is inconsistent with *in vivo* that data showed deltamethrin, enhances Ca^{2+} influx and neurotransmitter release. In the presence of deltamethrin, the V_{50act} of T422E underwent a depolarizing shift that was not consistent with our data showing a hyperpolarizing shift in V_{50act} of phosphorylated wild type $Ca_V2.2$ in the presence of deltamethrin (Symington *et al.*, 2007a). This difference between the T422E mutant and our wild type $Ca_V2.2$ data indicates that the other phosphorylation sites on $Ca_V2.2$ may contribute to Ca^{2+} influx in a way other than peak current. $V_{50inact}$ of phosphorylated $Ca_V2.2$ in the presence of deltamethrin also underwent a hyperpolarizing shift that was not consistent with increased Ba^{2+} (or Ca^{2+}) influx and subsequent neurotransmitter release. Increases in $\tau_{activation}$ or $\tau_{deactivation}$ would have been consistent with enhanced neurotransmitter release, however, other than a significant increase in $\tau_{deactivation}$ at 10 min post treatment and 30 mV, we did not observe any large changes compared to the control (Table 14). It has been shown (Fang *et al*., 2006) that $Ca_V2.2$ has five PKC-dependent phosphorylation sites of which, when phosphorylated, four are agonistic to channel function (Thr422, Ser1757, Ser2108 and Ser2132) while the other (Ser425) is antagonistic to channel function. Clearly, the current data supports the

Table 14. Summary of voltage-dependent $\tau_{activation}$ and $\tau_{deactivation}$ data endpoints of both unphosphorylated and phosphorylated $Ca_V2.2$modified by deltamethrin.

			Unphosphorylated + ΔM		Phosphorylated + ΔM	
		Voltage (mV)	Endpoint	Consistent w/ Neurotransmitter Release?	Endpoint	Consistent w/ Neurotransmitter Release?
4 min	$\tau_{activation}$	-30	4.80 ± 0.36	No	4.75 ± 0.39	No
		-20	3.90 ± 0.25	No	3.96 ± 0.29	No
		-10	3.17 ± 0.17	No	3.30 ± 0.21	No
		0	2.58 ± 0.12	No	2.75 ± 0.15	No
		10	2.10 ± 0.09	No	2.30 ± 0.11	No
		20	1.72 ± 0.08	No	1.92 ± 0.09	No
		30	1.40 ± 0.08 ◊(10)		1.60 ± 0.07	No
	$\tau_{deactivation}$	-80	1.55 ± 0.12	No	1.82 ± 0.17	No
		-70	1.8 ± 0.14	No	1.99 ± 0.14	No
		-60	2.09 ± 0.16	No	2.19 ± 0.10	No
		-50	2.43 ± 0.19	No	2.42 ± 0.09	No
		-40	2.83 ± 0.22	No	2.68 ± 0.14	No
		-30	3.29 ± 0.26 ♦(15)	Yes	2.98 ± 0.23	No
10 min	$\tau_{activation}$	-30	5.42 ± 0.32	No	5.07 ± 0.53	No
		-20	4.34 ± 0.21	No	5.19 ± 0.99 ♦(33)	No
		-10	3.47 ± 0.13	No	4.11 ± 0.58 ♦(28)	No
		0	2.78 ± 0.08	No	3.28 ± 0.3 ♦(20)	No
		10	2.23 ± 0.06	No	2.64 ± 0.13 ♦(23) ■(18)	No
		20	1.79 ± 0.06	No	2.14 ± 0.03 ♦(21) ■(20)	No
		30	1.44 ± 0.06	No	1.75 ± 0.07 ♦(20) ■(22)	No
	$\tau_{deactivation}$	-80	1.52 ± 0.08	No	1.62 ± 0.17	No
		-70	1.77 ± 0.1	No	1.89 ± 0.15	No
		-60	2.06 ± 0.13	No	2.22 ± 0.14	No
		-50	2.41 ± 0.17	No	2.61 ± 0.15	No
		-40	2.81 ± 0.22	No	3.08 ± 0.21	No
		-30	3.28 ± 0.28	No	3.65 ± 0.33	No

An open diamond (◊) indicates significant difference from No Treatment. A closed diamond (♦) indicates significant difference from DMSO. A square (■) indicates significant difference from deltamethrin. The values in parentheses (n) are percent increases or decreases. Significance was calculated using Student's T-test ($P<0.05$).

contention that T422 is not independent of the other phosphorylation sites.

The largest effect we observed on the unphosphorylated channel in the presence of deltamethrin was the decrease in both steady-state and voltage-dependent peak current. Since these results were in contrast to the effect of deltamethrin *in vivo*, they made clear the possibility that post-translational modification occurring on $Ca_V2.2$ within the *in vivo* system was either not present or not activated within the heterologous *Xenopus* oocyte expression system. When deltamethrin was applied to phosphorylated $Ca_V2.2$ expressed in *Xenopus* oocytes, we observed a reversal of deltamethrin inhibition of steady-state and voltage-dependent peak current. The largest of these changes was the enhancement of steady-state peak current, which remained significantly greater than did the DMSO or the deltamethrin treatments at 4 and 10 min post treatment, and was unlike voltage-dependent peak current which decreased over 10 min. The decrease in voltage-dependent peak current could be due to those channels sensitive to low levels of membrane depolarizations opening at those lower levels and being in the process of inactivating as the membrane undergoes increasing levels of step depolarization. We were able to replicate the steady-state peak current results of Symington *et al.* (2005) and Stea et al (1995) in regards to the action of deltamethrin and phosphorylation on $Ca_V2.2$ respectively. When treating PKC-phosphorylated $Ca_V2.2$ with deltamethrin, we also observed similar increases in voltage-dependent peak current compared to the T422E experiments by Symington et al. (2007a) but we also obtained results that had yet to be described.

We observed a novel increase in steady-state deactivation tau and a hyperpolarizing shift in V_{50act} of PKC-phosphorylated $Ca_V2.2$ in the presence of

deltamethrin that was not evident when the T422E mutant (Symington *et al*., 2007a) was treated with deltamethrin. The slowing of deactivation occurred when phosphorylated $Ca_V2.2$ was treated with deltamethrin and this effect remained significant over 10 min. This effect was not observed by Symington *et al.* (2007a) because unlike their T422E mutant, our use of PMA-activated PKC-dependent phosphorylation had the potential to phosphorylate some or all the PKC sites on $Ca_V2.2$, with one or more of them having the potential to prolong steady-state deactivation tau. Lastly, we observed a significant shift in V_{50act} of phosphorylated $Ca_V2.2$ in the presence of deltamethrin. This could mean that at least one of the PKC phosphorylation sites on $Ca_V2.2$ is responsible for making the channel more sensitive to membrane depolarization. Again, these novel results indicate that the simultaneous phosphorylation of multiple PKC-dependent phosphorylation sites creates $Ca_V2.2$ phosphoforms that yield unique kinetic profiles.

Isoflurane, a volatile anesthetic, inhibits $Ca_V2.2$ steady-state and voltage-dependent peak currents (Rajagopal *et al.*, 2011) in much the same way deltamethrin decreased steady-state and voltage-dependent peak current. Using Ser/Thr→Ala site-directed mutagenesis, Rajagopal *et al*. (2011) created constructs that eliminated either the stimulatory PKC-dependent phosphorylation site (Thr422, Ser1757, Ser2108 and S2132) or the inhibitory PKC phosphorylation sites (Ser425) to determine the effect of isofluorane currents. In the presence of isoflurane, modified $Ca_V2.2$ currents in which the stimulatory sites were eliminated and Ser425 was left unchanged, were significantly decreased compared to the wild type channel. A similar experiment using deltamethrin may yield a similar result since isoflurane and deltamethrin have similar effects on the wild type channel. Conversely, the elimination of only the inhibitory site Ser425 reversed

the isoflurane inhibition of $Ca_V2.2$ currents and again, treating the same mutant construct with deltamethrin may yield a similar response since the two compounds have similar effects on the wild type channel. The next steps to take to determine the extent to which the $Ca_V2.2$ stimulatory sites and the inhibitory site play a role in enhancement or inhibition of $Ca_V2.2$ currents via would be to use several mutant constructs of the $Ca_V2.2$ to determine what effects the different phosphorylation states have on $Ca_V2.2$ currents when exposed to deltamethrin. Fang *et al.* (2006) used several mutant constructs to observe the effects of phosphorylation on $Ca_V2.2$. They observed wildly varying responses to peak current when different PKC-dependent phosphorylation sites were made "permanently phosphorylated" while others were left "permanently unphosphorylated". Two of the major observations Fang *et al.* (2006) made was that residue Thr422 significantly increase peak current and residue Ser425 significantly reduced peak current. The other three PKC phosphorylation sites were also stimulatory but their effects were not nearly as significant as that of Thr422. In our experiments we observed an enhancement of wild type $Ca_V2.2$ currents in the presence of deltamethrin beyond the enhancement of peak current. Clearly phosphorylation of Thr422 is important in enhancing $Ca_V2.2$ currents, but if it were the only important site, we would not have observed changes in steady-state deactivation tau or V_{50act} which both contribute to enhanced Ca^{2+} influx and subsequent neurotransmitter release. In order to determine what role each of the PKC phosphorylation sites play in kinetic profile of $Ca_V2.2$ in the presence of deltamethrin we will have to implement an exhaustive site-directed mutagenesis study similar to the one performed by Fang *et al.* (2006).

APPENDIX

COMPOUNDS USED IN THIS STUDY

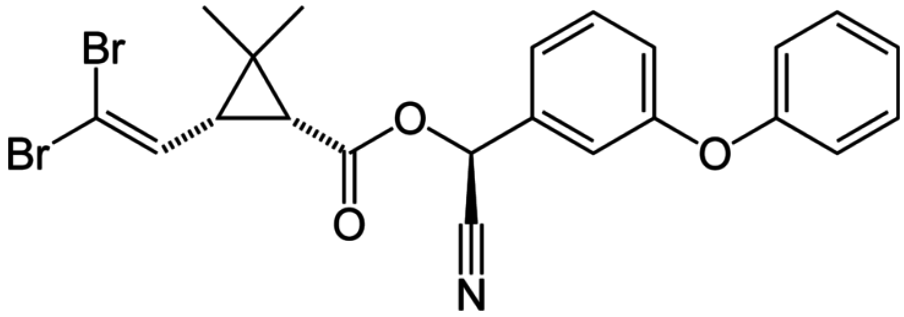

Deltmethrin

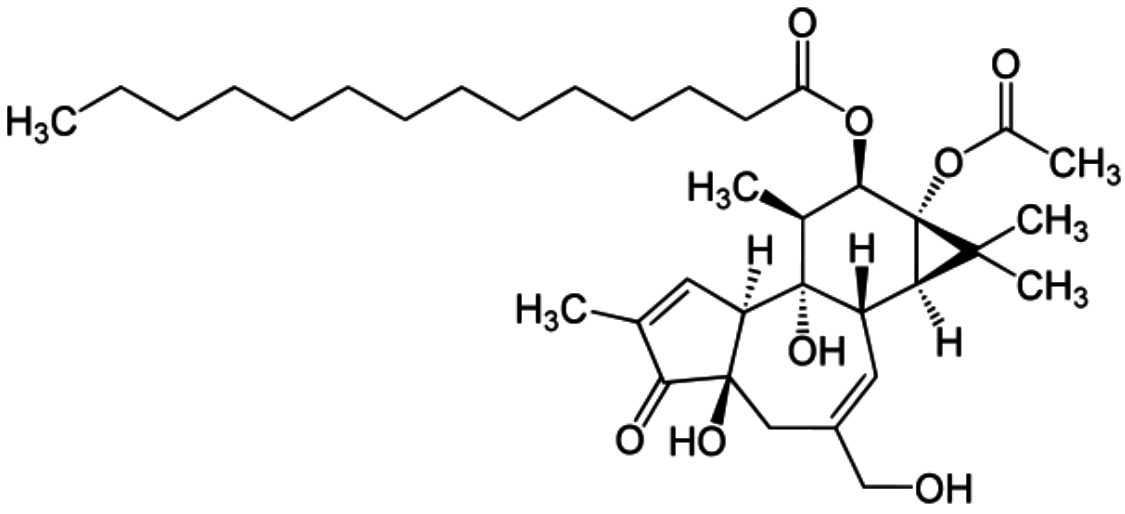

phorbol 12-myristate 13-acetate (PMA)

REFERENCES

Akopian, A.N., L. Sivilotti, and J.N. Wood. 1996. A tetrodotoxin-resistant voltage-gated sodium channel expressed by sensory neurons. *Nature*. 379:257-262.

Aldridge, W.N., B. Clothier, P. Forshaw, M.K. Johnson, V.H. Parker, R.J. Price, D.N. Skilleter, R.D. Verschoyle, and C. Stevens. 1978. The effect of DDT and the pyrethroids cismethrin and decamethrin on the acetyl choline and cyclic nucleotide content of rat brain. *Biochemical Pharmacology*. 27:1703-1706.

Alves, A.-M., S.B. Symington, S.H. Lee, and J.M. Clark. 2010. PKC-dependent phosphorylations modify the action of deltamethrin on rat brain N-type ($Ca_V2.2$) voltage-sensitive calcium channel. *Pesticide Biochemistry and Physiology*. 97: 101-108.

Armstrong, C.M. 1981. Sodium channels and gating currents. *Physiol Rev*. 61:644-683.

Augustine, G.J., M.P. Charlton, and S.J. Smith. 1987. Calcium action in synaptic transmitter release. *Annu Rev Neurosci*. 10:633-693.

Barrett, C.F., and A.R. Rittenhouse. 2000. Modulation of N-type calcium channel activity by G-proteins and protein kinase C. *J Gen Physiol*. 115:277-286.

Bourinet, E., F. Fournier, J. Nargeot, and P. Charnet. 1992. Endogenous *Xenopus*-oocyte Ca-channels are regulated by protein kinases A and C. *Federation of European Biochemical Societies*. 299:5-9.

Breckenridge, C.B., L. Holden, N. Sturgess, M. Weiner, L. Sheets, D. Sargent, D.M. Soderlund, J.-S. Choi, S. Symington, J.M. Clark, S. Burr, and D. Ray. 2009. Evidence for a separate mechanism of toxicity for the Type I and the Type II pyrethroid insecticides. *NeuroToxicology*. 30:S17-S31.

Brooks, M.W., and J.M. Clark. 1987. Enhancement of norepinephrine release from rat brain synaptosomes by alpha cyano pyrethroids. *Pesticide Biochemistry and Physiology*. 28:127-139.

Castagna, M., Y. Takai, K. Kaibuchi, K Sano, U. Kikkawa, and Y. Nishizuka.1982. Direct activation of calcium-activated, phospholipid-dependent protein kinase by tumor-promoting phorbol esters. *The Journal of Biological Chemistry*. 257:7847-7851.

Catterall, W. 1997. Modulation of sodium and calcium channels by protein phosphorylation and G proteins. *Adv Second Messenger Phosphoprotein Res*. 31:159-181.

Catterall, W. 2000a. Structure and regulation of voltage-gated Ca2+ channels. *Annu Rev Cell Dev Biol*. 16:521-555.

Catterall, W.A. 2000b. From ionic currents to molecular mechanisms: the structure and function of voltage-gated sodium channels. *Neuron*. 26:13-25.

Catterall, W.A., J. Striessnig, T.P. Snutch, and E. Perez-Reyes. 2003. International Union of Pharmacology. XL. Compendium of Voltage-Gated Ion Channels: Calcium Channels. *Pharmacological Reviews*. 55:579-581.

Choi, J.-S., and D.M. Soderlund. 2006. Structure-activity relationships for the action of 11 pyrethroid insecticides on rat $Na_V1.8$ sodium channels expressed in Xenopus oocytes. *Toxicology and Applied Pharmacology*. 211:233-244.

Clark, J., and M. Brooks. 1989. Role of ion channels and intraterminal calcium homeostasis in the action of deltamethrin at presynaptic nerve terminals. *Biochem Pharmacol*. 38:2233-2245.

Clark, J.M., S.J. Edman, S.R. Nagy, A. Canhoto, F. Hecht, and J. Van Houten. 1995. Action of DDT and Pyrethroids on Calcium Channels in *Paramecium tetraurelia*. J.M. Clark, editor. American Chemical Society. 591:173-190.

Cooper, C.B., M.I. Arnot, Z.P. Feng, S.E. Jarvis, J. Hamid, and G.W. Zamponi. 2000. Cross-talk between G-protein and protein kinase C modulation of N-type calcium channels is dependent on the G-protein beta subunit isoform. *J Biol Chem*. 275:40777-40781.

Corbalán-García, S., and J.C. Gómez-Fernández. 2006. Protein kinase C regulatory domains: the art of decoding many different signals in membranes. *Biochim Biophys Acta*. 1761:633-654.

Doering, C.J., A.E. Kisilevsky, Z.P. Feng, M.I. Arnot, J. Peloquin, J. Hamid, W. Barr, A. Nirdosh, B. Simms, R.J. Winkfein, and G.W. Zamponi. 2004. A single Gβ subunit locus controls cross-talk between protein kinase C and G protein regulation of N-type calcium channels. *J Biol Chem*. 279:29709-29717.

Drean, G., C. Leclerc, A.M. Duprat, and M. Moreau. 1995. Expression of L-type Ca^{2+} channel during early embryogenesis in Xenopus laevis. *Int J Dev Biol*. 39:1027-1032.

Eells, J.T., and M.L. Dubocovich. 1988. Pyrethroid insecticides evoke neurotransmitter release from rabbit striatal slices. *Journal of Pharmacology and Experimental Therapeutics*. 246:514-521.

Elliott, M., A.W. Farnham, N.F. Janes, P.H. Needham, and D.A. Pulman. 1974. Insecticidally active conformations of pyrethroids. *In* G.K. Kohn, editor. American Chemical Society, Washington, D.C. 80-91.

Fang, H., S. Patanavanich, S. Rajagopal, X. Yi, M.S. Gill, J.J. Sando, and G.L. Kamatchi. 2006. Inhibitory role of Ser-425 of the α_1 2.2 subunit in the enhancement of $Ca_V2.2$ currents by phorbol-12-myristate, 13-acetate. *J Biol Chem*. 281:20011-20017.

Finkbeiner, S., and M.E. Greenberg. 1998. Ca^{2+} channel-regulated neuronal gene expression. *J Neurobiol*. 37:171-189.

García-Ferreiro, R.E., E.O. Hernández-Ochoa, and D.E. García. 2001. Modulation of N-type Ca^{2+} channel current kinetics by PMA in rat sympathetic neurons. *Pflugers Arch*. 442:848-858.

Ginsburg, K., and T. Narahashi. 1993. Differential sensitivity of tetrodotoxin-sensitive and tetrodotoxin-resistant sodium channels to the insecticide allethrin in rat dorsal root ganglion neurons. *Brain Res*. 627:239-248.

Goldin, A. 1992. Maintenance of Xenopus laevis and oocyte injection. *Methods Enzymol*. 207:266-279.

Goldin, A.L., R.L. Barchi, J.H. Caldwell, F. Hofmann, J.R. Howe, J.C. Hunter, R.G. Kallen, G. Mandel, M.H. Meisler, Y.B. Netter, M. Noda, M.M. Tamkun, S.G. Waxman, J.N. Wood, and W.A. Catterall. 2000. Nomenclature of voltage-gated sodium channels. *Neuron*. 28:365-368.

Hamid, J., D. Nelson, R. Spaetgens, S.J. Dubel, T.P. Snutch, and G.W. Zamponi. 1999. Identification of an integration center for cross-talk between protein kinase C and G protein modulation of N-type calcium channels. *J Biol Chem*. 274:6195-6202.

Hanlon, M.R., and B.A. Wallace. 2002. Structure and function of voltage-dependent ion channel regulatory β subunits. *Biochemistry*. 41:2886-2894.

Hartzell, C., I. Putzier, and J. Arreola. 2005. Calcium-Activated Chloride Channels. *Annual Review of Physiology*. 67:719-758.

Hildebrand, M.E., J.E. McRory, T.P. Snutch, and A. Stea. 2004. Mammalian voltage-gated calcium channels are potently blocked by the pyrethroid insecticide allethrin. *J Pharmacol Exp Ther*. 308:805-813.

Hodgkin, A.L., and A.F. Huxley. 1952. A quantitative description of membrane current and its application to conduction and excitation in nerve. *J Physiol*. 117:500-544.

Hossain, M.M., T. Suzuki, I. Sato, T. Takewaki, K. Suzuki, and H. Kobayashi. 2004. The modulatory effect of pyrethroids on acetylcholine release in the hippocampus of freely moving rats. *Neurotoxicology*. 25:825-833.

Isom, L.L., K.S.D. Jongh, D.E. Patton, B.F.X. Reber, J. Offord, H. Charbonneau, K. Walsh, A.L. Goldin, and W.A. Catterall. 1992. Primary Structure and Functional Expression of the β_1 Subunit of the Rat Brain Sodium Channel. *Science*. 256:839-842.

Isom, L.L., D.S. Ragsdale, K.S. De Jongh, R.E. Westenbroek, B.F.X. Reber, T. Scheuer, and W.A. Catterall. 1995. Structure and function of the β_2 subunit of brain sodium channels, a transmembrane glycoprotein with a CAM motif. *Cell*. 83:433-442.

Kass, R.S. 2004. Sodium Channel Inactivation Goes with the Flow. *The Journal of General Physiology*. 124:7-8.

Kellenberger, S., T. Scheuer, and W.A. Catterall. 1996. Movement of the Na1 Channel Inactivation Gate during Inactivation. *The Journal of Biological Chemistry*. 271:30971-30979.

Kostyuk, P.G., and R.E. Shirokov. 1989. Deactivation kinetics of different components of calcium inward current in the membrane of mice sensory neurones. *J Physiol*. 409:343-355.

Li, D., F. Wang, M. Lai, Y. Chen, and J.F. Zhang. 2005. A protein phosphatase 2cα-Ca^{2+} channel complex for dephosphorylation of neuronal Ca^{2+} channels phosphorylated by protein kinase C. *J Neurosci*. 25:1914-1923.

Lin, Z., S. Haus, J. Edgerton, and D. Lipscombe. 1997. Identification of functionally distinct isoforms of the N-type Ca^{2+} channel in rat sympathetic ganglia and brain. *Neuron*. 18:153-166.

Liu, W.S., and C.A. Heckman. 1998. The Sevenfold Way of PKC Regulation. *Cellular Signaling*. 10:529-542.

Maeno-Hikichi, Y., S. Chang, K. Matsumura, M. Lai, H. Lin, N. Nakagawa, S. Kuroda, and J.F. Zhang. 2003. A PKC epsilon-ENH-channel complex specifically modulates N-type Ca^{2+} channels. *Nat Neurosci*. 6:468-475.

Martinez-Pinna, J., E.M. McLachlan, and R. Gallego. 2000. Distinct mechanisms for activation of Cl^- and K^+currents by Ca^{2+} from different sources in mouse sympathetic neurones. *Journal of Physiology*.249â€”264.

Mosior, M., and A.C. Newton. 1996. Calcium-Independent Binding to Interfacial Phorbol Esters Causes Protein Kinase C To Associate with Membranes in the Absence of Acidic Lipidsâ€ 35:1612-1623.

Narahashi, T. 1992. Nerve Membrane Na+ Channels as targets of insecticides. *Trends in Pharmacological Sciences*. 13:234-241.

Narahashi, T., A. Tsunoo, and M. Yoshii. 1987. Characterization of two types of calcium channels in mouse neuroblastoma cells. *J Physiol (Lond)*. 383:231-249.

Narahashi, T., and T. Yamasaki. 1960. Mechanism of Increase in Negative After-Potential by Dicophanum (DDT) in the Giant Axons of the Cockroach. *Journal of Physiology*. 152:122-140.

Neal, A.P., Y. Yuan, and W.D. Atchinson. 2010. Allethrin Differentially Modulates Voltage-Gated Calcium Channel Subtypes in Rat PC12 Cells. *Toxicological Sciences*. 116:604-613.

Newton, A.C. 2001. Protein kinase C: structural and spatial regulation by phosphorylation, cofactors, and macromolecular interactions. *Chem Rev*. 101:2353-2364.

Nichols, R.A., J.W. Haycock, J.K. Wang, and P. Greengard. 1987. Phorbol ester enhancement of neurotransmitter release from rat brain synaptosomes. *J Neurochem*. 48:615-621.

Nishizuka, Y. 1992. Intracellular signaling by hydrolysis of phospholipids and activation of protein kinase C. *Science*. 258:607-614.

Ogata, N., and H. Tatebayashi. 1993. Kinetic analysis of two types of Na^+ channels in rat dorsal root ganglia. *J Physiol*. 466:9-37.

Perez-Reyes, E. 2003. Molecular Physiology of Low-Voltage-Activated T-Type Calcium Channels. *Physiol Rev*. 83:117-161.

Rajagopal, S., H. Fang, C. Lynch Iii, J.J. Sando, and G.L. Kamatchi. 2011. Effects of isoflurane on the expressed Cav2.2 currents in Xenopus oocytes depend on the activation of protein kinase C [delta] and its phosphorylation sites in the Cav2.2[alpha]1 subunits. *Neuroscience*. 182:232-240.

Ray, D.E., and J.R. Fry. 2006. A reassessment of the neurotoxicity of pyrethroid insecticides. *Pharmacology and Therapeutics*. 111:174-193.

Rossie, S. 1999. Regulation of voltage-sensitive sodium and calcium channels by phosphorylation. *Adv Second Messenger Phosphoprotein Res*. 33:23-48.

Roy, M.L., and T. Narahashi. 1992. Differential Properties of Tetrodotoxin-sensitive and Tetrodotoxin-resistant Sodium Channels in Rat Dorsal Root Ganglion Neurons. *The Journal of Neuroscience*. 12:2104-2111.

Shafer, T.J., and D.A. Meyer. 2004. Effects of pyrethroids on voltage-sensitive calcium channels: a critical evaluation of strengths, weaknesses, data needs, and relationship to assessment of cumulative neurotoxicity. *Toxicol Appl Pharmacol*. 196:303-318.

Shafer, T.J., D.A. Meyer, and K.M. Crofton. 2005. Developmental Neurotoxicity of Pyrethroid Insecticides: Critical Review and Future Research Needs. *Environmental Health Perspectives*. 113:123-136.

Shih, T.M., R.D. Smith, L. Toro, and A.L. Goldin. 1998. High-level expression and detection of ion channels in Xenopus oocytes. *Methods Enzymol*. 293:529-556.

Soderlund, D.M., and J.R. Bloomquist. 1989. Neurotoxic actions of pyrethroid insecticides. *Annu Rev Entomol*. 34:77-96.

Soderlund, D.M., J.M. Clark, L.P. Sheets, L.S. Mullin, V.J. Piccirillo, D. Sargent, J.T. Stevens, and M.L. Weiner. 2002. Mechanisms of pyrethroid neurotoxicity: implications for cumulative risk assessment. *Toxicology*. 171:3-59.

Soderlund, D.M., and S.H. Lee. 2001. Point Mutations in Homology Domain II Modify the Sensitivity of Rat Nav1.8 Sodium Channels to the Pyrethroid Insecticide Cismethrin. *NeuroToxicology*. 22:755-765.

Stea, A., T.W. Soong, and T.P. Snutch. 1995. Determinants of PKC-dependent modulation of a family of neuronal calcium channels. *Neuron*. 15:929-940.

Swanson, R., and K. Folander. 1992. In vitro synthesis of RNA for expression of ion channels in Xenopus oocytes. *Methods Enzymol*. 207:310-319.

Swartz, K.J. 1993. Modulation of Ca^{2+} channels by protein kinase C in rat central and peripheral neurons: disruption of G protein-mediated inhibition. *Neuron*. 11:305-320.

Swartz, K.J., A. Merritt, B.P. Bean, and D.M. Lovinger. 1993. Protein kinase C modulates glutamate receptor inhibition of Ca^{2+} channels and synaptic transmission. *Nature*. 361:165-168.

Symington, S., R. Frisbie, H. Kim, and J. Clark. 2007a. Mutation of Threonine 422 to Glutamic Acid Mimics the Phosphorylation State and Alters the Action of Deltamethrin on CaV2.2. *In*. Pesticide Biochemistry and Physiology. 312-320.

Symington, S., A. Zhang, and J. Clark. 1999a. The action of pyrethroids on the voltage-sensitive calcium channel of Paramecium tetraurelia. *In*. Pesticide Science. 1035-1037.

Symington, S., A. Zhang, W. Karstens, J. Van Houten, and J. Clark. 1999b. Characterization of pyrethroid action on ciliary calcium channels in Paramecium tetraurelia. *In*. Pesticide Biochemistry and Physiology. 181-193.

Symington, S.B., and J.M. Clark. 2005. Action of deltamethrin on N-type ($Ca_V2.2$) voltage-sensitive calcium channels in rat brain. *In*.

Symington, S.B., R.K. Frisbie, K.D. Lu, and J. Marshall Clark. 2007b. Action of cismethrin and deltamethrin on functional attributes of isolated presynaptic nerve terminals from rat brain. *Pesticide Biochemistry and Physiology*. 87:172-181.

Tan, J., and D.M. Soderlund. 2009. Human and rat $Na_V1.3$ voltage-gated sodium channels differ in inactivation properties and sensitivity to the pyrethroid insecticide tefluthrin. *NeuroToxicology*. 30:81-89.

Vais, H., S. Atkinson, N. Eldursi, A.L. Devonshire, M.S. Williamson, and P.N.R. Usherwood. 2000. A single amino acid change makes a rat neuronal sodium channel highly sensitive to pyrethroid insecticides. *FEBS Letters*. 470:135-138.

Vance, C.L., C.M. Begg, W.L. Lee, H. Haase, T.D. Copeland, and M.W. McEnery. 1998. Differential expression and association of calcium channel α_{1B} and β subunits during rat brain ontogeny. *J Biol Chem*. 273:14495-14502.

Wang, S.-Y., and G.K. Wang. 2003. Voltage-gated sodium channels as primary targets of diverse lipid-soluble neurotoxins. 15:151-159.

Weiner, M.L., M. Nemec, L. Sheets, D. Sargent, and C. Breckenridge. 2009. Comparative functional observational battery study of twelve commercial pyrethroid insecticides in male rats following acute oral exposure. *NeuroToxicology*. 30:S1-S16.

Xiao, H., X.-C. Zhang, L. Zhang, X.-Q. Dai, W. Gong, J. Cheng, R. Gao, and X. Wang. 2006. Fenvalerate modifies T-type Ca2+ channels in mouse spermatogenic cells. *Reproductive Toxicology*. 21:48-53.

Xu, Y.F., S.J. Hewett, and W.D. Atchison. 1998. Passive Transfer of Lambert-Eaton Myasthenic Syndrome Induces Dihydropyridine Sensitivity of I_{Ca} in Mouse Motor Nerve Terminals. *Journal of Neurophysiology*. 80:1056-1069.

Yoshii, M. 1985. Effects of pyrethroids and veratridine on two types of calcium channels in neuroblastoma cells. *Society for Neuroscience Abstracts*. 11:158.159.

Yu, F.H., and W.A. Catterall. 2003. Overview of the voltage-gated sodium channel family. *Genome Biology*. 4:207.

Zamponi, G.W., E. Bourinet, D. Nelson, J. Nargeot, and T.P. Snutch. 1997. Crosstalk between G proteins and protein kinase C mediated by the calcium channel α_1 subunit. *Nature*. 385:442-446.

Zhu, Y., and S. Ikeda. 1994. Modulation of Ca2+-channel currents by protein kinase C in adult rat sympathetic neurons. *Journal of Neurophysiology*. 72:1549-1560.